

1-1-2013

# Characterizing Hypoxia and Its Behavioral Effects In 3-Dimensional Cell Aggregates

Matthew Lorincz Skiles  
*University of South Carolina*

Follow this and additional works at: <http://scholarcommons.sc.edu/etd>

---

## Recommended Citation

Skiles, M. L. (2013). *Characterizing Hypoxia and Its Behavioral Effects In 3-Dimensional Cell Aggregates*. (Doctoral dissertation). Retrieved from <http://scholarcommons.sc.edu/etd/533>

This Open Access Dissertation is brought to you for free and open access by Scholar Commons. It has been accepted for inclusion in Theses and Dissertations by an authorized administrator of Scholar Commons. For more information, please contact [SCHOLARC@mailbox.sc.edu](mailto:SCHOLARC@mailbox.sc.edu).

Characterizing Hypoxia and its Behavioral Effects in 3-Dimensional Cell Aggregates

by

Matthew L. Skiles

Bachelor of Science  
University of South Carolina, 2006

---

Submitted in Partial Fulfillment of the Requirements

For the Degree of Doctor of Philosophy in

Biomedical Engineering

College of Engineering and Computing

University of South Carolina

2013

Accepted by:

Dr. James Blanchette, Major Professor

Dr. Ehsan Jabbarzadeh, Committee Member

Dr. Susan Lessner, Committee Member

Dr. John Baynes, Committee Member

Lacy Ford, Vice Provost and Dean of Graduate Studies

© Copyright by Matthew L. Skiles, 2013  
All Rights Reserved.

## Dedication

A portion of my life has been invested into the work that culminates with this dissertation. It is therefore dedicated to those who prepared me for the effort, helped me through it, and will (hopefully) enjoy the fruits that its labor bears: my parents, Pamela and Samuel, my wife, Jean, and my son, Robert Gabriel.

## Acknowledgments

I would like to acknowledge, and thank, my advisor, Dr. James Blanchette, for the wisdom, guidance, and insight freely offered and invaluable to my growth and accomplishment as a researcher. I also offer appreciation to those who contributed to and/or facilitated the work that is presented here: Suchit, Romone, Nathan, Lindsay, Pritesh, and Kevin; the labs of Dr. Melissa Moss, Dr. Tarek Shazly, Dr. Ehsan Jabbarzadeh, Dr. Esmail Jabbari, and Dr. Michael Matthews at the University of South Carolina; the lab of Dr Kristi Anseth at the University of Colorado; and the Instrument Resource Facility at the University of South Carolina School of Medicine.

## Abstract

Cell transplantation can be considered a regenerative therapy, an intervention which attempts to replace or restore the function of compromised tissue by harnessing innate properties of cells that cannot be replicated artificially. For such therapies to succeed, it will be necessary to understand and closely match the physiological conditions that govern cell behaviors *in vivo*. One important factor is low oxygen tension, termed hypoxia, which is often overlooked *in vitro*. Because oxygen insufficiency can lead to cell death, hypoxia has traditionally been viewed as a negative condition. However, hypoxia can also serve as a potent regulator of crucial cell behaviors involved in normal development, adaptation, and regeneration through transcriptional activity of hypoxia-inducible factors (HIFs). Characterizing HIF activity, especially in three-dimensional tissues which can experience oxygen heterogeneities, will be useful in investigating how culture parameters impact local microenvironmental conditions to affect cell behavior.

In the present work, a novel fluorescent reporter system was used to detect cellular HIF activity in islet-like clusters of pancreatic  $\beta$ -cells and adipose-derived stem cell (ADSC) spheroids, two cell systems used in transplantation therapies. Fluorescent signaling was observed in cultures incubated in reduced oxygen conditions and in large cultures, indicating the development of tissue size-dependent oxygen gradients. HIF activity could be monitored in the same samples over time and could be correlated to

other cell behaviors. In  $\beta$ -cells, signal was observed in all clusters incubated in 1% or 2% oxygen and in the center of large clusters ( $>300\mu\text{m}$ ) incubated in 20% oxygen. In clusters that exhibited HIF activity, insulin secretion and cluster morphology were severely impaired. In ADSC spheroids, both reduction of external oxygen concentration and an increase in spheroid size increased HIF activity. Moderate HIF activity corresponded with increased vascular endothelial growth factor (VEGF) secretion from spheroids, while intense HIF activity corresponded with regional reduction of cell viability; therefore, an optimal size for VEGF secretion could be demonstrated. Altogether, the HIF reporter system represents a useful tool in monitoring cellular hypoxia so that culture parameters such as external oxygenation and culture size can be properly considered in order to guide desired cell behaviors in cell transplantation.

## Table of Contents

Dedication.....	iii
Acknowledgements.....	iv
Abstract.....	v
List of Tables .....	viii
List of Figures .....	ix
List of Abbreviations.....	xi
Introduction .....	1
Chapter 1: Literature Review .....	3
1.1 Oxygen’s Role as a Nutrient .....	3
1.2 Oxygen’s Role in Cell Signaling .....	13
1.3 Regulating Hypoxia to Affect Cell Behaviors in Transplantation Therapies....	39
Chapter 2: Correlating Hypoxia with Insulin Secretion Using a Fluorescent Hypoxia Detection System.....	56
Chapter 3: Identifying HIF Activity in 3D Cultures of Islet-Like Clusters .....	79
Chapter 4: Influence of Culture Geometry on Hypoxia and Hypoxia-Induced Secretion of VEGF in Human Adipose-Derived Stem Cell Spheroid .....	101
Chapter 5: Conclusions .....	126
References .....	131

## List of Tables

Table 1.1 Normal pO <sub>2</sub> values reported in different human tissues .....	10
Table 1.2 Direct transcriptional targets of HIF-1 .....	29
Table 2.1 Analysis of MIN6 aggregate sizes.....	70
Table 4.1 Mean values and standard deviation of VEGF release from ADSC cultures .....	117
Table 4.2 Table indicating statistical significance of differences in mean VEGF release from the cultures under study .....	118

## List of Figures

Figure 1.1 Production of energy-carrying molecules in aerobic cellular respiration .....	5
Figure 1.2 Schematic of the ETC and production of ATP by proton motive force.....	6
Figure 1.3 Oxygen-dependent mechanisms of HIF regulation .....	22
Figure 1.4 Schematic of development of hypoxia in 3D cultures .....	42
Figure 2.1 Schematic of a novel hypoxia detection system in living MIN6 cells .....	66
Figure 2.2 Dissolved oxygen concentrations measured in 2 mL of growth medium.....	68
Figure 2.3 Daily one hour insulin release over 2 weeks.....	71
Figure 2.4 Fluorescently imaged aggregates .....	73
Figure 3.1 400,000 MIN6 cells aggregated to form islet-like clusters .....	88
Figure 3.2 Brightfield microscopy images of islet-like clusters for the analysis of morphology .....	90
Figure 3.3 Top) Schematic of HIF-induced cellular fluorescence.....	92
Bottom) Hypoxic signaling in islet-like clusters of MIN6 cells.....	92
Figure 3.4 GSIS in clusters of MIN6 cells .....	93
Figure 3.5 Analysis of viability in clusters of MIN6 cells.....	95
Figure 4.1 Flow cytometry analysis of cell surface markers CD44 and CD105 in P6 ADSCs .....	107
Figure 4.2 Diameter of spheroids formed by centrifugally pelleting different numbers of ADSCs .....	112
Figure 4.3 Fluorescent DsRed signaling as an indicator of HIF activity in 5k, 10k, 20k, and 60k ADSC spheroids .....	113

Figure 4.4 Fluorescent HIF reporter signal displayed at 1/5 the exposure length as in Figure 4.2 .....	115
Figure 4.5 Levels of daily and total per-cell VEGF release from ADSC monolayers and 5k, 10k, 20k, and 60k spheroids.....	116
Figure 4.6 H&E staining of ADSC spheroid sections.....	120
Inset) Live/Dead viability assessment of ADSCs .....	120

## List of Abbreviations

°C	Degrees Celsius
I	ETC complex I (NADH-ubiquinone oxidoreductase)
II	ETC complex II (Succinate-ubiquinone oxidoreductase)
III	ETC complex III (Ubiquinol-cytochrome c oxidoreductase)
IV	ETC complex IV (Cytochrome c oxidase [COX])
3D	Three-dimensional
5k	5,000
10k	10,000
20k	20,000
60k	60,000
Acetyl CoA	Acetyl co-enzyme A
A.C.S.	American Chemical Society
ADP	Adenosine diphosphate
ADSC	Adipose-derived stem cell
ANG-1	Angiopoietin 1
ARNT	Aryl hydrocarbon receptor nuclear translocator
ATP	Adenosine triphosphate
Bcl-2	B-cell lymphoma 2
bFGF	Basic fibroblast growth factor
bHLH-PAS	basic helix-loop-helix PER-ARNT-SIM
bNGF	Basic nerve growth factor
BNIP3	BCL2/adenovirus E1B 19 kDa protein-interacting protein 3
cAMP	Cyclic adenosine monophosphate
CBP/p300	CREB binding protein/p300 transcriptional coactivator
cm <sup>2</sup>	Square centimeters
CMV	Cytomegalovirus
CO <sub>2</sub>	Carbon dioxide
COX	Cytochrome-c oxidase
CREB	cAMP response element-binding protein
CSF	Colony stimulating factors
CTAD	C-terminal transactivation domain
Cyt C	Cytochrome C
Da	Dalton
DNA	Deoxyribonucleic acid
DsRed-DR	Destabilized variant of the DsRed protein
ELISA	Enzyme-linked immunosorbent assay
EPAS1	Endothelial PAS domain protein 1

EPO	Erythropoietin
ETC	Electron transport chain
FADH <sub>2</sub>	Flavin adenine dinucleotide (reduced form)
Fe <sup>2+</sup>	Iron II; Ferrous iron
FIH	Factor inhibiting HIF
g	Force of gravity
GFP	Green fluorescent protein
GSIS	Glucose-stimulated insulin secretion
<sup>1</sup> H NMR	Proton nuclear magnetic resonance
H <sub>2</sub> O <sub>2</sub>	Hydrogen peroxide
HBSS	Hank's Balanced Salt Solution
HGF	Hepatocyte growth factor
HIF	Hypoxia-inducible factor
HO·	Hydroxide radical
HRE	Hypoxia responsive element
Hrs.	Hours
IGF-1	Insulin-like growth factor 1
IL	Interleukin
IU	International units
kDa	KiloDalton
K <sub>m</sub>	Michaelis-Menten constant (half maximal rate of reaction)
L	Liter
LDH	Lactate dehydrogenase
LOX	Lysyl oxidase
LOXL2	Lysyl oxidase-like 2
MCP	Monocyte chemoattractant protein
mg	Milligram
Min	Minutes
MIN6	Murine insulinoma 6
mL	Milliliter
miRNA	MicroRNA
mm	Millimeters
mM	Millimolar
mmHG	Millimeters of mercury
MMP	Matrix metalloproteinases
M <sub>n</sub>	Number average molar mass
MOI	Multiplicity of infection
MRI	Magnetic resonance imaging
mRNA	Messenger ribonucleic acid
MSC	Mesenchymal stem cell
mTOR	Mammalian target of rapamycin
mW	Milliwatt
NADH	Nicotinamide adenine dinucleotide (reduced form)
nm	Nanometers

NTAD.....	N-terminal transactivation domain
O <sub>2</sub> .....	Oxygen (dioxygen gas, molecular oxygen)
·O <sub>2</sub> <sup>-</sup> .....	Superoxide anion
O <sub>2</sub> Hb.....	Oxyhemoglobin
Oct4.....	Octamer-binding transcription factor 4
ODD.....	Oxygen-dependent degradation domain
OS-9.....	Osteosarcoma amplified 9 protein
P4H2.....	Prolyl 4-hydroxylase 2
PDGF.....	Platelet-derived growth factor
PEG.....	Poly(ethylene glycol)
PEGDM.....	PEG dimethacrylate
PER.....	Period circadian protein
PEST.....	Proline, glutamic acid, serine, threonine sequence
PET.....	Positron emission tomography
PHDs.....	Prolyl-4-hydroxylases
PKM2.....	Pyruvate kinase isoform M2
pO <sub>2</sub> .....	Oxygen partial pressure
pVHL.....	von Hippel-Lindau tumor suppressor protein
Q.....	Ubiquinone (oxidized) / ubiquinol (reduced)
RACK-1.....	Receptor for activated C kinase 1
rcf.....	Relative centrifugal force
ROS.....	Reactive oxygen species
rpm.....	Revolutions per minute
RPMI 1640.....	Roswell Park Memorial Institute medium 1640
RT-PCR.....	Real-time polymerase chain reaction
Sbstr. lvl.....	Substrate-level
SDF-1.....	Stromal cell-derived factor 1
SIM.....	Single-minded protein
SIP1.....	Survival of motor neuron protein-interacting protein 1
SIRT-3.....	NAD-dependent deacetylase sirtuin-3, mitochondrial
SSAT2.....	Spermidine/Spermine N1-Acetyltransferase 2
t <sub>1/2</sub> .....	Half-time
T1DM.....	Type 1 diabetes mellitus
TGF-β.....	Transforming growth factor-β
TNF-α.....	Tumor necrosis factor α
UV.....	Ultraviolet
VEGF.....	Vascular endothelial growth factor
Vol.....	Volume
W.....	Watts
Wt.....	Weight
wt%.....	Weight percent
μg.....	Microgram
μm.....	Micrometer
μL.....	Microliter

## Introduction

This dissertation is concerned with presenting and discussing experimental data which contributes novel findings to the field of cell transplantation. Specifically, results from the included studies provide a better understanding of how hypoxia develops within 3-dimensional (3D) cultures of pancreatic  $\beta$ -cells and adipose-derived stem cells (ADSCs) and how knowledge of this hypoxic status can be used to rationally direct desired cell behaviors (insulin secretion and VEGF secretion, respectively) to improve outcomes in transplantation therapies intended to restore lost tissue function. The structure of this dissertation, then, is intended to both communicate peer-reviewed results from several separate studies and to make clear the underlying impetus by which they are unified. The document is structured in the following manner:

- Chapter 1 consists of a literature review intended to develop a framework explaining why the research was undertaken. This includes relevant historical studies, recent findings and advancements in the field, and identification of areas in which the current knowledge appears to be incomplete. Specifically, the essential role of oxygen as a both a nutrient and as a cell signaling molecule is first discussed. Next, the mechanism of hypoxia-mediated regulation of cell behavior is explained, and it is suggested that rational control of culture parameters can be used to regulate hypoxic status, thus driving desired cell function. A novel approach to identifying cellular hypoxia is also advocated.

Finally, the importance of hypoxic status is considered in two specific cell systems which exhibit potential usefulness in transplantation therapies: islet-like  $\beta$ -cell clusters and ADSC spheroids. The advantages of tracking hypoxia by use of a novel reporter system as well as the potential benefits of characterizing hypoxia in these two systems are highlighted.

- Chapters 2-4 are research studies that have been published or submitted for publication in peer-reviewed research journals. These chapters each include a brief introduction, description of experimental methods and design, study results, and discussion of the findings. Section, figure, and reference numbering has been altered to conform to the formatting of this dissertation. Chapter 2 reports on the use of the hypoxia reporter in encapsulated islet-like clusters of  $\beta$ -cells of different sizes cultured in 20% or 1% oxygen. Chapter 3 compares hypoxic status, function, and viability of encapsulated clusters of the same size cultured in 20%, 2%, or 1%. Chapter 4 reports how overall hypoxic status of ADSC spheroids, as indicated by the reporter, can be intentionally affected by spheroid size and culture oxygenation in order to direct optimal secretion of proangiogenic growth factors from the cells.
- Chapter 5 discusses the overall findings of the previous three chapters, tying together the results and making an argument for the importance of considering oxygen tension in cell-based therapies. The novel results of these studies as well as their contribution to the advancement of  $\beta$ -cell and ADSC transplantation are presented.

## Chapter 1

### Literature Review

#### 1.1 Oxygen's Role as a Nutrient

Oxygen is an abundant element in nature, existing commonly as colorless, odorless dioxygen gas ( $O_2$ ), or forming oxides with most other elements. Estimates suggest that oxygen presently accounts for roughly 49% (wt.) of Earth's crust and 21% (vol.) of Earth's atmosphere [1 Duursma and Boissan, 1994]. Furthermore, molecular oxygen has been present in the environment, at varying levels, for the majority of the time span over which life has been evolving [2 Castresana 1995],[3 Dismukes 2001],[4 Kump 2008],[5 Stamati 2011]. From its ubiquity, it is not surprising, then, that oxygen plays an integral role in the biochemical processes of most known species. While certain unicellular organisms with ancient evolutionary origins have retained the capability to survive without oxygen, most other unicellular organisms, and virtually all multicellular ones, are dependent upon oxygen for survival. Indeed, incorporation of oxygen into biotic biochemistry may have been a prerequisite for the development of metazoan life [3 Dismukes 2001],[5 Stamati 2011]. The importance of oxygen to human biology, for instance, is evidenced by the complex mechanisms that have evolved to facilitate its availability: respiratory organs (lungs) to take in oxygen, carrier molecules (hemoglobin) to bind it, and a circulatory system (heart and blood vessels) to distribute

it throughout the body. In this regard, oxygen can be considered a nutrient, a chemical used in an organism's metabolism that is required to sustain its life and which must be taken in from its external environment [6 Whitney 2005].

### 1.1.1 Aerobic Respiration

In living organisms, the presence of oxygen allows for increased efficiency in energy production. Organisms that do not utilize oxygen for energy production depend solely upon the process of glycolysis for the direct formation of adenosine triphosphate (ATP) and are termed "anaerobes". Anaerobes are typically unicellular and prokaryotic. Alternatively, aerobes use oxygen as the final electron receptor in the process of oxidative phosphorylation, a series of reactions that generate 16-18 times more ATP than glycolysis. In aerobic cells, mitochondria, the organelles in which the oxidative phosphorylation process occurs, can account for 85-90% of cellular oxygen consumption [7 Solaini 2010].

In the process of oxidative phosphorylation, pyruvate, the product of glycolysis, is further broken down in the citric acid cycle to produce more ATP as well as the reduced form of the molecules nicotinamide adenine dinucleotide (NADH) and flavin adenine dinucleotide (FADH<sub>2</sub>), which act as energy carriers (Figure 1.1). NADH and FADH<sub>2</sub> donate electrons to the electron transport chain (ETC), a series of membrane-associated protein complexes that are sequentially reduced by the electrons, resulting in protons being pumped out of the inner mitochondrial compartment against their concentration gradient. The electrons are finally passed to the enzyme, cytochrome-c oxidase (COX), which uses four electrons to catalyze the reduction of one molecule of O<sub>2</sub>

to two molecules of water [8 Brunori 1987]. The proton gradient generated by the ETC is used by the transmembrane protein complex, ATP synthase, to generate ATP (Figure 1.2). It is estimated that nearly 40% of the energy represented in the oxidation of glucose is converted to energy in the form of ATP [9 Bergamini 2004], making aerobic respiration a highly efficient biological reaction.

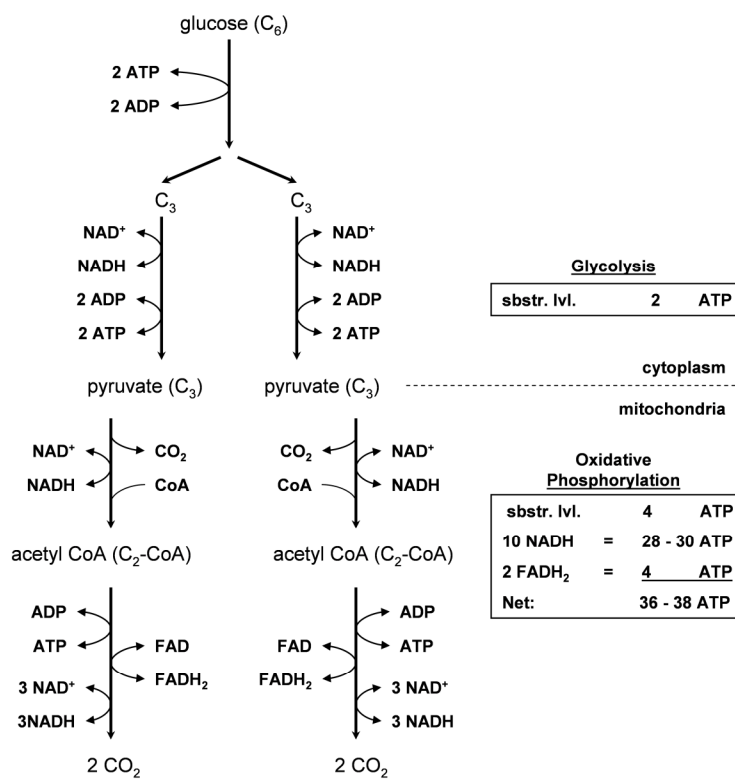


Figure 1.1 Production of energy-carrying molecules in aerobic cellular respiration. Comparison of ATP production in the aerobic and anaerobic processes is also shown. (ADP: adenosine diphosphate; CO<sub>2</sub>: carbon dioxide; acetyl CoA: acetyl co-enzyme A)

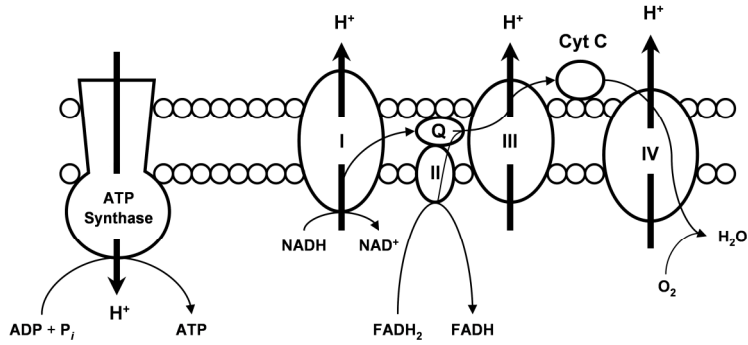


Figure 1.2 Schematic of the ETC and production of ATP by proton motive force. NADH and FADH<sub>2</sub> initially donate electrons to different complexes in the ETC, resulting in the transfer of a different number of protons for the two molecules.

#### 1.1.1.1 Aerobic Respiration and Organismal Complexity

The energy yield from anaerobic respiration is relatively small in comparison to aerobic respiration. This energy limitation necessarily limits the diversity of molecules that can be produced in anaerobic species, and, in turn, restricts their potential size and complexity. Raymond and Serge predicted that at least 1000 metabolic reactions which occur in aerobic metabolism cannot occur under anaerobic processes [10 Raymond 2006]. Specifically, these tend to be synthesis reactions of larger, more hydrophilic macromolecules. Additionally, certain molecules, such as sterols, that are essential to complex, compartmentalized cells, require oxygen for their biosynthesis and are thus typically lacking in anaerobic organisms [11 Summons 2006]. Furthermore, elevated metabolic levels resulting from aerobic respiration have been suggested to have contributed to the development of nuclear signaling pathways in eukaryotes, as many nuclear factors are products of respiration [12 Jiang 2010]. Thus, it is clear that the rise

of atmospheric oxygen and the emergence of aerobic metabolism were critical to the evolution of complex metazoans whose energy demands cannot be met by glycolysis alone [5 Stamati 2011],[12 Jiang 2010],[13 Thannickal 2009]. In fact, oxygen is noted to be among the most commonly-used molecules in the metabolic and biosynthetic processes of multicellular animals [10 Raymond 2006].

#### 1.1.1.2 Aerobic Respiration and Reactive Oxygen Species

Evolution of the ability to use oxygen in the production of energy was a boon to organismal complexity. However, use of oxygen in metabolism presents a set of challenges for aerobic life forms. The large energy release from the reduction of O<sub>2</sub> to water is harnessed during oxidative phosphorylation in a series of less energetic reduction reactions in the ETC. Electron “leak” during these steps can result in premature and incomplete reduction of O<sub>2</sub> and formation of several different oxygen metabolites such as hydrogen peroxide (H<sub>2</sub>O<sub>2</sub>), superoxide anions ( $\cdot\text{O}_2^-$ ), or hydroxide radicals (HO $\cdot$ ). These products, known as reactive oxygen species (ROS), are significantly less stable than molecular oxygen and interact with other biomolecules much more readily than O<sub>2</sub>.

At least nine mitochondrial enzymes in the ETC have been found to measurably contribute to ROS production in mammalian cells [14 Andreyev 2005]. In fact, it has been estimated that 2-3% of the molecular oxygen utilized by mitochondria in oxidative phosphorylation is incompletely reduced [15 Gibson 2008]. If not neutralized, excessive ROS levels can be extremely toxic to a cell. ROSs have the ability to damage lipids, proteins, and deoxyribonucleic acids (DNA), among other cell constituents [9 Bergamini

2004],[16 Chance 1955]. Furthermore, oxidative damage by ROSs to certain enzyme complexes involved in the ETC can cause an increased generation of more ROSs in a feed-forward manner. Cellular damage caused by ROSs is collectively referred to as “oxidative stress” and can result in cell death. The negative impact that ROSs can have on cellular function can be implied from the considerable number of protective mechanisms that aerobic cells have developed for detoxifying ROSs or mitigating their damage [14 Andreyev 2005].

### 1.1.2 Hypoxia

In 1772, Joseph Priestley showed that depletion of an essential element in air by a mouse in a sealed glass jar resulted in the animal’s death, and that a plant placed in the jar could restore the air’s vitality [17 Priestley 1772]. The element was subsequently isolated and identified as oxygen [18 Lavoisier 1789]. The word “hypoxia” (“hypo” – low or less, and “oxia” – referring to oxygen), then, denotes a state of reduced oxygenation within a biotic environment, often used to mean “oxygen insufficiency”. In humans, some common causes of hypoxia within bodily tissues include environmental limitation (thin air), respiratory disorder, blood disorder (anemia), vascular damage/occlusion, and elevated metabolic use (exercise). From Priestley’s experiment, it is clear that the dire, organismal-level effects of hypoxia have long been known.

Different species can exhibit different tolerances to hypoxia. For instance, loggerhead turtles, marine reptiles, have been found to dive underwater for up to seven hours before resurfacing [19 Hochscheid 2005], while sperm whales, marine mammals, can dive for thirty minutes to an hour [20 Watkins 2002]. For many common terrestrial

mammals, including humans, the survival time without oxygen is generally found to be 4-6 minutes. (Indeed, Irving estimated that the maximal theoretical store of oxygen in an average adult male would be completely consumed by resting metabolism in no more than 11 minutes [21 Irving 1939].) Resistance to hypoxia also varies among different types of tissue, depending largely upon their metabolic activity and energy requirement. For instance, the estimated survival times of different human tissues without oxygen vary widely: brain, < 3 min.; kidney and liver, 15-20 min.; skeletal muscle, 60-90 min.; vascular smooth muscle, 24-72 hrs.; hair and nails, several days [22 Leach 1998]. However, no matter the cellular or organismal tolerance for hypoxia, all forms of life that are dependent upon aerobic respiration succumb to oxygen deprivation of sufficient severity or duration.

#### 1.1.2.1 Hypoxia: Notes on Terminology

The term “hypoxia” is applied somewhat ambiguously in the biomedical literature, describing either an oxygen range, typically 0% – 5% O<sub>2</sub>, or a comparative oxygen tension that is below the physiological norm for a given tissue. The difference is subtle yet relevant, as the native oxygen environment can vary significantly between different tissues in the body. For instance, from Table 2.1 it can be seen that some tissues constantly reside in an environment that is traditionally considered hypoxic, while others can experience a significant reduction in oxygen from normal levels while remaining above an oxygen partial pressure (pO<sub>2</sub>) of 5% [23 Carreau 2011],[24 Fermor 2007].

Table 1.1 Normal pO<sub>2</sub> values reported in different human tissues.

Tissue	pO <sub>2</sub>	
	mmHg	%
Articular Cartilage		
superficial	53	7
deep zone	<7.6	<1
Bone Marrow	52-55	6.8-7.2
Brain	24-48	3.2-6.3 (>4.6 ensures normal function)
Intestine		
small bowel wall	61	8.0
solon wall	34	4.5
Kidney		
cortex	50	6.6
medulla	10-20	1.3-2.6
Liver	31-42	4.1-5.5
Lungs		
alveolar surface	100-120	13.2-15.8
Muscle		
biceps	25	3.3
deltoid	34	4.5
gastrocnemius	29	3.8
quadriceps femoris	32	4.2
tibial muscle	21	2.8
Skin		
superficial region	8	1.1
dermal papillae	24	3.2
sub-papillary plexus	35	4.6
Compiled from references in <b>24</b> Carreau 2011 and <b>24</b> Fermor 2007.		

Due to such imprecise terminology, attempts to clarify the language have been sporadically, though increasingly, seen. The more accurate terms “atmospheric normoxia” and “hyperoxia” have been used to describe atmospheric oxygen pressure, while “physiological normoxia”, “physioxia”, and “in situ normoxia” have been used to express normal physiological oxygen pressure [23 Carreau 2011],[25 Ivanovic 2009]. For such discriminating authors, “hypoxia” is reserved to denote an abnormally reduced pO<sub>2</sub>. Such descriptions are further complicated, however, by the somewhat variable reports

of the “physionormal”  $pO_2$  range, e.g. 3-10% [23 Carreau 2011], 2-9% [26 Simon 2008], 3-5% [27 Semenza 2012a], 1-14% [5 Stamati 2011]. Additionally, normal tissue oxygen pressure can vary from individual to individual and can be affected by various activities. In any case, the traditional use of “normoxia” to represent atmospheric oxygen pressure (21%) and “hypoxia” to represent oxygen pressures below 5% persists in the vast majority of the published literature.

That conditions which are traditionally viewed as “hypoxic” can be both physionormal and pathological depending upon the local microenvironment is a central theme of the present work. In either case, oxygen tension acts as a stimulus, affecting cell behavior and function. Therefore, this work will attempt to characterize “hypoxia” in such terms.

#### 1.1.2.2 Hypoxia: Effects of $O_2$ Limitations on Aerobic Respiration

Lack of oxygen is lethal to cells that rely on aerobic respiration, though the process of hypoxic cell death is not always straightforward. Some cellular effects of hypoxia can include dramatically reduced protein production and turnover, mitochondrial derangement, loss of osmotic balance, increased oxidative stress, and cell death by necrosis, apoptosis, or autophagy [7 Solaini 2010],[28 Hochachka 1996],[29 Shimizu 1996], [30 Zhang 2008],[31 Azad 2008],[32 Kumar 2010]. As  $O_2$  is required to accept electrons at the end of the ETC, it would be reasonable to assume that a paucity of oxygen would result in the dysfunction of oxidative phosphorylation. Indeed, in a traditional view, hypoxic cell death proceeds as follows: inhibition of the ETC, cessation of ATP production, depletion of ATP pools through utilization in cellular processes,

failure of membrane ion pumps, loss of osmotic balance, and, finally, necrotic cell death. However, more thorough investigations over the past several decades have found that disruption of the ETC due to oxygen limitation is not normally the precipitating cause of death in hypoxic cells.

By examining the relationship between oxygen concentration and electron flux in isolated mitochondria, it was found that COX activity did not become oxygen limited until oxygen concentrations fell below  $<0.1\%$  [33 Wilson 1979],[34 Erecinska 1982],[35 Rumsey 1990]. In other words, the ETC could still function to produce ATP even at oxygen concentrations well below the levels of physiological hypoxia. Interestingly, global cellular responses to hypoxia are often seen at oxygen concentrations in the range of 1-3%  $O_2$ , higher than the concentration at which oxygen becomes limiting for ETC function [36 Schumacker 1993] [37 Budinger 1996],[38 Chandel 1997],[39 Budinger 1998]. Such changes include reduction of energy-intensive processes, activation of glycolytic pathways, and changes in mitochondrial respiratory rate. This implies, somewhat counter intuitively, that instead of oxygen-limited mitochondrial function altering cellular function, altered cell function triggered by hypoxia seems to alter mitochondrial function. Indeed, it was found that cellular ATP utilization is the primary factor influencing respiration rate in most cells, accounting for up to 50% of the control over the process, while the ETC account for only 0-15% [40 Brown 1990a],[41 Brown 1990b].

Suppression of mitochondrial oxygen consumption in the range of 1-3%  $O_2$  is referred to as oxygen conformance and is a well-documented phenomenon [28

Hochachka 1996]. When this occurs, an increase in glycolytic respiration is usually seen. Though much less efficient than the aerobic process, glycolysis can proceed quickly and makes ATP available directly into the cytoplasm. Thus it can provide a significant amount of ATP for a cell in the short term. However, glycolysis also uses glucose much more rapidly than aerobic respiration. In conditions where *both* oxygen and nutrient availability are limited (such as ischemia, or severe hypoxia in cells with a high energy demand) glycolytic glucose insufficiency can result in ATP depletion, loss of osmotic balance, and necrosis, as predicted by the traditional view of hypoxia [42 Eguchi 1997].

That the oxygen-dependent chemical reaction in the aerobic metabolic pathway is not oxygen-limited when cells begin to exhibit a response to hypoxia indicates that nutritional oxygen (i.e. oxygen as a simple metabolic substrate) cannot be responsible for the changes in cell behavior. However, such adaptive behaviors are clearly a direct response to changes in oxygen concentration, implying that oxygen must be involved in affecting behavior by some other oxygen-sensitive pathways. Thus, it is clear that beyond simply serving as a nutrient, oxygen must also play a role in cell signaling events. This role, and the mechanisms by which it is facilitated, will be discussed in the following section.

## **1.2 Oxygen's Role in Cell Signaling**

The ability of cells to react/adapt to low oxygen tension implies the existence of cellular mechanisms for sensing oxygen and subsequently transmitting signals to alter cell behavior. One of the earliest examples of such signaling to be discovered was the ability of low  $pO_2$  to alter the ionic conductance of cells within the carotid body in the

carotid artery, triggering electrical signaling of the central nervous system to affect breathing and arterial tone [43 López-Barneo 1988]. Another such oxygen-sensitive response is the upregulation of erythropoietin (EPO), the hormone responsible for red blood cell maturation, in oxygen deficient kidney and liver cells, also investigated in the mid eighties [44 Bondurant 1986],[45 Schuster 1989]. Following these observations, the subsequent, pervading assumption held that oxygen sensing in the body was accomplished primarily by such variously-distributed, specialized cells. However, work in the early 1990's by the Semenza group uncovered a universal oxygen-sensing/signaling mechanism common to all nucleated cells in humans and well conserved in most vertebrates. This mechanism was determined to be the primary means by which all cells regulate oxygen homeostasis, adapting energy consumption to oxygen supply and avoiding excessive ROS formation. Furthermore, continued research over the ensuing two decades has slowly revealed how low oxygen tension and the cellular behaviors that it drives are an ordinary and indispensable part of many cell functions and of normal organismal development. As tissue engineering and regenerative medicine perspectives take an increasingly prominent position in the advancement of medical therapies, it will be essential to consider oxygen's role not only as a nutrient but as a potent signaling molecule, influencing a myriad of cell behaviors.

### 1.2.1 Hypoxia Inducible Factors: The Master Regulators of Response to Hypoxia

Hypoxia-inducible factor-1 (HIF-1), first identified by Semenza and Wang in 1992 [46 Semenza 1992], is an oxygen-regulated transcription factor, commonly referred to as the master regulator of hypoxia. Since its discovery, two other HIF-family proteins,

HIF-2 and HIF-3, have been identified. Beyond simply helping cells cope with reduced oxygenation, HIF proteins have been found to drive important cell behaviors involved in embryonic development, cell commitment and maturation, and healing, as well as pathologies such as cancer. As HIF-proteins appear to regulate the majority of observable changes in cell behavior in response to reduced oxygen tension, the presence of cellular HIF activity has the potential to be more instructive regarding cell behavior than measuring local oxygen concentration.

### 1.2.2 HIFs: Discovery

The observation of oxygen conformance in mitochondria suggested a widespread mechanism of oxygen sensing common to all cells [28 Hochachka 1996]. Using DNase I protection assays to examine the mechanism of EPO responsiveness to oxygen in human hepatoma cells, Semenza et al. first identified a 256-base-pair region in the EPO gene that bound at least two anemia-induced nuclear factors and which conferred hypoxia inducibility when transiently expressed in other genes [47 Semenza 1991]. Further examination of this region delineated the essential 50-nucleotide enhancer sequence, which was termed the hypoxia responsive element (HRE) and identified a nuclear factor, HIF-1 $\alpha$ , which exhibited hypoxia-inducible binding to the HRE [46 Semenza 1992]. In the hepatoma cells, presence of a functional HRE resulted in a seven-fold increase in EPO production in response to hypoxia (1% O<sub>2</sub>).

Maxwell et al. soon showed that the HRE elicited hypoxia-responsive transcription in a number of other cell types as well [48 Maxwell 1993]. Human fetal lung fibroblasts, human skin fibroblasts, human monocyte/macrophage cells, monkey

renal fibroblasts, pig retinal epithelial cells, rat aortic endothelial cells, Chinese hamster lung fibroblasts, Chinese hamster ovary cells, mouse renal adenocarcinomas, and mouse erythroleukemias were transiently transfected with a plasmid containing the HRE enhancer fused to a broadly active promoter and the  $\alpha_1$ -globin gene as a reporter. In 1% oxygen, 11 of the 12 tested lines demonstrated a 3- to 11- fold induction of  $\alpha_1$ -globin production, similar to the original observations in hepatomas [48 Maxwell 1993]. This implied that the same hypoxia-responsive nuclear factor responsible for HRE binding and EPO upregulation in hepatomas must be present in a range of cell types and may represent a widespread mechanism for response to hypoxia. Indeed, Wang and Semenza observed that a number of mammalian cell types which did not express the EPO gene still exhibited binding of HIF-1 to DNA and that the binding site was the same conserved HRE sequence [49 Wang 1993a]. Weiner et al. later demonstrated HIF-1 expression in every mammalian tissue they tested: brain, kidney, liver, heart, placenta, pancreas, and skeletal muscle tissue in mice, rats, and humans [50 Weiner 1996]. Subsequent investigation has found that HIF-1 and its oxygen-sensitive regulator mechanism are conserved in all aquatic and terrestrial vertebrates [51 Rytönen 2011].

### 1.2.3 HIFs: Structure

HIF-family proteins are heterodimeric transcription factors comprising a constitutively-expressed and stable  $\beta$  subunit and one of three constitutively-expressed  $\alpha$  subunits, subject to post-transcriptional, oxygen-dependent regulation. The  $\beta$  subunit is also known as the aryl hydrocarbon receptor nuclear translocator (ARNT). The  $\alpha$  subunits are termed HIF-1 $\alpha$ , HIF-2 $\alpha$ , and HIF-3 $\alpha$ , with HIF-1 $\alpha$  being the most prominent

and most well-studied (though the importance of non-redundant activities regulated by HIF-2 $\alpha$  is becoming more well-elucidated).

Both  $\alpha$  and  $\beta$  subunits have been identified as members of the basic Helix-Loop-Helix PER-ARNT-SIM (bHLH-PAS) family of transcription factors [52 Wang 1995]. Kewley et al. review the biology of this family of proteins [53 Kewley 2004]. bHLH-PAS transcription factors are often signal-regulated and bind to non-traditional variants of the classic E-box enhancer. In the case of HIF heterodimers, the specific recognition sequence is the HRE found in the promoter region of target genes. The conserved portion of this recognition sequence is 5'-(A/G)CGTG-3' [54 Semenza 1996]. The PAS domain is named for three proteins in which the domain was originally identified: Period Circadian Protein (PER), ARNT, and Single-Minded Protein (SIM). Signals mediated by PAS domains in various organisms include redox state, xenobiotic metabolism, light detection, and oxygen balance [55 Taylor 1999].

Members of the bHLH-PAS family must dimerize to become functional and are defined by two major domains: 1) a bHLH domain near the N-terminus, termed the N-terminal transactivation domain (NTAD), responsible for nonspecific dimerization [56 Murre 1989],[57 Reisz-Porszasz 1994],[58 Ema 1996],[59 Jiang 1996a],[60 Kobayashi 1997], with the basic region being the site of DNA binding [61 Ferré-D'Amaré]; and 2) a PAS homology domain which establishes dimerization partner specificity and target gene specificity [55 Taylor 1999],[62 Pongratz 1998],[63 Crews 1999]. In addition, HIF- $\alpha$  subunits contain an oxygen-dependent degradation domain (ODD), while HIF-1 $\alpha$  and HIF-2 $\alpha$  contain a C-terminal transactivation domain (CTAD) which interacts with

transcriptional co-activators to help initiate transcription [64 Jiang 1997],[65 Huang 1998],[66 Ema 1999],[67 O'Rourke 1999],[68 Maynard 2003]. While HIF- $\beta$  is known to interact with a number of other bHLH-PAS proteins, HIF-1 $\alpha$  dimerizes almost exclusively with HIF- $\beta$ . In humans, HIF-1 $\alpha$  is encoded by the HIF1A gene, HIF-2 $\alpha$  is encoded by the endothelial PAS domain protein 1 (EPAS1) gene, and HIF-3 $\alpha$  is expressed as multiple splice variants of the HIF3A gene [52 Wang 1995], [68 Maynard 2003],[69 Makino 2002].

#### 1.2.4 HIFs: Transcriptional Activity

HIF- $\alpha$  is constitutively produced in the cytoplasm where it is rapidly degraded in the presence of oxygen. When oxygen concentrations drop and HIF- $\alpha$  levels rise, the protein is translocated to the nucleus where it is free to dimerize with HIF- $\beta$  [70 Chilov 1999]. Translocation may be partially dependent upon mitochondrial succinate [71 Brière 2005]. In the nucleus, the HIF heterodimer binds to HRE sequences in target genes and recruits the CREB-binding protein/p300 (CBP/p300) transcriptional coactivator complex to initiate transcription [66 Ema 1999],[72 Arany 1996],. Both HIF stability and the ability of HIF dimers to interact with the CBP/p300 complex are regulated in an oxygen-dependent manner.

#### 1.2.5 HIFs: Regulation

Following its discovery, it was known that HIF-1 $\alpha$  was regulated by oxygen but was not itself responsible for oxygen sensing. Due to their direct chemical interactions with molecular oxygen, COX and heme proteins were first suggested as likely oxygen-sensing candidates [28 Hochachka 1996]. (It was later shown that HIF- $\alpha$  can be

stabilized even in the absence of functional ETC machinery, including COX [73 Brunelle 2005].) In 2001, however, it was discovered that a member of the conserved family of prolyl-4-hydroxylases (PHDs) [74 Epstein 2001],[75 Bruick 2001], specifically prolyl 4-hydroxylase 2 (P4H2) [76 Berra 2003], was the cellular oxygen sensor and regulator of oxygen-dependent degradation of HIF- $\alpha$ . Since then, several other mechanisms of HIF regulation, either directly or indirectly dependent on oxygen, have been identified or suggested.

#### 1.2.5.1 Regulation of HIF- $\alpha$ Protein Stability

Activation of HIF-1 is oxygen-dependent and is regulated by stability of the HIF-1 $\alpha$  protein subunit. Both HIF-1 $\alpha$  and HIF-1 $\beta$  messenger ribonucleic acids (mRNAs) are constitutively expressed intracellularly, but HIF-1 $\alpha$  protein levels are nearly undetectable in normoxic cells, even when HIF-1 $\alpha$  is overexpressed. In hypoxic cells, high levels HIF-1 $\alpha$  are observed, but HIF-1 $\beta$  levels are unaffected. Both intracellular levels of HIF-1 $\alpha$  and DNA binding of HIF-1 rapidly decrease upon re-introduction to normoxia [77 Huang, 1996].

Examination of HIF-1 $\alpha$  by Ratcliffe et al. revealed a region of the protein between amino acids 530 and 652, the ODD, which conferred oxygen-dependent repression when transferred to a reporter gene system [78 Ratcliffe 1998]. They suggested that the mechanism of regulation may be mediated by proteolytic degradation. It was later found that P4H2 was responsible for hydroxylating HIF-1 $\alpha$  within this region [76 Berra 2003]. Specifically, it was shown that P4H2 hydroxylates two key proline residues, proline 564 [79 Ivan 2001] and proline 402 [80 Masson 2001],

in the ODD which allows for its recognition by the E3-ubiquitin ligase complex. Activity of the HIF PHD family of enzymes is dependent on  $\text{Fe}^{2+}$ ,  $\alpha$ -ketoglutarate (2-oxoglutarate), and ascorbic acid as co-factors and  $\text{O}_2$  as a cosubstrate. In the case of HIF-1 $\alpha$ , P4H2 catalyzes a dioxygenase reaction in which one oxygen atom is inserted into the proline residue and the other is inserted into  $\alpha$ -ketoglutarate to form succinate and  $\text{CO}_2$  [81 Schofield 2004]. Thus P4H2 serves as the global, cellular oxygen sensor. In the presence of oxygen, P4H2 mRNA is upregulated [74 Epstein 2001] and the hydroxylation reaction with HIF-1 $\alpha$  proceeds. When oxygen is limited, the reaction does not take place and HIF1 $\alpha$  is not hydroxylated. In addition, the protein, OS-9 can interact with both HIF-1 $\alpha$  and P4H2 to promote degradation [82 Baek 2005]. The requirement of  $\text{Fe}^{2+}$  as a cofactor explains the ability of iron chelating agents, such as cobalt chloride and desferoxamine, to induce a hypoxic response in cells.

Hydroxylated HIF-1 $\alpha$  is recognized by the von Hippel-Lindau tumor suppressor protein (pVHL), the  $\beta$ -domain of which interacts with the hydroxylated moieties in the HIF-1 $\alpha$  ODD. The  $\alpha$ -domain of pVHL then recruits elongin B, elongin C, cullin-2, and ring-box 1 to form a complex which covalently links a chain of ubiquitin moieties to the ODD. Polyubiquitinated HIF-1 $\alpha$  docks with the 26S proteasomal complex which selectively degrades ubiquitinated proteins [83 Maxwell 1999],[84 Ohh 2000]. The protein, SSAT2, helps to stabilize the interaction of pVHL with elongin C thus facilitating ubiquitination of HIF-1 $\alpha$ . [85 Baek 2007]. Degradation by this pathway is rapid; cytoplasmic HIF-1 $\alpha$  is nearly undetectable under normoxic conditions, and the half-life of stabilized HIF-1 $\alpha$  is approximately 5 minutes upon cellular reoxygenation.

The canonical pathway of HIF protein regulation, then, is as follows: In the presence of oxygen, P4H2 hydroxylates HIF-1 $\alpha$ , which can then be recognized by pVHL and quickly degraded by the E3-ubiquitin ligase complex. In the absence of oxygen, hydroxylation of HIF-1 $\alpha$  does not occur and intracellular levels of the molecule increase.

#### 1.2.5.2 Regulation of HIF- $\alpha$ Transcriptional Activity

The transcriptional activity of HIFs can also be regulated in an oxygen dependent manner. HIF- $\alpha$  contains a nuclear localization signal in its CTAD, allowing stable HIF- $\alpha$  to rapidly bind to nuclear pore proteins and translocate into the nucleus [86 Kallio 1998]. Once there, it is free to pair with HIF- $\beta$  to form a functional HIF dimer. Ema et al. found that the CTAD of HIF- $\alpha$  in the nucleus interacts with CBP/p300 to initiate transcription of target genes [66 Ema 1999]. A key asparagine residue in this region (asparagine-803 in HIF-1 $\alpha$  and asparagine-851 in HIF-2 $\alpha$ ) can be hydroxylated by another hydroxylase-domain protein, termed factor inhibiting HIF (FIH), in the presence of oxygen [87 Lando 2002a]. The modification sterically inhibits HIF- $\alpha$  from interacting with CBP/p300, necessary components of the transcription machinery [88 Lando 2002b]. P4H2 has a  $K_m$  for oxygen that is approximately 3 times greater than FIH; therefore, in moderately reduced oxygen conditions in which HIF- $\alpha$  is beginning to be stabilized due to declining P4H2 activity, FIH can still repress HIF activity by inhibiting DNA binding [89 Koivunen 2004].

As both major mechanisms for regulating HIF activity are hydroxylase-dependent, it is clear that hydroxylases are central to cellular hypoxic responses. It is not surprising then that, like HIF proteins themselves, the HIF regulatory hydroxylases also appear to

be highly conserved in vertebrates. Figure 1.3 summarizes how hydroxylase-domain proteins act in regulating HIF.

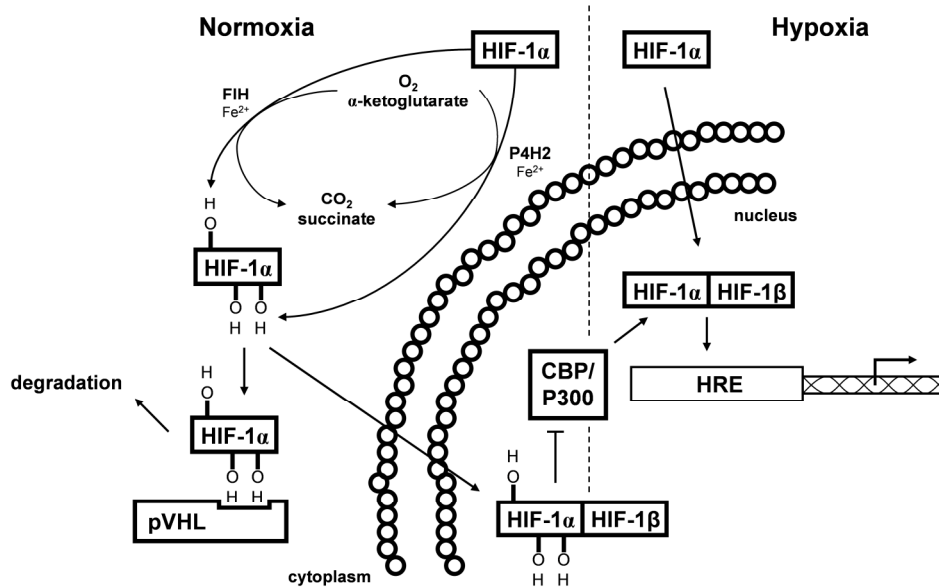


Figure 1.3 Oxygen-dependent mechanisms of HIF regulation. In normoxia, HIF-1 $\alpha$  is constitutively expressed but protein levels are kept low by rapid ubiquitination and proteosomal degradation. Activity of any non-degraded HIF-1 $\alpha$  is suppressed by the failure of the p300 co-activator to bind. In hypoxic conditions, oxygen dependency of both hydroxylases, P4H2 and FIH, prevents HIF-1 $\alpha$  modification, inhibiting degradation and allowing for dimerization and binding of co-activators.

### 1.2.5.3 Additional Factors in HIF regulation

Though there seems to be limited redundancy in HIF regulation, several factors other than PHDs can influence HIF activity in both oxygen-sensitive and oxygen-independent manners. Specifically, agents which have the ability to affect HIF mRNA stability, PHD catalytic activity, pVHL affinity/polyubiquitination, and complexing of HIF/BCP/p300/HRE can modulate HIF activity. Several miRNAs and mRNA-destabilizing proteins have been shown to interfere with HIF- $\alpha$  mRNA stability [90 Taguchi 2008],[91

Bruning 2011],[92 Chamboredon 2011]. It has also recently been shown that the protein RACK-1 can bind to HIF- $\alpha$  and elongin C to recruit an E3 ubiquitin protein-ligase complex in lieu of pVHL [93 Liu 2007]. This process is not dependent upon oxygen. ROSs also appear to play a role in HIF regulation, presumably by oxidizing hydroxylase-bound Fe<sup>2+</sup> and abrogating its ability to serve as a cofactor in hydroxylating reactions [94 Pan 2007]. SIRT-3 was shown to help destabilize HIF- $\alpha$  by inhibiting ROS production [95 Finley 2001]. It is interesting to note that ROSs contribute to stabilizing HIF, as one of the major behaviors regulated by HIF is oxygen conformance of the mitochondria. Reducing oxidative phosphorylation in conditions of low oxygen presumably help limit excessive ROS production which would lead to cell damage. It is not surprising to find, then, that several metabolic intermediates of the citric acid cycle have also been reported to inhibit hydroxylase activity, including citrate, isocitrate, malate, oxaloacetate, pyruvate, succinate, and fumarate, [96 Kaelin 2008]. Luo et al. also found that pyruvate kinase isoform M2 (PKM2), the enzyme that catalyses the final step in glycolysis, can function as a coactivator of HIF- $\alpha$  [97 Luo 2011]. PKM2 can associate directly with HIF-1/2 $\alpha$  and p300 to enhance their binding to HREs. Additionally, the mammalian target of rapamycin (mTOR) protein has been shown to enhance HIF activity, and this enhancement could be inhibited by rapamycin [98 Semenza 2003],[99 Land 2007]. Finally, very recent studies have suggested that epigenetics are involved in the regulation of HIF, with DNA and histone modifications altering accessibility and transcribability of HIF target genes [100 Tanimoto 2010],[101 Mimura 2011],[102 Xu 2012],[103 Vanharanta 2013],[104 Nguyen 2012].

### 1.2.6 Gradation of HIF Response

The sensitivity of P4H2 to changes in oxygen concentration also imparts a graded responsiveness of HIF-1 to O<sub>2</sub>. Jiang et al. exposed HeLa cells to oxygen concentrations ranging from 0% to 20% and measured levels of both HIF-1 subunit proteins as well as HIF-1 DNA binding [105 Jiang 1996b]. As expected, the HIF-1 $\alpha$  subunit was dramatically responsive to oxygen concentration. Between 20% and 6% oxygen, HIF-1 $\alpha$  levels and DNA binding modestly increased as oxygen concentration decreased. However, below 6% oxygen both HIF-1 $\alpha$  and HIF-1 DNA binding increased exponentially to reach maximal values at 0.5% oxygen. Half-maximal responses were observed between 1.5 and 2% oxygen. Thus, the majority of HIF-1 activity takes place over a physiologically relevant range of oxygen (0 - 5%), with the largest response occurring at physiologically hypoxic levels (0.5 - 1.5%).

Bracken et al. tested the graded response of HIF-1 in a similar set of experiments with a variety cell lines: HEK293T, HeLa, COS-1, HepG2, CACO-2, and PC12 cells [106 Bracken 2006]. In every case, they also found an exponential increase in HIF-1 $\alpha$  protein levels as oxygen was decreased from 5% to <1%. However, though HIF-1 activity, as measured by reporter protein production, was also maximal below 1% oxygen, the response did not always match HIF-1 $\alpha$  protein levels. In addition to differences in maximal reporter protein production levels between cells types, they noted two categories of response. Some cells gradually increased reporter protein production as oxygen decreased from 10% to <1%. Others required an oxygen concentration of <2% before exhibiting a dramatic increase in reporter protein production, which much more

closely coincides with changes in HIF-1 $\alpha$  levels. This indicates that hypoxia is better defined by cellular response than by absolute oxygen concentration.

### 1.2.7 Kinetics of HIF Response

The rate of HIF degradation/stabilization is also important to the responsiveness of its activity. Traditional immunoprecipitation assays reveal a half-life for HIF- $\alpha$  of approximately 5-8 minutes in normoxic conditions [65 Huang 1998],[107 Jaakkola 2001],[108 Jeong 2002]. Using a firefly luciferase reporter protein fused to the HIF-1 $\alpha$  gene, Moroz et al. reported a half-life of 4-6 minutes for the factor [109 Moroz 2009]. However, though HIF- $\alpha$  is very unstable in normoxia, HIF- $\alpha$  mRNA is constitutively expressed and the protein is constantly produced. Additionally the  $K_m$  of P4H2 for O<sub>2</sub> is just above the concentration of O<sub>2</sub> in air. This high value ensures that even a small decrease in oxygen is likely to have a significant effect on P4H2 activity [110 Hirsila 2003]. Thus HIF-1 can be both a highly-sensitive and rapidly-responsive initiator of hypoxia response.

Wang and Semenza studied the kinetics of HIF-1 $\alpha$  protein stabilization and DNA binding in hepatoma cells exposed to 1% oxygen for 0-4 hours [111 Wang 1993b]. They found that HIF-1 activity was first detectable within 15 minutes, with 8% maximal activity at 30 minutes, 50% maximal activity between 1 and 2 hours, and maximal activity at 4 hours. After rapid re-exposure to 20% oxygen, HIF-1 activity was reduced to 34% within 5 minutes and was eliminated by 15 minutes. The group also showed that binding of stabilized HIF-1 to DNA occurred rapidly, with 77% binding within 1 minute

and 100% binding within 5 minutes. Likewise, DNA binding decay occurred with a  $t_{1/2}$  of 1 minute upon reoxygenation of the cells.

More recently, Jewell et al. used tonometers to rapidly equilibrate suspensions of HeLaS3 cells to various oxygen conditions and study the time-course of HIF-1 $\alpha$  accumulation and degradation [112 Jewell 2001]. Presence and DNA binding of nuclear HIF-1 $\alpha$  was detected within 2 minutes of hypoxic exposure, with nuclear HIF-1 $\alpha$  protein levels reaching a maximal value by 1 hour. Within 2 minutes of reoxygenation, DNA binding was reduced while nuclear HIF-1 $\alpha$  protein levels were reduced within 4-8 minutes and undetectable by 32 minutes. These studies point to the capability of both rapid onset and rapid cessation of hypoxic signaling by the HIF mechanism.

#### 1.2.8 Transcriptional Targets of HIFs

The primary role of HIF-mediated transcriptional regulation is to promote cell survival in acute hypoxia and cellular adaptation to prolonged hypoxia. As a rapid response to hypoxia, HIF mediates global changes in metabolism in order to reduce overall cellular ATP consumption. A traditional view of hypoxia held that lack of oxygen would inhibit oxidative phosphorylation, limiting the production of ATP which would be rapidly depleted if normal cell activities continued. As discussed, more detailed analyses suggest that oxidative phosphorylation is not limited under normal physiological hypoxia, but reduced oxygen concentrations affect its efficiency, resulting in higher levels of premature electron loss from the ETC and greater ROS formation. In order to avoid cellular ROS damage, HIF mediates the reduction of oxidative phosphorylation and the activation of glycolytic metabolism. However, because glycolytic metabolism cannot

sustain the level of ATP production achieved by oxidative phosphorylation, HIF also mediates cell-wide reduction of ATP-intensive activities to avoid depletion.

HIF additionally mediates cell behaviors which function to adapt a cell to prolonged hypoxia or to remediate the hypoxic state. For instance, HIF-induced upregulation of EPO helps to increase the number of oxygen-carrying red blood cells in the local vicinity. Such hypoxia-driven behavioral response are often observed during embryonic development, where the local microenvironmental oxygen concentration helps to inform cells about their relative bodily location and direct the behavioral sequences that are required for normal organismal growth. It is not surprising, then, to find that HIF functioning is mandatory to embryogenesis, with absence of HIF-1 function being embryonic lethal [113 Maltepe, 1997],[114 Iyer 1998],[115 Ryan 1998]. *Hif1a*<sup>-/-</sup> mice die at embryonic day 9 due to vascular and cardiac defect/deformity [114 Iyer 1998],[116 Melillo 1995].

Because of the number of processes that are linked to cell metabolism, and therefore at least indirectly dependent upon oxygen, HIF has the potential for enormous regulatory oversight in cells. To date, over 100 genes have been identified as direct targets of HIF-1/2 [117 Loboda 2010]. These genes are involved in any number of cell processes, including energy metabolism, transcriptional regulation, cell cycle and growth, viability and apoptosis, transport, signaling, migration, matrix and barrier function, paracrine activity, and differentiation [81 Schofield 2004],[118 Semenza 2000],[119 Ke 2006]. A list of well-known HIF targets are presented in Table 1.2. Furthermore, because HIFs govern transcription of a large number of other transcription

factors, the number of genes that are indirectly regulated by HIFs is much larger. In fact, by some estimates, as many as 5% of the genes in the human genome are HIF-regulated in hypoxic conditions [98 Semenza 2003]. In gene expression profiles performed in arterial endothelial cells, Manalo et al. found that the largest group of genes up-regulated by HIF-1 included transcription factors, with cytokines/growth factors, receptors, and other signaling proteins also displaying significant upregulation [120 Manalo 2005]. Genes downregulated in hypoxia are generally involved in cell growth and proliferation [120 Manalo 2005],[121 Goda 2003]. Using chromatin immunoprecipitation and comparing results to genome-wide transcript profiling, other groups likewise found a large number of genes to be up- and downregulated in hypoxia, but reported that only upregulated genes appeared to contain an HRE sequence in the promoter [122 Mole 2009],[123Schodel 2011]. This implies that direct transcriptional regulation by HIF is accomplished almost entirely by gene upregulation (in fact over 20% of genes upregulated in hypoxia were direct HIF targets [122 Mole 2009]), while down regulation is accomplished indirectly. Indeed, of 191 genes downregulated in hypoxia in five different cell types, Ortiz-Barahona et al. found none of them to be directly targeted by HIF in all five cell types [124 Ortiz-Barahona 2010].

Table 1.2 Direct transcriptional targets of HIF-1.

Function	Gene/Gene Product	Function	Gene/Gene Product	
<b>Glucose Metabolism</b>	Adenylate kinase 3	<b>Vasomotor Regulation</b>	Adrenomedullin	
	Aldolase A/C		Atrial natriuretic peptide	
	Carbonic anhydrase-9		Endothelial nitric-oxide synthase	
	Enolase-1		Endothelin-1	
	Glucose transporter-1/3		Heme oxygenase-1	
	Glyceraldehyde-3-phosphate dehydrogenase		Inducible nitric-oxide synthase	
	Hexokinase-1/2		Nitric oxide synthase 2	
	Lactate dehydroxygenase A		Tyrosine hydroxylase	
	6-Phosphofructo-2-kinase/fructose-2,6-bisphosphate-3		$\alpha_{1B}$ -adrenergic receptor	
	Phosphofructokinase L		<b>Erythropoiesis and Iron Metabolism</b>	Ceruloplasmin
Phosphoglycerate kinase-1	Erythropoietin			
Pyruvate kinase M	Multidrug-resistance P-glycoprotein			
<b>Survival, Growth, and Apoptosis</b>	Bcl-2/adenovirus E1B 19kD-interacting protein-3	Transferrin		
	Calcitonin-receptor-like receptor	Transferrin receptor		
	Endoglin	<b>Matrix Function/ Metabolism</b>	Collagen prolyl hydroxylase	
	Insulin-like growth factor-2		Ecto-5'-nucleotidase	
	Insulin-like growth-factor-binding protein-1/3		Intestinal trefoil factor	
	Nip3-like protein X		Matrix metalloproteinases	
	p21		Procollagen prolyl hydroxylase- $\alpha$ 1	
	Transforming growth factor- $\alpha$	<b>Cell Migration</b>	Chemokine receptor CXCR4	
	Wilms' tumour suppressor		c-Met	
	$\alpha$ -Fetoprotein		<b>Transcriptional Regulation</b>	DEC1
<b>Angiogenesis</b>	Endothelial-gland-derived vascular endothelial growth factor			DEC2
	Leptin			ETS1
	Plasminogen-activator inhibitor-1	p35srj		
	Transforming growth factor- $\beta$ 3			
	Vascular endothelial growth factor A			
Vascular-endothelial-growth-factor receptor-1				

Compiled from references in **81** Schofield 2004, **118** Semenza 2000, and **119** Ke 2006.

### 1.2.9 Cell Type Variation in HIF Responses

HIF-mediated responses to hypoxia also display heterogeneity between cell types [125 Stroka 2001],[126 Chi 2006],[127 Gardener 2008],[128 Brachen 2006],[129 Lendahl 2009]. Benita et al. examined hypoxia-responsive genes in 7 different cell types and found wide variability in HIF activity [130 Benita 2009]. Monocytes displayed 486 genes that were differentially expressed in hypoxia while HeLa cells displayed 2119 such genes. Of these genes, 159 and 555, respectively, displayed an HRE sequence in the promoter region. Furthermore, only 17 genes responded to hypoxia in all of the studied cell types. The group concluded that a small subset of HIF direct-target genes, generally involved in the shift from oxidative to glycolytic metabolism and cessation of cellular growth/proliferation, represent the “core” HIF response to hypoxia. Genes that displayed variable responsiveness to hypoxia between cell types were less likely to contain an HRE sequence, suggesting that cell-type variation in gene expression is controlled indirectly by HIF.

Secondary factors that are involved in HIF indirectly-regulated pathways are often affected by a cell’s phenotype and current physiologic context. This helps to explain how cellular responses to hypoxia can vary despite similar levels of HIF mRNA expression in most hypoxic cells. For instance, while most cells undergo inhibition of proliferation in hypoxic conditions, vascular endothelial cells are often triggered to divide and migrate under hypoxia as part of the angiogenic response. Likewise, Bcl2/adenovirus E1B 19 kDa protein-interacting protein 3 (BNIP3) and p53 contribute to HIF-regulated apoptotic cell death, while B-cell lymphoma 2 (Bcl-2) family proteins can

promote HIF-regulated cell survival in hypoxia [127 Gardener 2008]. Because cellular activity can impact the effect of HIF-signaling, it is reasonable to predict that cells whose primary functions involve energy-intensive activities will be more negatively impacted by hypoxia, while cells with low energy requirements should be tolerant of hypoxia. Indeed, this appears to be the case: neurons, pancreatic  $\beta$ -cells, and cardiomyocytes are all highly oxygen dependent, with their primary functions (de/re-polarization, muscle contraction, and insulin secretion, respectively) being severely diminished in hypoxic conditions. Alternatively, articular chondrocytes have very low metabolic requirements and tolerate prolonged hypoxic exposure for the majority of their mature life cycle.

Of recent interest has been how the various HIF isoforms contribute to differential hypoxic responses in different cell types. While HIF-1 is expressed in all metazoan cells, HIF-2 is restricted to specific cell types in vertebrates [131 Semenza 2011a]. Furthermore while HIF-1 and HIF-2 exhibit some of the same target genes, they can also mediate regulation of different cell functions without overlap. This means that because both HIFs recognize the same HRE sequence in target genes, HRE and PHD binding affinity for HIF-1 versus HIF-2 can influence which responsive cell behaviors are elicited in hypoxia [132 Kenneth 2008]. While HIF-1 globally regulates genes involved in glycolytic metabolism and complex patterns of genes affecting cell survival versus apoptosis decisions, HIF-2 is only expressed in certain cells of the kidney, liver, pancreas, lung, heart, intestine, and epithelium and does not contribute to affecting glycolysis [117 Loboda 2010],[133 Hu 2003]. HIF-2 is prominently expressed in the vascular endothelium during embryonic development and may contribute to maintenance of

normal vascular architecture. It has also been shown to be the primary HIF isoform mediating transcriptional regulation of octamer-binding transcription factor 4 (Oct4), which is crucial to stem cell self-renewal, and transforming growth factor  $\beta$  (TGF- $\beta$ ) [134 Raval 2005],[135 Covello 2006]. HIF-3 acts as an antagonist to HIF-1 and HIF-2 by forming a functionally inactive dimer with HIF- $\beta$  [136 Makino 2001]. Elucidating the different expression profiles, activities, and roles of the HIF isoforms in different cells/tissues remains an active area of cellular research [128 Brachen 2006].

#### 1.2.10 HIF: Implications for Identifying Hypoxia

Given the broad array of cellular behaviors that HIFs can mediate, and knowing that physiological hypoxia is a normal and often required condition in organismal growth, development, and activity, it is clear that identification of hypoxic status is of import to biomedical research. However, identifying hypoxia, especially on the cellular level, is tricky. Krohn et al. adroitly explain:

*“Hypoxia is therefore a phenomenologic concept. There is no specific value of O<sub>2</sub>Hb [oxyhemoglobin] concentration, % Hb saturation by oximetry, or tissue partial pressure, PO<sub>2</sub> measured with electrodes, that results in a transition from normoxia to hypoxia... The biologic consequences of hypoxia depend on duration and the needs of individual cells...”* [137 Krohn 2008]

Hypoxia, therefore, may be best defined in terms cell behavioral responses. The following section offers a discussion of current techniques for detecting hypoxia at the tissue and cellular levels, highlighting advantages and disadvantages of each, and

proposes that a fluorescent HIF reporter system is particularly well suited for identifying hypoxia in 3D tissue cultures and engineered tissue constructs *in vitro*.

#### 1.2.10.1 Current Methods for Detecting Hypoxia

Current strategies for identifying hypoxia are typically aimed at either tissue- or cell-level detection. At the tissue level, evaluation usually consists of measuring or analyzing some biomolecule present in the blood or interstitial fluid that is differentially affected in hypoxic conditions. At the cell level, stains or markers are often used to detect intracellular changes indicative of hypoxia. Hypoxia detection strategies can also be categorized by whether they measure environmental conditions (oxygen concentration) or biochemical conditions (behavioral changes).

##### 1.2.10.1.1 Indirect Measures of Hypoxia

Many indirect techniques for imaging hypoxia at the tissue level have come from cancer research, where hypoxia in tumors has been found to be associated with poor outcomes. Magnetic resonance imaging (MRI) can be used to distinguish between oxygenated hemoglobin and deoxyhemoglobin, giving an indication of local oxygen availability in the vasculature of a given tissue [138 Kim 2005],[139 Leontiev 2007]. While this technique can be used to assess temporal changes in relative tissue oxygenation, it is not capable of providing quantitative information. MRI can also be used to measure increases in tissue lactate, which builds up as a result of increased glycolytic metabolism. Both of these approaches measure downstream consequences of hypoxia, which can exhibit some lag and also persist for a time even after normoxia

has been restored. MRI can also be used to measure  $pO_2$  directly, using an oxygen-sensitive reporter perfluorocarbon injected into the site of interest [140 Mason 1993],[141 Zhao 2004]. This technique is dependent upon adequate perfluorocarbon perfusion of the study tissue. However, for routine *in vitro* studies, use of MRI is impractical. Furthermore, these techniques focus on identifying hypoxia on a tissue-wide scale and may not have the resolution to identify hypoxia on the cellular level.

Various oxygen probes are also used to detect hypoxia. Microelectrodes can precisely measure the local oxygen concentration down to a very small scale, and may offer quantitative information about the oxygen conditions at a specific location, even at the cellular level [142 Vaupel 1991],[143 Collingridge 1999],[144 Kim 2003],[145 Mason 2003]. However, they require  $O_2$  for detection, meaning that as oxygen concentrations become very small, readings become less reliable. Fluorescent needle type oxygen probes contain a fluorophore which is quenched in the presence of oxygen, eliminating the variability of readings at low oxygen levels [146 Jorge 2006]. However, oxygen probes of any kind provide only very local information about oxygen concentration and require a large number of evaluations to obtain meaningful spatial information about oxygen distribution. Furthermore, any such probe requires placement in the tissue, leading to damage and inflammatory responses that can alter local tissue oxygen levels.

Nitroimidazoles represent a more direct method for identifying hypoxia. Nitroimidazoles can act as oxygen mimetics, accepting terminal electrons from the ETC. Their affinity for electrons is less than  $O_2$ , so that under normal oxygen conditions only low levels of nitroimidazoles are reduced. These molecules are only singly reduced and

can still be easily oxidized by O<sub>2</sub>. However, under hypoxic conditions, without competition from oxygen, nitroimidazoles become doubly reduced, forming alkylating agents that react indiscriminately with cellular macromolecules, thus trapping nitroimidazole within the cell [137 Krohn 2008]. For tissue-wide analysis, the nitroimidazole can be radiolabeled for positron emission tomography (PET) [147 Adamsen 2005]. Antibodies to the nitroimidazole, pimonidazole (commonly available as Hypoxyprobe-1), have also been prepared. This allows for immunohistochemical staining and analysis of samples for the identification of hypoxia down to the cellular level [148 Varia 1998],[149 Olive 2000],[150 Nordmark 2003]. A primary disadvantage of histological analyses is that they require the sacrifice of the tissue/construct under study. Therefore, it is not possible to monitor the hypoxic status of the sample over time or in response to changing conditions.

Another approach is to predict the occurrence of hypoxia by computational modeling [151 Gross 2007],[152 Cheema 2008],[153 Buchwald 2009]. Models provide the ability to draw predictive conclusions about expected oxygen concentrations and gradients without the need for cell culture. However, while modeling is a powerful tool, results are only as powerful as the assumptions on which the model is based, which in turn are guided by current knowledge of the system being modeled. Therefore, an incomplete understanding of cellular processes can lead to models which do not accurately recapitulate observed phenomena.

The methods represent indirect approaches to detecting hypoxia. In these techniques, indicators of hypoxia are evaluated but the immediate effector of response

to hypoxia, HIF, is not. Alternatively, direct HIF detection may be a better determinant of hypoxia within a cell as it is the mediator which transitions a cell's status from "normal" to "hypoxic".

#### 1.2.10.1.2 Direct Measures of Hypoxia: HIF Detection

Direct detection of HIF is perhaps a more telling indicator of whether or not a cell is experiencing hypoxic stress than measurements of oxygen or detection of metabolites involved in secondary hypoxia responses. HIF-1 stability is highly sensitive to oxygen concentration with a graded and rapid response to hypoxia. Thus, intracellular levels of HIF-1 both directly correspond to a cell's immediate state of oxygenation and are predictive of imminent biochemical cellular responses that occur as HIF activity affects transcription. Real-time polymerase chain reaction (RT-PCR) can be performed to quantify changes in HIF- $\alpha$  mRNA levels; however, as HIF- $\alpha$  is constitutively expressed in most cells, this is not a good indication of transition of a cell to a hypoxic state. Alternatively, the HIF- $\alpha$  protein itself can be identified. This is commonly done by immunohistochemical/immunofluorescent staining, which can indicate HIF localization in a tissue, or by Western blotting which allows for quantification by densitometry. These methods directly measure a cell's hypoxic status. However, they do suffer from a number of drawbacks. First, the short half-life of HIF- $\alpha$  makes accurate capture and determination of protein levels difficult. Secondly, basal and elevated HIF- $\alpha$  levels can vary among cell types, meaning that specific concentrations of HIF- $\alpha$  do not always correspond directly to a consistent level of transcriptional changes in a cell. Most importantly, however, is that both immunostaining and Western blotting protocols

require the sacrifice of the tissue of interest. This means that repeated analysis of hypoxic status within the same sample cannot be performed. Thus by these methods, it is difficult to develop a temporal profile of the hypoxic response within a cell.

An alternative approach to HIF protein detection is the use of a reporter system. Several groups have detailed the use of an engineered vector containing repeats of the HRE enhancer and a minimal promoter to allow for hypoxia-induced expression of a fused gene. Given the appropriate reporter protein, this approach conveniently allows for the kinetics and magnitude of HIF-mediated effects on transcription to be observed. Furthermore, if the reporter protein is non-toxic to the cell and is easily detected, repeated observations of the same sample can be made.

The majority HIF reporter vectors detailed in the literature have been constructed as potential targeted gene-therapies for cancer treatment or diagnostic tools for the identification of hypoxia in tumors. Shibata et al. prepared a vector containing five HRE repeats from the human VEGF gene coupled to a minimal cytomegaloviral (CMV) promoter with luciferase as a reporter gene [154 Shibata 2000]. They reported a 500-fold increase in luciferase expression in response to hypoxia in transfected cells. This type of vector was suggested as a means to selectively express a therapeutic agent (in lieu of the luciferase reporter gene) in tumors which are generally hypoxic compared to normal tissues [154 Shibata 2000],[155 Payen 2001]. Indeed, a similar vector containing a suicide gene (herpes simplex virus thymidine kinase) under HRE control was used to induce tumor regression in mice [156 Koshikawa 2000]. Similarly, Harada et al. used a HRE-luciferase reporter system to observe changes in the

number of hypoxic cells within a tumor to evaluate the effectiveness of cancer drugs [157 Harada 2005].

The recent characterization and marketing of a number of genes whose products are stable fluorescent proteins has also allowed for the construction of imagable hypoxia reporter systems. Vordermark et al. reported the suitability of green fluorescent protein (GFP) as a reporter gene product for identifying HIF activity at oxygen concentrations as low as 0.02% [158 Vordermark 2001]. Serganova et al. transfected C6 glioma cells with an HRE-GFP reporter vector and observed green fluorescence, indicating HIF-mediated transcriptional activity, in tumor masses comprised of the cells [159 Serganova 2004]. They noted the particular usefulness of this approach for determining dynamics and spatial heterogeneity of HIF-1-specific transcriptional activity [159 Serganova 2004].

A fluorescent reporter of HIF activity appears to be a relevant and useful tool for determining whether or not a cell is hypoxic and investigating different microenvironmental conditions that can result in HIF-induced changes in cell behavior. Such a system identifies cellular hypoxia in terms of cell behavior and offers a good estimate of the expression of other direct HIF targets. The method also avoids a number of the problems inherent in other hypoxia detection techniques, such as the need to sacrifice the study sample. However, very little use of such a system outside of tumor hypoxia has been reported. As discussed, low oxygen conditions can be common in the human body and can be necessary to drive normal and appropriate biological processes. As researchers make increasing efforts to simulate *in vivo* conditions in their

*in vitro* studies, there is an apparent need to understand how environmental signals, like oxygen tension, in a cell's physiological environment contribute to affecting its function. Use of a fluorescent reporter system to identify HIF activity and correlate it to other relevant changes in cell behavior should begin to fulfill this need.

### **1.3 Regulating Hypoxia to Affect Cell Behaviors in Transplantation Therapies**

The loss or failure of tissues and organs due to damage and disease is one of the most prevalent and expensive problems encountered in medicine today [160 Laschke 2006]. Since it was officially defined by the National Science foundation in 1987, the field of tissue engineering has offered the promise of addressing this issue through development of functional replacement tissues that are transplanted into the recipient [161 Langer 1993]. With the subsequent discovery and utilization of embryonic and adult stem cells, tissue engineering has slowly become encompassed under the umbrella of “regenerative medicine”, which, as defined by Mason and Dunnill, “...replaces or regenerates human cells, tissues or organs to restore or establish normal function” [162 Mason 2008]. By this definition, any cell-transplantation therapy qualifies as regenerative medicine. Regenerative medicine combines the use of cells, materials, and bio-physical/chemical stimuli in a rational effort to produce functional tissues that are closely analogous to native tissues for the treatment of defects or disease. A key feature of regenerative medicine is the harnessing of innate properties and capabilities of cells that are difficult, if not impossible, to reproduce artificially. The cellular genome contains all of the inherent instructions required to run the myriad biological processes that together result in a living organism. Through evolution, these

have developed into a highly regulated and enormously complicated pattern of conserved and emergent cell behaviors that allow for survival and reciprocal interaction with the world. Tissue engineers, then, have the difficult task of applying, in an intelligent manner, what information has been learned about these preprogrammed cell functions in order to drive desired cell behaviors while restricting undesired ones in an effort to develop therapies for tissue restoration.

It has become increasingly noted that for cell transplantation and tissue engineering endeavors to succeed, the *in vitro* conditions in which tissue growth/fabrication takes place will need to closely mimic the native physiological environment. Differences between the conditions that cells encounter in culture and in the body can lead to discrepancies between *in vitro* and *in vivo* results. One of the most non-physiological conditions encountered by cells in routine cell culture is elevated exposure to oxygen. In atmospheric culture conditions, cells are exposed to nearly 21% O<sub>2</sub>, whereas oxygenation of a typical tissue in the body is much lower. Therefore, investigators using standard culture conditions may not observe the same responses from cells as might typically be seen *in vivo*. As more research is performed at physiornormal oxygen concentrations, it will be important to monitor the hypoxic status of cells in culture and observe the effects of reduced oxygen on cell behavior. Furthermore, tissue engineering is often concerned with the production of 3D tissues, which differ widely from the monolayers typical of standard culture. Because oxygen delivery occurs by diffusion from the media *in vitro*, oxygen gradients can easily form in 3D tissues, thus exposing cells to heterogeneous oxygen conditions. Because of this,

oxygen tension in many tissue engineered constructs may exert a significant, and potentially more complicated, effect on cell behavior than is typically considered.

A fluorescent hypoxia reporter system, described in the present work, provides a means for evaluating hypoxia and its effects in different cell systems. Though its role in signaling has become much better understood, “hypoxia” is still often viewed with a negative connotation, as it can lead to aberrant cell behavior and cell death. However, many beneficial behaviors, such as vascularization and wound healing, can also be triggered by hypoxia. Thus, hypoxia’s role in cell transplantation and tissue engineering is phenomenological and context dependent. In the present work, it is hypothesized that for different 3D tissue systems, tissue dimensions and external oxygen concentration (both controllable culture parameters *in vitro*) contribute to the hypoxic status experienced by cells within the culture, and can work to promote desirable, hypoxia-induced behaviors or, alternatively, to inhibit cell function (Figure 1.4). This dual nature of hypoxia in cell-based, tissue engineering therapies, as well as the versatility of a fluorescent HIF reporter for use in its study, is highlighted in two systems which were the subject of the present work: islet-like  $\beta$ -cell clusters, and ADSC spheroids. In  $\beta$ -cell clusters, beneficial cell behavior is achieved by avoiding hypoxia, while in ADSC spheroids, hypoxia promotes the desired behavior. The importance of these systems as transplantation therapies as well as the role of hypoxia in each is discussed in the following sections.

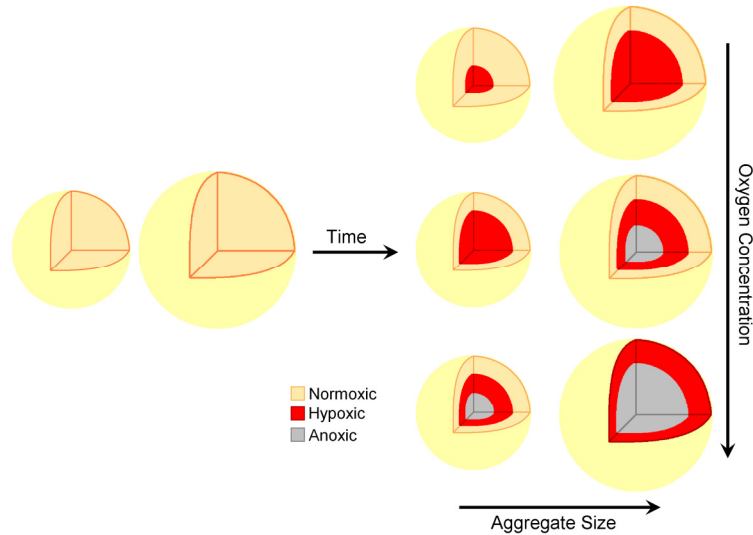


Figure 1.4 Schematic of development of hypoxia in 3D cultures. The extent of hypoxia within a cell aggregate should be affected by aggregate size and external oxygen concentration. To achieve the desired cell behavior, it may be possible to vary these parameters to optimize hypoxic status throughout the aggregate.

### 1.3.1 Encapsulated $\beta$ -cells as a Treatment for Type I Diabetes Mellitus

Type 1 diabetes mellitus (T1DM) is a chronic inflammatory disease of the pancreas resulting in the body's inability to produce insulin.  $\beta$ -cells, the cells responsible for insulin production and secretion, reside within specialized tissue clusters called the islets of Langerhans found within the pancreas. In T1DM, the  $\beta$ -cells are destroyed, presumably through a dysfunctional autoimmune process. Without the insulin produced by  $\beta$ -cells, the body tissues are unable to take in and utilize glucose, the primary energy product of metabolism and the body's main energy source. If untreated, T1DM is fatal.

There are currently several treatment options for T1DM, offering the potential to improve patient prognosis considerably. Exogenous insulin administration via injection

is the most prevalent such option. By constantly monitoring blood glucose levels and administering insulin when needed, diabetic patient quality of life and life expectancy can be much improved. However, besides the discomfort of repeated blood draw and hypodermic injection, this method also inadequately replicates what the body does naturally. In the body, islets are well perfused with blood and  $\beta$ -cells can continually monitor blood glucose levels and respond by secreting the appropriate amount of insulin. This continual monitor/secrete system is called responsive release, and it ensures that at any given moment the amount of insulin and glucose in the blood are appropriately balanced to achieve the correct physiological function. Exogenous supplementation of insulin, however, occurs in doses. Doses are administered periodically in amounts estimated to adequately process the glucose load of a meal over a given time period. Such periodic administration means that insulin concentration is not necessarily matched to glucose concentration at all times. Thus, exogenous insulin supplementation often fails to prevent the chronic, systemic complications of T1DM, such as retinopathy, glaucoma, neuropathy, and hypertension, over time.

In the normal physiological state, the body naturally secretes insulin in a responsive manner dependent upon blood glucose concentration at a given moment. It stands to reason, then, that an ideal method for treating T1DM would do the same. Because  $\beta$ -cells are specifically specialized to perform this task, transplantation of functional pancreatic tissue to replace compromised islets offers an appealing treatment approach. Transplantation was first attempted as a treatment for severe T1DM in 1966, with allotransplantation of a pancreas, duodenum, and kidney

concurrently [163 Kelly 1967]. This and other subsequent early attempts offered poor outcomes due to complications from the invasive surgery and the requirement of immunosuppressive drugs to prevent organ rejection. Later transplantation attempts made use of the fact that islets represent only a small percentage of the total pancreatic mass but are sufficient for remediating T1DM. Islets were isolated and purified from donor pancreata and transplanted into recipients, greatly reducing surgical invasiveness but still requiring a life-long immunosuppressant regimen to prevent rejection. Besides issues with long-term immunosuppressant drug use, transplantation procedures also suffer from donor limitations. The islets from as many as three donors are required to satisfy the needs of single recipient. Thus, although positive outcomes have been achieved by islet transplantation, methods to improve the procedure and overcome limited tissue supply continue to be explored.

Encapsulation has been considered as means of overcoming the main shortcomings of islet transplantation. Encapsulation separates the transplanted tissues from the cells of the immune system and offers two benefits. First, possibility of immune rejection is greatly reduced so that immunosuppressive drugs are not required. Secondly, the avoidance of an immune response makes utilization of xenotypic tissue sources a potential way to overcome limited donor supply. Lim and Sun first evaluated the potential of this technique by encapsulating rat islets in semipermeable, cross-linked alginate [164 Lim 1980]. They then examined viability and function of the islets *in vitro* and in chemically induced diabetic rats. They found that encapsulated islets exhibited glucose-stimulated insulin secretion (GSIS) similar to unencapsulated islets and could

restore normoglycemia in the mice for at least 20 days, compared to six day survival of mice receiving unencapsulated islets. More recent trials have shown xenotransplantation proof of concept, with alginate-encapsulated pig islets functioning to remediate hyperglycemia in diabetic monkeys [165 Dufrane 2006a] and dogs [166 Abalovich 2009] for several months without immune rejection. Elliott et al. even reported viability of alginate-encapsulated pig islets 9.5 years after transplantation into a human (function was lost after 14 months) [167 Elliott 2007], though a second group was unable to duplicate the result [168 Tuch 2009]. However, limited duration of viability/function of encapsulated islets has largely restricted the overall success of transplantation therapies. Capsule material and nutrient delivery (especially oxygen) are the two major parameters that appear to most affect encapsulated islet performance.

#### 1.3.1.1 Poly(Ethylene Glycol) as a Favorable Material for $\beta$ -Cell Encapsulation

A majority of current encapsulation trials utilize hydrogels as the semipermeable matrix which separates  $\beta$ -cells from immune cells. Hydrogels are appealing for their ability to hold many times their volume in water, which provides a large aqueous environment for the encapsulated cells. Though alginate-based gels are traditionally the most utilized, poly(ethylene glycol) (PEG) hydrogels represent a promising alternative. A shortcoming of alginates has been their propensity to become fibrotically overgrown if not adequately purified [169 Langlois 2009] and their batch-to-batch variability making comparisons between studies difficult. Recent direct comparisons have shown that, in these two respects, PEG yields superior performance [170 Liu 2010]. In addition to

being highly biocompatible, PEG is also easily functionalized and non-degrading when covalently crosslinked. PEG hydrogels have already been shown to support a number of cell types including chondrocytes [171 Bryant 2002],[172 Rice 2004], osteoblasts [173 Burdick 2002], valvular interstitial cells [174 Benton 2009], and mesenchymal stem cells [175 Nuttelman, 2004]. PEG network permeability, a function of mesh size, is also easily manipulated by varying macromer concentration and size in the photoactive solution [176 Cruise 1998]. Lin-Gibson et al. provided a method for photopolymerizing PEG dimethacrylates (PEGDM) that had been prepared by microwave methacrylation of PEG [177 Lin-Gibson 2004]. Using this method, Weber et al. showed that polymer mesh size was easily controlled by appropriate selection of initial macromer size [178 Weber 2008] and that such hydrogels were suitable for sustaining  $\beta$ -cells [179 Weber 2006]. Bryant et al. showed that neither the photoinitiator nor time of UV exposure used in the photopolymerization process was toxic to the cells [180 Bryant 2000].

#### 1.3.1.2 Hypoxia in Islet Encapsulation

Loss of function and/or viability is often observed in a significant percentage of cells following tissue isolation and encapsulation procedures. This has been especially noted of islets of Langerhans, transplanted as a treatment for T1DM [181 De Vos 1997],[182 Suzuki 1998],[183 De Vos 1999]. While a variety of factors have been investigated, hypoxia has increasingly been implicated as the primary cause for this observed device failure, with insulin secretion by the pancreatic  $\beta$ -cells being particularly sensitive to changes in oxygen concentration [184 Dionne 1989],[185 Dionne 1993],[186 de Groot 2003]. Low oxygen tension in explanted islets can be

directly attributed to their removal from the rich vasculature of the pancreas. Encapsulation exacerbates this problem in two ways: 1) by prohibiting islet revascularization and 2) by adding an additional barrier to oxygen transport. Outcomes in unencapsulated islet transplants have shown that diffusion of oxygen and nutrients to islets in well-perfused sites of the body prior to revascularization can be sufficient to maintain viability and function [187 Shapiro 2000],[188 Shapiro 2006]. A capsule, however, may hinder diffusion of oxygen to encapsulated tissues because of permeability limitations and increased diffusional distance [189 Schrezenmeir 1994]. However, besides material and geometric considerations of capsule design, a variety of factors such as islet size [190 Lehmann 2007],[191 Cavallari 2007], rate of oxygen consumption [192 Sweet 2002],[193 Wang 2005], and site of implantation [194 Dufrane 2006b] all play a part in determining how much oxygen may be available to any particular cell.

Oxygen insufficiency is known to inhibit  $\beta$ -cell function by decoupling glucose sensing from insulin exocytosis [195 Zehetner 2008],[196 Cantley 2009],[197 Puri 2009]. Studies characterizing how size, encapsulation material, and external oxygen conditions affect the hypoxic status of islets as well as how techniques such as re-aggregation and hypoxic preconditioning contribute to hypoxic tolerance (if at all) are obviously important to optimizing implant function. However, direct characterization of hypoxia, in terms of HIF activity, in  $\beta$ -cells is scarcely reported. In the present work, use of a fluorescent HIF reporter was shown to facilitate such investigations, allowing for the determination of temporal and spatial profiles of hypoxia in 3D, islet-like clusters and

observation of how cluster size and external oxygen concentration contribute to hypoxia-mediated effects on cell function.

### 1.3.2 ADSC Spheroids as a Cell-Based Method to Drive Angiogenesis

Despite its promise, tissue engineering has offered relatively few clinical successes to date [198 Griffith 2002],[199 Ikada 2006]. Lack of vascularity has consistently been cited as the largest obstacle to the development of clinically relevant engineered tissues over the past several years [160 Laschke 2006],[200 Rauwkema 2008],[201 Lovett 2009],[202 Santos 2010],[203 Novosel 2011],[204 Horch 2012],[205 Laschke 2012]. Most cells in the body reside within 100-200 $\mu$ m of a blood vessel, a distance which corresponds closely the theoretical limit of oxygen diffusion in a tissue [206 Folkman 1973],[207 Colton 1995]. For engineered tissues, which are avascular, this diffusional restraint limits the size of tissues that can be effectively transplanted. Following transplantation, local inflammation and healing processes at the implant site resulting from the surgical procedure can help to induce infiltration of host vessels into the implant. However, the rate of vessel progression is slow and interior cells of the implant often do not survive long enough to be vascularized. Several strategies for enhancing vascularization of engineered tissues have been described, including administration of pro-angiogenic growth factors, cell co-culture, and pre-vascularization. These strategies either attempt to promote angiogenesis, the sprouting of vascular branches from existing vasculature, or vasculogenesis, the *de novo* formation of microvessel networks from disorganized precursor cells.

Growth factors are known to be potent mediators of angiogenesis and vasculogenesis *in vivo*. VEGF is the most powerful stimulator of angiogenesis, often working in concert with basic fibroblast growth factor (bFGF) [208 Carmeliet 2011]. When triggered by these growth factors, endothelial cells in existing vessel walls secrete matrix metalloproteinases (MMPs), branch off from the vessel, and begin to migrate in the direction of the growth factor source. Endothelial cells directly behind these migrating cells begin to proliferate rapidly, extending a new capillary sprout toward the tissue of need. Subsequent vessel maturation is important to reducing capillary leakiness and preventing vessel regression. Platelet-derived growth factor (PDGF), TGF- $\beta$ , and angiopoietin 1 (Ang-1) are involved in vessel stabilization and maturation by reducing MMP secretion, stimulating matrix production, and recruiting supporting cells such as smooth muscle cells and pericytes [200 Raukema 2008],[209 Carmeliet 2000],[210 Hirschi 2002].

In regenerative medicine applications, administration of angiogenic factors can help to stimulate blood vessel growth and promote more rapid vascularization of tissue implants. For this purpose, recombinant VEGF is often applied. VEGF can be administered by direct injection; however, high dose requirements due to VEGF instability and negative systemic side-effects, including ectopic blood vessel development and excessive capillary leak, make this delivery technique unfavorable [160 Laschke 2006]. An alternative strategy has been to localize VEGF to the implant site by controlling its release from the implant itself, often a biomaterial scaffold that serves as the matrix component of an engineered tissue. Many demonstrations of

material-based constructs for VEGF delivery are reported in the literature, displaying a wide variety of release profiles and mechanisms [211 Zisch 2003],[212 Sokolsky-Papkov 2007],[213 Übersax 2009],[214 Fu 2010]. However, material-based delivery systems do face a number of hurdles. First, they require both a prior knowledge of the appropriate delivery dosage/duration and the ability to achieve this release profile from a material construct. Also, the maximal cumulative dose is predefined by the loading process during fabrication and cannot be augmented after implantation. Furthermore, few systems are capable of responding to cellular and other microenvironmental cues that would modulate delivery to match physiological need. Finally, the process of angiogenesis is driven by concurrent action of multiple factors each displaying different availability profiles which change over time; however, the appropriate relative profiles of many growth factors are not fully characterized in many cases, and most material-based growth factor delivery systems have difficulty incorporating and delivering multiple factors differentially.

#### 1.3.2.1 Cell-Based Delivery for Therapeutic Angiogenesis in Tissue Engineering

A more recent technique has been to use cells as a growth factor source, an approach termed cell-based delivery. In cell-based delivery, a particular cell type is chosen for incorporation into the engineered tissue to promote tissue angiogenesis, either natively or by some inducing stimulus. Cell-based delivery techniques are attractive, as researchers are able to take advantage of natural biological mechanisms that cells already possess. This approach offers three key benefits [200 Rauwkema 2008]. First, unlike most biomaterials, cells can participate in innate biological signaling

processes that regulate angiogenic factor secretion to maintain factor concentrations in the physiological range and adapt them to meet the requirements of different stages of vessel formation. Secondly, growth factors secreted from cells often interact with the extracellular matrix to form three dimensional microgradients which contribute to directing capillary arrangement [215 Helm 2005]. Finally, cells may have the capability to produce and secrete a variety of different angiogenic factors, in physiological profiles, that act together to direct several stages of vessel migration, stabilization, and maturation [205 Laschke 2012].

For cell-based delivery to be effective, a cell source must be chosen that is capable of producing the factors of interest and providing the appropriate signals within the implant microenvironment. The recently-characterized ADSCs represent a very promising cell population for the promotion of angiogenesis. ADSCs are readily isolated from lipoaspirates which can be collected through a minimally invasive procedure. The stem cell yield from adipose tissue is large, approximately 500 times greater than from bone marrow, where similar stromal cell populations were first identified [216 Mizuno 2009]. Ease of culture and rapid expansion make ADSCs ideal for autologous use. ADSCs have also been shown to be capable of secreting a number of factors of relevance to angiogenesis in regenerative medicine, including VEGF; bFGF; hepatocyte growth factor (HGF); basic nerve growth factor (bNGF); angiogenin; Ang-1; insulin-like growth factor 1 (IGF-1); interleukins (IL)-6, -7, -8, -11, and -17; monocyte chemoattractant protein (MCP)-1 and -2; granulocyte/monocyte-, granulocyte-, and macrophage colony stimulating factors (CSF); tumor necrosis factor  $\alpha$  (TNF- $\alpha$ ), and stromal cell-derived

factor 1 (SDF-1) [217 Kilroy 2007],[218 Hong 2010],[219 Rasmussen 2011]. Furthermore, ADSCs have shown the potential to differentiate into a variety of mature lineages of mesodermal and non-mesodermal origin, including adipogenic, chondrogenic, osteogenic, skeletal muscle, smooth muscle, cardiac muscle, epithelial, hepatocytic, pancreatic, and hematopoietic support cells [216 Mizuno 2009]. Of particular relevance are studies indicating that ADSCs can differentiate directly into endothelial precursor and endothelial cells [220 Planat-Benard 2004],[221 Miranville 2004],[222 Cao 2005],[223 Colazzo 2010],[224 Keerl 2010],[225 Shi 2012].

In recent years, ADSCs have been shown to contribute to improved tissue repair in dermal wounds [226 Kim, W.S. 2007],[227 Lu 2008],[228 Kim 2009],[229 Nambu 2009], mouse ischemic hindlimbs [221 Miranville 2004],[222 Cao 2005],[230 Nakagami 2005],[231 Moon 2006],[232 Kim, Y. 2007], and myocardial infarcts [233 Miyahara 2006],[234 Valina 2007],[235 Cai 2009],[236 Schenke-Layland 2009],[237 Wang 2009]. Usually, the cells are directly injected into the deficient tissue as a dispersion, or a seeded into a tissue scaffold for implantation. The restorative effects of ADSCs have mostly been attributed to their enhancement of angiogenesis, which appears to be accomplished through one or more of the following mechanisms. First, current evidence supports a primary paracrine activity of ADSCs, with secretion of pro-angiogenic and anti-apoptotic growth factors contributing to enhanced tissue survival and increased capillary density. (VEGF and IGF-1, for instance, have been shown to function in both roles [219 Rasmussen 2011].) ADSCs also secrete factors which can recruit circulating stem and endothelial precursor cells, as well as various support cells

such as fibroblasts and pericytes [238 Takahashi 1999],[239 Crosby 2000],[240 Ceradini 2005],[241 Nakao 2010]. In particular, SDF-1, appears to function in stem cell homing [242 Askari 2003],[243 Ceradini 2004]. Finally, as mentioned, ADSCs can differentiate into endothelial cells to directly integrate into developing vasculature. ADSCs also share many common characteristics with pericytes, cells which support the vascular endothelium and have been shown to contribute to superior angiogenesis and vessel stabilization when co-cultured with endothelial cells [244 Traktuev 2008],[245 Traktuev 2009]. Taken together, these properties suggest that ADSCs are capable of modulating the stem cell niche to create a local microenvironment that is highly primed to promote angiogenesis [246 Gimble 2007].

#### 1.3.2.2 Hypoxia and the Angiogenic Potential of ADSCs

In order to fully take advantage of the angiogenic potential of ADSCs for regenerative medicine, researchers will need to develop techniques to control and possibly amplify their pro-angiogenic behaviors. To this end, a better understanding of the stimuli that encourage these behaviors will be advantageous. In the body, ADSCs reside in a perivasacular niche with oxygen concentrations ranging from 2-8% O<sub>2</sub>, an environment that has been described as locally hypoxic [247 Matsumoto 2005],[248 Pasarica 2009],[249 Mohyeldin 2010]. This concentration encompasses the range over which HIFs are exponentially stabilized, suggesting that HIF activity plays an important part in regulating typical ADSC functions. Indeed, hypoxia appears to be one of the primary motivating factors promoting ADSC paracrine activity and affecting differential potential. Hypoxic culture of ADSCs has been reported to upregulate expression of

VEGF, bFGF, IGF-1, and HGF *in vitro* [219 Rasmussen 2011],[250 Rehman 2004],[251 Rosová 2008], [252 Lee 2009],[253 Liu 2013]. In particular, the VEGF gene is known to contain HRE repeats in its promoter region, making it a direct target of HIF-1 [254 Levy 1995],[255 Liu 1995],[256 Forsythe 1996]. In animal studies, hypoxic preconditioning of ADSCs resulted in superior survival, healing, and vascularity of ischemic skin flaps and myocardial infarcts in mice [257 Tang 2009],[258 Yue 2013]. Hypoxia has also been suggested to contribute to an increase in stem cell survival and to the secretion of pro-survival factors from stem cells [259 Chacko 2010]. However, despite the fact that the potent angiogenic properties of ADSCs are largely regulated by hypoxia over physiornormal oxygen tensions, relatively little work has focused on developing a better understanding of how cellular hypoxia is encountered by ADSC cultures. Furthermore, Abdollahi et al. have recently concluded that “...further study is needed to optimize the use of hypoxia as a stimulus for various stem cell functions, including its potential role in therapeutic angiogenesis” [260 Abdollahi 2011].

Realization that oxygen is one of the key regulators of stem cell function has a profound significance on how current cell-based and tissue engineering applications using ADSCs can be further improved [261 Zachar 2011]. While upregulation of angiogenic growth factors by genetic engineering has been shown to enhance the therapeutic outcomes with stem cells [262 Geiger 2007], hypoxia can be used to a similar effect while eliciting a more global and complex cell response and avoiding potential concerns such as oncogene formation [263 Baraniak 2010]. As discussed previously, oxygen diffusion in a 3D tissue is known to affect oxygen tension. Therefore,

in the present work, it is suggested that 3D and hypoxic culture can be used to illicit upregulation of angiogenic behavior in ADSCs. In addition to the potential paracrine effects, 3D culture has been shown to enhance survival of cells within a spheroid through contact-dependent signaling and upregulation of pro-survival factors [264 Shweiki 1995],[265 Bates 200],[266 Gaedtke 2007],[267 Bhang 2012a]. Furthermore, 3D culturing may serve to precondition the cells for hypoxic conditions encountered at the ischemic implant site [268 Saleh 2011],[269 Baraniak 2012]. Application of a fluorescent HIF reporter system allows for a unique characterization of hypoxia within 3D ADSC cultures which should serve as a supplement to the few investigations of hypoxia in ADSC spheroids. Furthermore, it is hypothesized that spheroid size and external oxygen concentration can be adjusted to affect hypoxic status of cells throughout a culture, and thus control the output of angiogenic factors. This hypothesis is investigated in the current work. Using culture size to control hypoxia for tissue engineering has not been previously reported in the literature and has implications for optimizing tissue designs for angiogenic cell-therapies in regenerative medicine.

## Chapter 2

# Correlating Hypoxia with Insulin Secretion Using a Fluorescent Hypoxia Detection System<sup>1</sup>

---

<sup>1</sup> M.L. Skiles, R. Fancy, P. Topiwala, S. Sahai, J.O. Blanchette. Correlating hypoxia with insulin secretion using a fluorescent hypoxia detection system. *J Biomed Mater Res B Appl Biomater* 2011, 97(1);148-55. (published) [**270** Skiles 2011a]

## 2.1 Abstract

A common obstacle to the survival of encapsulated tissue is oxygen insufficiency. This appears particularly true of encapsulated pancreatic  $\beta$ -cells. Our work investigates a fluorescent hypoxia detection system for early recognition of hypoxic stress in encapsulated pancreatic tissue. Murine insulinoma (MIN6) cells were engineered to produce a red fluorescent protein under the control of hypoxia-inducible-factor-1. Aggregates of these cells were encapsulated in poly(ethylene glycol) hydrogels at densities of 200,000, 600,000, and 1 million cells per capsule then incubated in either a 1% or 20% oxygen environment. Cell function was evaluated by daily measurement of glucose-stimulated insulin secretion. Encapsulated cells were also fluorescently imaged periodically over 72 hours for expression of the marker signal. Results indicate that oxygen insufficiency severely impacts insulin release from MIN6 cells, and that large aggregates are especially vulnerable to oxygen limitations. Our marker was found to be successfully indicative of hypoxia and could be used as a predictor of subsequent insulin release. Further work will be required to fully characterize signal dynamics and to evaluate *in vivo* efficacy. The method presented here represents a unique and valuable approach to detecting hypoxic stress in living tissues which may prove useful to a variety of fields of biological research.

## 2.2 Introduction

Loss of function and/or viability is often observed in a significant percentage of cells following tissue isolation and encapsulation procedures. This has been especially noted of islets of Langerhans, transplanted as a treatment for T1DM [181 de Vos

1997],[182 Suzuki 1998],[183 de Vos 1999]. While a variety of factors have been investigated, hypoxia has increasingly been implicated as the primary cause for this observed device failure, with insulin secretion by the pancreatic  $\beta$ -cells being particularly sensitive to changes in oxygen concentration [184 Dionne 1989], [185 Dionne 1993],[186 de Groot 2003].

Low oxygen tension in explanted islets can be directly attributed to their removal from the rich vasculature of the pancreas. Encapsulation exacerbates this problem in two ways: 1) by prohibiting islet revascularization and 2) by adding an additional barrier to oxygen transport. Outcomes in unencapsulated islet transplants have shown that diffusion of oxygen and nutrients to islets in well perfused sites of the body prior to revascularization can be sufficient to maintain viability and function [187 Shapiro 2000],[188 Shapiro 2006]. A capsule, however, may hinder diffusion of oxygen to encapsulated tissues by permeability limitations and an increased diffusional distance [189 Schrezenmeir 1994]. For many commonly used materials, oxygen can easily permeate and diffuse within the capsule. Weber, et al. [178 Weber 2009], for instance, have shown that the diffusion coefficients of small molecules within a poly(ethylene glycol) (PEG) hydrogel polymerized from 10 kDa macromers approach their values for diffusion in water. This implies that in terms of oxygenation, combined effects of capsule geometry and material may largely influence device success. However, beyond material and geometric considerations, a variety of factors such as islet size [190 Lehmann 2007],[191 Cavallari 2007], rate of oxygen consumption [192 Sweet 2002],[193 Wang 2005], and site of implantation [194 Dufrane 2006b] all play a part in determining

how much oxygen may be available to any particular cell. As such, a method for quickly detecting hypoxia in individual living cells would provide obvious benefits to the field of cell encapsulation.

Our work reports the development of such a detection system. HIF-1, a heteromeric dimer, has previously been identified as central to cellular hypoxia response [271 Semenza 2001]. In particular, presence of the HIF-1 $\alpha$  subunit, necessary for HIF-1 activity, has been shown to increase exponentially in cells exposed to oxygen levels lower than 6% [105 Jiang 1996b]. We have developed a transfer vector capable of inserting a gene coding for production of a red fluorescent protein under the control of HIF-1. In response to diminished oxygen availability, HIF-1 $\alpha$  is upregulated, dimerizes with HIF-1 $\beta$ , and attaches to HREs in the genome, initiating transcription of native hypoxia response genes as well as the inserted red fluorescent protein gene. Signal can be observed in living cells under a fluorescent microscope.

To better characterize this marker, we have employed it in PEG-encapsulated murine  $\beta$ -cells. Covalently crosslinked PEG networks have been shown to provide a suitable environment for  $\beta$ -cell survival [179 Weber 2006]. Among their favorable characteristics, PEG hydrogels are highly biocompatible, non-degrading, and readily functionalized. Within the hydrogels, hypoxia signal expression and cell function, as defined by GSIS, were compared in normoxic and hypoxic conditions. As a rapid indicator of hypoxia in living cells, we believe this detection system could prove useful not only in cell encapsulation but also in other fields in which hypoxia plays an important role, such as the directionalization of stem cell differentiation.

## 2.3 Materials and Methods

### 2.3.1 Materials

PEG (linear,  $M_n = 10,000 \text{ g mol}^{-1}$ ) and 1-Hydroxycyclohexyl phenyl ketone (99%) (Irgacure 184) were purchased from Sigma-Aldrich (St. Louis, MO, USA) and used as received. Methacrylic anhydride (94%) and reagent A.C.S. grade dichloromethane ( $\geq 99.5\%$ ), and anhydrous diethyl ether ( $\geq 99.5\%$ ) were also purchased from Sigma-Aldrich and used as received.

### 2.3.2 PEGDM Synthesis and Functional PEGDM Solution Preparation

Polymer was prepared in a manner similar to that described by Lin-Gibson et al. [177 Lin-Gibson 2004]. Methacrylic anhydride and PEG were combined in a scintillation bottle at a molar ratio of 10:1 by addition of 0.308g of methacrylic anhydride to 2.0g of PEG. PEG was evenly melted by irradiating the bottle in a standard domestic microwave (1050 W) for 2 minutes, vortexing, then irradiating for another 5 minutes. This process allowed for covalent addition of a methacrylate group to each PEG chain end forming PEGDM. The heated solution was allowed to cool briefly before being re-dissolved in excess dichloromethane (~6 mL). PEGDM was precipitated out of solution in cold anhydrous diethyl ether and collected by vacuum filtration. After drying, PEGDM was dissolved in deionized water and transferred into cellulose ester dialysis tubing with a molecular weight cut-off of 1,000 Da (Spectra/Por Dialysis Membrane, Spectrum Laboratories, Los Angeles, California, USA). The solution was dialyzed against deionized water for 5 days to purify the product. Water was replaced every 24 hours. After

purification, the PEGDM solution was transferred into an appropriate container and placed in a freezer at  $-80^{\circ}\text{C}$  overnight. The frozen solution was then lyophilized on a freeze-drier (Freezone 2.5, Labconco, Kansas City, MO, USA) for 4 days to obtain the final powder form. To prepare the photoactive PEGDM solution, PEGDM was dissolved in Hank's Balanced Salt Solution (HBSS, Invitrogen, Carlsbad, CA, USA) to form a 10 wt% solution. Irgacure 184 was added at 0.025 wt% as a photoinitiator. The final solution was sterilized by filtration through a  $0.2\ \mu\text{m}$  syringe filter and stored in the dark. Crosslinking was achieved by exposure of the desired volume of photoactive PEGDM solution to long wavelength UV light (352 nm). Upon exposure, degradation of Irgacure 184 results in production of free radicals which attack the vinyl carbon-carbon double bonds of the methacrylate end groups resulting in covalent crosslinking of PEG chains and formation of the hydrogel.

In their work, Lin-Gibson et al. noted near stoichiometric conversion of PEG ( $M_n = 1,000$  and  $4,000$ ) to PEGDM after 5 minutes of reaction with methacrylic anhydride at a 1:10 molar ratio (96% and 99% methacrylation, respectively, with no significant difference) [177 Lin-Gibson 2004]. Initial monomer size was not observed to impact resultant percent methacrylation. The procedure described in our work for the preparation and purification of PEGDM is identical to a similar procedure used by Weber et al. for 10 kDa PEG monomers [179 Weber 2006]. Their group reports  $95 \pm 3\%$  methacrylation of PEGDM prepared by this method as determined by  $^1\text{H}$  NMR. Byproducts of the microwave methacrylation reaction are methacrylic acid, which

should be easily removed during purification, and un-methacrylated or mono-methacrylated PEG which should only comprise a small percentage of the final product.

### 2.3.3 Cell Culture

MIN6 cells are an immortalized mouse pancreatic  $\beta$ -cell line exhibiting GSIS comparable to native mouse  $\beta$ -cells. Cells were cultured in RPMI 1640 medium (Invitrogen) supplemented with 10% fetal bovine serum (Invitrogen), 1% penicillin-streptomycin (Invitrogen), and 0.5 $\mu$ g/mL Fungizone (Invitrogen). Cells were plated on 75 cm<sup>2</sup> treated tissue culture flasks and incubated at ambient oxygen levels at 37°C and 5% CO<sub>2</sub> in humid conditions.

### 2.3.4 Dissolved Oxygen Studies

Nitrogen-purged programmable incubators were used to maintain constant oxygen levels for cellular studies (Napco Series 8000 WJ, Thermo Electron, USA). All “high” oxygen studies were maintained at 5% CO<sub>2</sub> and 20% oxygen. All “low” oxygen studies were maintained at 5% CO<sub>2</sub> and 1% oxygen. To determine the corresponding dissolved oxygen content in culture medium during incubation, measurements were taken with a dissolved oxygen probe (Pasport Xplorer GLX and Pasport Dissolved Oxygen Sensor, PASCO, Roseville, CA, USA). The probe was calibrated with deionized water at 25°C. Then, 2 mL of RPMI 1640 growth medium was placed into the well of a 24-well suspension plate, the probe was inserted, and the plate was incubated for at least 12 hours. The media remained uncovered and unagitated throughout study of both high and low oxygen conditions. Incubator temperatures were maintained at 37°C. To

determine if dissolved oxygen concentration was measurably impacted by cellular utilization of oxygen, 1 million dispersed MIN6 cells were seeded into a well and allowed to incubate in 2 mL of medium while dissolved oxygen concentration was measured. Concentrations were again recorded for both high and low oxygen conditions.

### 2.3.5 Encapsulation of Cells

Cultures of MIN6 cells were trypsinized and counted with a hemocytometer on a Nikon Eclipse *Ti* microscope (Nikon, Tokyo, Japan). A range of densities were seeded into 6-well suspension plates in a total volume of 2 mL of growth medium: 100,000 cells/mL, 300,000 cells/mL, and 500,000 cells/mL. Dissociated  $\beta$ -cells have been shown to rapidly lose viability and function, but can spontaneously reaggregate if allowed [272 Matta 1994]. Therefore, cells were incubated at 37°C and 20% oxygen on a rotational shaker at 100 rpm for 24 hours to allow for aggregate formation.

To prepared vessels for capsule polymerization, clear, 1mL syringes were placed tip up in a rack and decapitated to remove the tapered point. Capsules were formed in two steps. Bottom halves of capsules were prepared first, by addition of 20  $\mu$ L of photoactive PEGDM solution into the tips of standing syringes followed by photopolymerization by UV irradiation for 10 minutes. Then, cells that had been aggregating for 24 hours were centrifuged at 200 rpm for 2 minutes and medium was removed. Aggregates were re-suspended in 20  $\mu$ L of photoactive PEGDM solution, with care taken to not dissociate the aggregates. This volume was added into the syringe on top of previously polymerized capsule bottom and polymerization was continued for an additional 10 minutes. In this manner, settling of suspended aggregates in their

respective aliquot resulted in a finished capsule with aggregates fixed in the medial plane. Finished capsules were cylindrical in shape, approximately 6 mm in diameter and 2 mm thick. Capsules were ejected from the syringe tubes, washed with HBSS, and placed in 24-well suspension plates in 1 mL of growth media.

### 2.3.6 Characterization of Aggregate Sizes

Representative images of aggregates at Time 0 (initial time of encapsulation) were analyzed for each of the three cell densities prepared using Nikon NIS-Elements imaging software. Long axis diameter and shortest orthogonal diameter were determined. Average aggregate diameter and standard deviation were calculated from long-axis measurements. A shape factor was also calculated as the ratio of the short-axis to long-axis diameter for each aggregate. The number of aggregates determined to be large (diameter > 150  $\mu\text{m}$ ) and extremely large (diameter > 250  $\mu\text{m}$ ) were additionally determined and reported along with the average size of large and extremely large aggregates.

### 2.3.7 Insulin Release Studies

To assess degree of device function, GSIS from encapsulated aggregates was measured over two weeks. Capsules containing 200,000, 600,000 and 1 million aggregated cells were studied. One day after encapsulation, culture medium was removed and 1 mL of a low concentration buffered glucose solution (1.1 mM) was introduced to each well. Capsules were incubated for one hour before removal of this solution and addition of a high concentration buffered glucose solution (16.7 mM).

After an hour of incubation, samples from the high glucose solution were removed for later analysis and capsules were returned to culture medium. These conditions were used to replicate a starved-state/fed-state cycle. One set of capsules was then returned to incubation in the high oxygen condition while the second set was placed in low-oxygen incubation. Glucose stimulation was repeated in this manner every 24 hours for 2 weeks. At the end of the study, insulin concentration in samples was determined via mouse insulin ELISA assay (Merckodia, Uppsala, Sweden). Capsules of each cellular density were studied in identical experimental setups.

### 2.3.8 Construction of the Hypoxia Marker Virus

A schematic of the mechanism of hypoxia signaling is shown in Figure 2.1. The marker virus is a recombinant adenovirus generated using the pAdEasy-1 system (QBiogene, Montreal, Canada). The red fluorescent protein is a destabilized variant of the DsRed protein. The destabilized protein (termed DsRed-DR) has a portion of mouse ornithine decarboxylase fused to the C-terminus of the DsRed protein which contains a PEST sequence. The DsRed-DR sequence was removed from its vector and inserted into the multiple cloning site of the AdEasy transfer vector under the control of a minimal SV40 promoter with a trimer of the HRE sequence from murine lactate dehydrogenase (LDH). A transfer vector with the LDH HRE SV40 promoter was generously donated by Dr. Rachel Cowen (University of Manchester, UK). The HRE trimer upstream of the SV40 promoter allows hypoxia-dependent transcription of the DsRed-DR protein. After insertion of the DsRed-DR sequence, the transfer vector was allowed to undergo homologous recombination with the pAdEasy vector to produce the recombinant

adenoviral genome which was linearized, transferred and amplified according to the manufacturer's specifications. Following purification of the virus, a plaque assay was performed to determine the concentration of the resulting HRE DsRed-DR viral stocks which allowed infection at specified multiplicities of infection (MOI). This value was determined to be  $3.7 \times 10^7$  plaque-forming units per microliter.

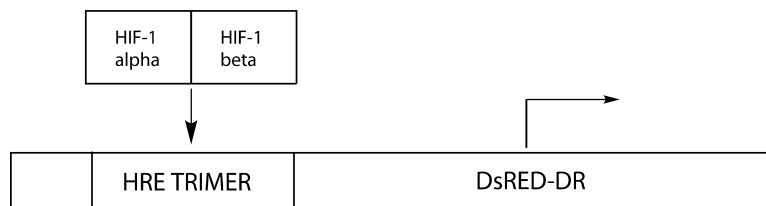


Figure 2.1 Schematic of a novel hypoxia detection system in living MIN6 cells. In response to hypoxia, HIF-1 $\alpha$  is stabilized and dimerizes with HIF-1 $\beta$ . This unit initiates transcription at HREs in target genes producing hypoxia-response proteins as well as the fluorescent DsRed-DR protein.

### 2.3.9 Fluorescent Hypoxia Detection Studies

Cells were infected at an MOI of 100 by addition of the vector to the medium just prior to the 24 hour aggregation incubation period. They were then encapsulated as described in the methods and imaged on an inverted fluorescent microscope with an excitation wavelength of 556 nm at a time denoted as Time 0. One set of capsules was returned to the high oxygen condition while a second set was incubated in the low oxygen condition. Capsules were then re-imaged approximately every 10 -12 hours for 2 to 3 days. Capsules containing 200,000, 600,000, and 1 million aggregated cells were studied. Growth medium was replaced every 24 hours.

### 2.3.10 Statistical Analysis

For capsules prepared at each of the described cell densities, mean insulin secretion at the high and low oxygen conditions were compared. An unpaired Student's t-test assuming unequal variances and with  $\alpha = 0.05$  was used to determine significance of differences between each condition. Significance of differences in size and shape factor between groups was also determined by the same test. Some measured insulin concentrations were at the maximum detectable limit of the performed assay. For these samples, the maximum detectable value (an absorbance of 4.0 at 450 nm) was used. Reported means calculated with inclusion of an estimated maximum value are indicated by <sup>†</sup>.

## 2.4 Results

### 2.4.1 Dissolved Oxygen

Dissolved oxygen concentrations in RPMI 1640 medium incubated in high and low oxygen conditions overnight are shown in Figure 2.2A. After 13.5 hours, medium in the high oxygen condition exhibited a dissolved oxygen concentration of 3.9 mg/L. This value was reached within the first 1.5 hours of incubation. Medium in the low oxygen condition displayed a dissolved oxygen concentration of 0.6 mg/L after 13.5 hours while showing a more gradual decline to this value. A dissolved oxygen concentration of 3.9 mg/L, which represents the end concentration reached in the high oxygen condition, was reached within 15 minutes in the low oxygen trial.

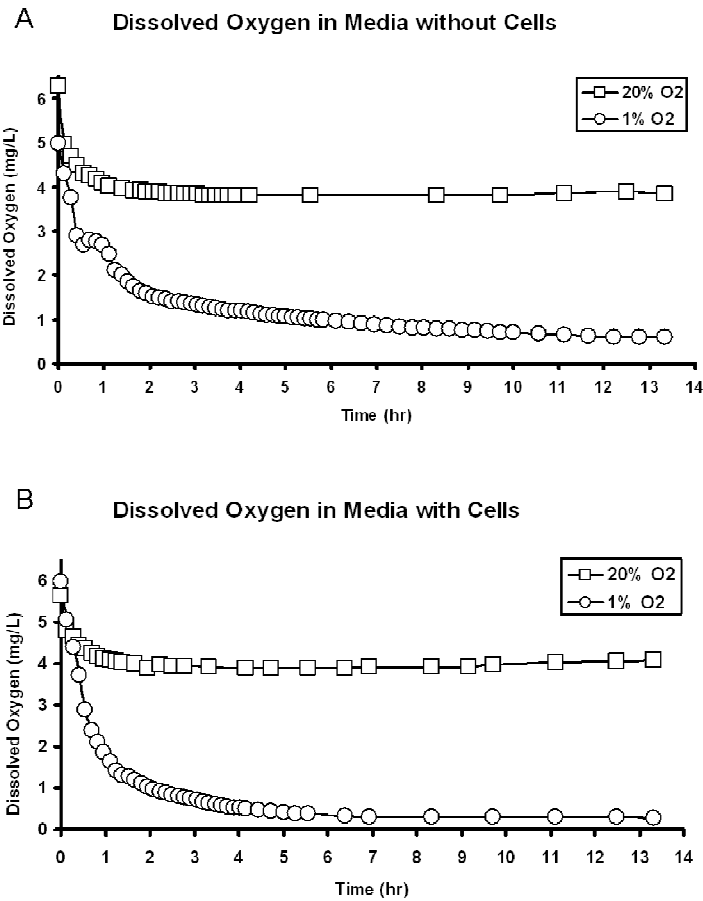


Figure 2.2 A) Dissolved oxygen concentrations measured in 2 mL of growth medium incubated at 37°C in 20% and 1% oxygen. B) Dissolved oxygen concentrations measured in 2 mL of growth medium containing 1 million MIN6 cells incubated in high and low oxygen conditions.

In the second trial, 1 million MIN6 cells were added to the media in both high and low oxygen conditions. Figure 2.2B shows the dissolved oxygen concentrations obtained from these trials. Media containing 1 million cells displayed a dissolved oxygen concentration of approximately 4.0 mg/L after 13.5 hours in high oxygen incubation. This showed no decrease from the value observed in the high oxygen condition in the absence of cells. However, after 13.5 hours of low oxygen incubation, media containing

1 million cells displayed a dissolved oxygen concentration of 0.2 mg/L. This value is approximately one-third of the value observed for media free of cells in the low oxygen condition.

#### 2.4.2 Aggregate Sizes

Capsules were imaged immediately following polymerization to ensure that cells were fully encapsulated and to determine the size of encapsulated aggregates. Centrifugation and re-suspension of cells during the encapsulation procedure was not observed to cause dissociation of aggregates. At each encapsulated density, the bulk of aggregates had a diameter of 75-150  $\mu\text{m}$ . At every density, at least one exceptionally large aggregate ( $> 250 \mu\text{m}$ ) was observed. These were more frequent in higher density capsules, with 4 to 5 being observed in each capsule containing 1 million cells. Capsules containing 1 million aggregated cells additionally displayed significant association of averaged-sized aggregates to form larger fused aggregate networks.

Four representative images of encapsulated aggregates for each density were analyzed to better characterize aggregate size. Table 2.1 shows average aggregate size for aggregates formed at each of the seeded densities. The number and size of large and exceptionally large aggregates are also given, along with average aggregate size excluding large aggregates. Differences in average aggregate size between all groups, though small, were found to be significant ( $p < 0.05$ ). When excluding aggregates larger than 150  $\mu\text{m}$ , which were less prevalent and displayed greater variability in size, aggregates formed from 200,000 cells still displayed a statistically significant difference in size from aggregates formed from 600,000 ( $p = 0.002$ ) and 1 million ( $p = 0.0003$ ) cells,

though the differences in average size was small. Aggregates formed in the 600,000 and 1 million cell conditions did not display a significant difference in average size when excluding large aggregates. In evaluating shape, aggregates were best described as elliptical. Average shape factor was determined to be 0.72 and any difference in shape factor among aggregates from different cell densities or between aggregates of different sizes was not significant.

Table 2.1 Analysis of MIN6 aggregate sizes

Cell Density (per capsule)	Size ( $\bar{x}$ , $\mu\text{m}$ )	#>150 $\mu\text{m}$	%>150 $\mu\text{m}$	#>250 $\mu\text{m}$	%>250 $\mu\text{m}$	Size ( $\bar{x}$ , $\mu\text{m}$ ) <150 $\mu\text{m}$	Range ( $\mu\text{m}$ )
200k	75.7* $\pm$ 29.7	5	1.63	2	0.65	73.0* $\pm$ 20.1	17.3-322.6
600k	80.1* $\pm$ 33.4	9	1.67	2	0.37	77.4* $\pm$ 21.1	22.4-519.0
1M	96.4* $\pm$ 67.2	34	11.8	4	1.39	80.6 $\pm$ 30.0	27.4-835.2

\*Difference in value between groups is significant,  $p < 0.05$ .

#### 2.4.3 Glucose-Stimulated Insulin Secretion

GSIS was measured at high and low oxygen for each of the cell densities prepared. In high oxygen conditions, capsules containing 200,000 aggregated cells displayed an average ( $n = 4$ ) insulin release of 6.4<sup>†</sup>  $\mu\text{g/L}$  ( $\pm 3.1$   $\mu\text{g/L}$ ) at the end of two weeks. Insulin release from capsules containing 600,000 ( $n = 3$ ) and 1 million cells ( $n = 4$ ) was reported on average to be 10.7  $\mu\text{g/L}$  ( $\pm 0.9$   $\mu\text{g/L}$ ) and 8.2<sup>†</sup>  $\mu\text{g/L}$  ( $\pm 3.2$   $\mu\text{g/L}$ ), respectively, at the end of two weeks. For all three high-oxygen trials, insulin release remained relatively consistent and undiminished over the 14 day period. In 1% oxygen, cells encapsulated at a density of 200,000 exhibited insulin release of 0.6  $\mu\text{g/L}$  ( $\pm 0.4$   $\mu\text{g/L}$ ), cells encapsulated at a density of 600,000 exhibited insulin release of 0.3  $\mu\text{g/L}$  ( $\pm 0.1$   $\mu\text{g/L}$ ), and cells encapsulated at a density of 1 million exhibited insulin release of 2.1

$\mu\text{g/L}$  ( $\pm 0.7 \mu\text{g/L}$ ), after 14 days. In each case, drastic reduction in insulin release was observed by as early as day 2. Figures 2.3A, B, and C show high-oxygen and low-oxygen insulin release from capsules containing 200,000, 600,000, and 1 million aggregated cells, respectively.

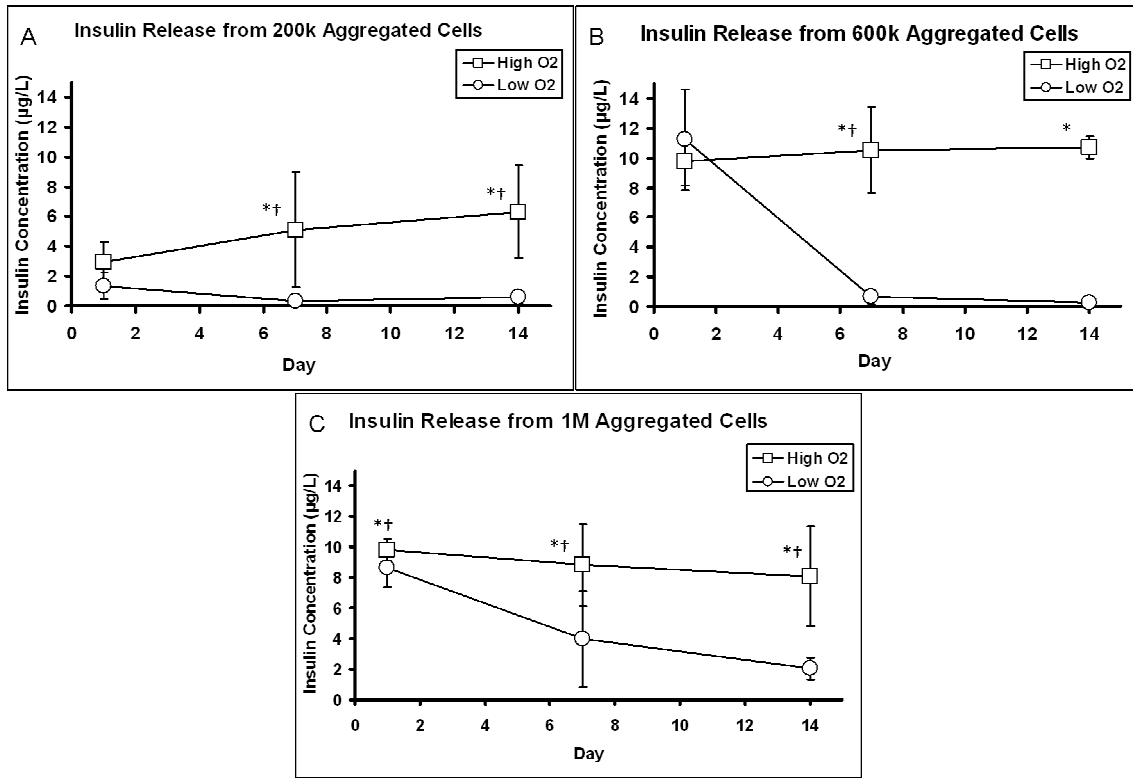


Figure 2.3 Daily one hour insulin release over 2 weeks from capsules containing (A) 200,000, (B) 600,000, and (C) 1 million aggregated MIN6 cells incubated in 20% or 1% oxygen. Statistical significance of differences between high and low oxygen insulin secretion values is indicated by ‘\*’, where  $p < 0.05$ . Data points denoted by ‘†’ include at least one estimated maximum value in determination of the mean.

Comparison of the low and high oxygen conditions showed no significant difference in mean insulin secretion on Day 1 for all three trials. However, on Days 7 and 14, secretion in the low-oxygen condition was found to be significantly lower than in the high-oxygen condition for each cell density tested. ( $p = 0.04$  and  $0.02$ ,  $p = 0.01$

and 0.0008, and  $p = 0.03$  and  $0.02$  for Days 7 and 14 for capsules containing 200,000, 600,000, and 1 million cells, respectively.)

#### 2.4.4 Fluorescent Detection of Hypoxia

After incubation with the hypoxia marker vector for 24 hours, capsules containing 200,000, 600,000, and 1 million aggregated MIN6 cells were incubated in either high or low oxygen. Capsules were fluorescently imaged over 96 hours with red signal indicative of hypoxic stress. For capsules incubated in high oxygen conditions, signal was not detected in aggregates smaller than 250  $\mu\text{m}$  over the three day study period (Figure 2.4a1, b1, c1, d). Signal was observed in aggregates of all sizes within 20 hours in capsules incubated in low oxygen conditions (Figure 2.4a2, b2, c2). In both low and high oxygen conditions, aggregates larger than 250  $\mu\text{m}$  displayed signal in core regions. With extended time, signal in low oxygen aggregates expanded to include the entire aggregate, but remained localized in the aggregate core in high oxygen capsules (Figure 2.4e, f). The largest aggregates ( $> 700 \mu\text{m}$ ) exhibited localized interior signal at the time they were encapsulated, immediately following the 24 hour aggregation period (Figure 2.4 g). In continued hypoxic conditions, maximum signal expression was reached by 48 hours and was sustained thereafter with maintenance of the low oxygen condition.

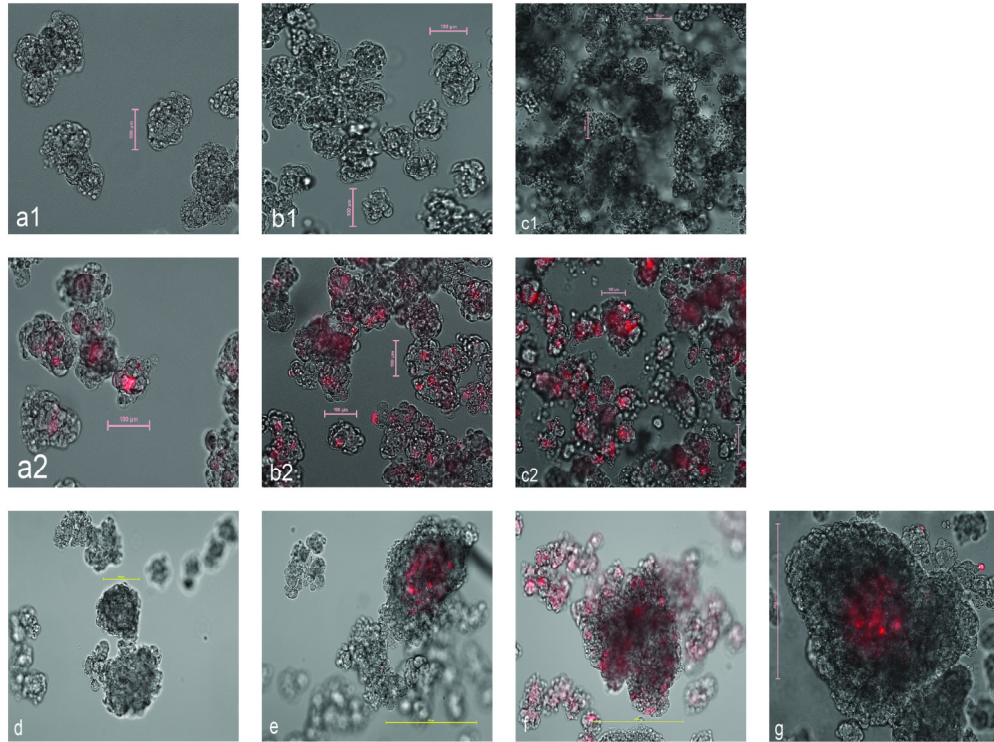


Figure 2.4 Fluorescently imaged aggregates from capsules containing 200,000 (a, bar=100 $\mu$ m), 600,000 (b, bar=100 $\mu$ m), and 1 million (c, bar=100 $\mu$ m) cells incubated in high (1) and low (2) oxygen conditions for 20 hours. At 20 hours in high oxygen, 250  $\mu$ m aggregates (d, bar=100 $\mu$ m) did not display signal, but 500  $\mu$ m aggregates showed centralized signal (e, bar=500 $\mu$ m). At 20 hours in low oxygen, 500  $\mu$ m aggregates displayed ubiquitous signal (f, bar=500 $\mu$ m), though signal onset also occurred in core regions. Exceptionally large aggregates ( $\sim$ 700  $\mu$ m shown) displayed central signal at Time 0 (g, bar=500 $\mu$ m). Fusion of smaller aggregates was noted in capsules with higher cell densities (b1,c1,b2,c2).

## 2.5 Discussion

As early as 1980, transplanted encapsulated pancreatic tissue was shown to have potential to alleviate diabetes [164 Lim 1980]. However, long-term success of such devices has remained elusive, with oxygen insufficiency suspected as a primary cause. Currently, most studies evaluating hypoxia in tissues do so indirectly, by quantifying functional changes in response to varying oxygen levels, or after the fact by

immunostaining fixed histological sections. However, the former approach does not easily account for the fact that functional changes may not be exhibited uniformly by all cells within a capsule, while the latter cannot indicate cellular responses at the time of occurrence nor retain viability of the tissue of interest. On the other hand, knowing the minimum cellular oxygen requirement, one could attempt to determine whether that value is met within a capsule, as has been done with microelectrode measurement of oxygen concentration [273 Carlsson 1998] and computational modeling [151 Gross 2007],[153 Buchwald 2009],[274 Dulong 2007]. However, although providing a good estimate, models are time consuming to develop and employ and must be re-adapted to any change in material or geometrical configuration. Furthermore, they still cannot take into account every factor affecting oxygen concentration throughout a capsule as some are not yet even fully understood. As an alternative approach, our fluorescent hypoxia marker system allows individual, living cells to report when they initiate a hypoxic stress response. This method both obviates the need to measure oxygen concentration and allows hypoxic conditions to be detected quickly, and potentially remediated, prior to tissue necrosis.

The hypoxia marker was evaluated in MIN6 aggregates encapsulated at different densities within crosslinked PEGDM hydrogels. No toxic effects should be expected from the method of encapsulation used in this work. Acrylated or methacrylated PEG as an encapsulation matrix has been shown to be supportive of a range of cell types. PEG itself is highly biocompatible while the Irgacure 184 photoinitiator has been shown to have no influence on viability at low concentrations [180 Bryant 2000]. Bryant et al. also

showed that 10 minutes of UV irradiation was likewise not detrimental to cell viability, and report that this length of exposure is within the clinically acceptable range [180 Bryant 2000]. Low-speed centrifugation prior to encapsulation did not result in aggregate disruption.

Results from both our functional studies and hypoxia detection studies are in good agreement with the published literature. Exposure of MIN6 aggregates to hypoxic conditions elicited an observable fluorescent response within 20 hours. Though future work will focus on timing of signal initiation, extremely large aggregates (> 500  $\mu\text{m}$ ) displayed central signal at the time of encapsulation. This indicates that signal onset occurs fairly quickly and agrees with Moritz et al. who found that response to hypoxia was observed in as little as 6 hours [275 Moritz 2002]. We also observed reduction in insulin secretion under hypoxic conditions, with effects beginning as early as day 2. Similar results have been widely reported [184 Dionne 1989],[185 Dionne 1993],[186 de Groot 2003].

When comparing signal expression and insulin secretion between capsules containing differing densities of cells, density of seeding did not appear to directly influence hypoxic signaling; at 1% oxygen all aggregates appeared to display signal, while at 20% oxygen signal was only seen in core regions of the largest aggregates. Thus aggregate size appears to exert more influence over aggregate oxygenation than overall cell number. As noted, though small, differences in average aggregate size between the tested cell densities were determined to be significant. However, it is unlikely that these average size differences contribute much to differences in signal expression and

insulin secretion (73  $\mu\text{m}$  and 80  $\mu\text{m}$  aggregates, for instance, did not exhibit differences in hypoxia signal expression and likely secreted insulin similarly). The percentage of large and exceptionally large aggregates present in the differing populations, on the other hand, may have contributed more significantly. In capsules containing 1 million cells, aggregates 150  $\mu\text{m}$  or larger represented nearly 12% of aggregates while making up less than 2% of aggregates in 200,000- and 600,000-cell capsules. Additionally, twice as many exceptionally large aggregates (>250  $\mu\text{m}$ ) were observed in 1 million-cell capsules. At this size, aggregates began to display hypoxia signaling in core regions, even in a 20% oxygen environment, again, consistent with findings by other groups [184 Dionne 1989],[275 Moritz 2002]. Thus, hypoxia signaling and insulin secretion were only indirectly affected by seeding density in capsules containing 1 million cells, insomuch that large aggregates were more prevalent. We point out that in our work it was desirable to observe the behavior of both large and small aggregates. However, in studies where stricter control of aggregate size may be important, consistency in size may be achieved by aggregating cells at a density of 100,000 cells per mL and then pooling aggregates to attain the desired number of cells per capsule.

Close observation of insulin secretion data may point to a tempting hypothesis – a greater percentage of large aggregates with hypoxic core regions explains an apparent “diminishing returns” in insulin secretion, where capsules containing 1 million cells incubated in high oxygen secreted statistically similar amounts of insulin as capsules containing 600,000 cells. Indeed, such an effect has been reported by Suzuki et al. [182 Suzuki 1998]. However, as noted, a number of the measured high-oxygen insulin

concentrations were at the maximal detectable limit of the assay and were estimated in calculations to be the maximal value. Because of this, accurate comparisons between the different seeding density groups cannot be made. However, the effect of these estimated values is not so detrimental to a comparison between the high and low oxygen conditions, on which this study is primarily focused. Even with relatively large standard deviation in some cases (attributable to small variability in cell number, precision of the assay, and the nature of insulin secretion), cells in high oxygen conditions secreted an amount of insulin that was, as calculated, significantly higher than cells in low oxygen conditions on Days 7 and 14. Because any true secretion value could only be the same or higher than the estimated value reported in this work, the difference between levels of insulin secreted in high and low oxygen conditions would only be increased by knowledge of the more accurate value. Thus our approach does not impact any conclusion drawn by a comparison of the functional effects of a 20% or 1% oxygen environment.

We report that hypoxia signaling was observed within 24 hours of exposure to low oxygen conditions while a drop in GSIS became apparent by day 2. In this sense, hypoxic signaling was predictive of future device function. Furthermore, signal onset was rapid enough to allow time for a remediating response prior to cell loss. Additional study will be required regarding signal extinction, though preliminary observations show that extinction occurs within 48 hours after re-exposure to the high oxygen condition. We hope that with modification of MOI, this system may be tuned to achieve real-time signaling. As a real-time indicator of hypoxia, the marker system might be particularly

useful to study of encapsulated tissues *in vivo*. Strength of emission will determine if signal is detectable, but we would expect utility at least in small animal models with an implantation site near to the skin. A possible modification in order to increase *in vivo* applicability could be to substitute a bioluminescent marker for the DsRed-DR gene used in this work. Though quantification of either type of signal is difficult, current work is focused on measuring HIF-1 $\alpha$  levels to compare to fluorescent intensities and determining threshold intensities corresponding to specific cellular responses.

Finally, though in this work MIN6 cells were particularly suited to demonstrating our method of hypoxia detection, we believe that the marker system may be favorably utilized in other cell types as well. We have recently, for instance, observed marker expression in native islets of Langerhans isolated from Balb/c mice. In this regard, degree of HIF-1 expression may vary among tissue types and will have large implications as to whether the marker could be considered for use [275 Moritz 2002]. Nonetheless, recent works suggesting the role of hypoxia in directing stem cell differentiation offer another exciting field in which our method of hypoxia detection could be helpfully employed [260 Abdollahi 2010],[276 Ma 2009],[277 He 2010]. We hope to investigate such applications in future work.

## Chapter 3

### Identifying HIF Activity in 3D Cultures of Islet-Like Clusters<sup>2</sup>

---

<sup>2</sup>M.L.. Skiles, N.B. Wilder, S. Sahai, J.O. Blanchette. Identifying HIF activity in three-dimensional cultures of islet-like clusters. *Int J Artif Organs* 2013, 36(3);175.83. (published) [278 Skiles 2013]

### 3.1 Abstract

**Purpose:** Hypoxia is a major cause for failure of encapsulated islet grafts. 3D re-aggregation and hypoxic preconditioning are used to help overcome this obstacle. However, it is still difficult to identify hypoxic cells in a 3D system. We evaluate the efficacy of a fluorescent system for detecting HIF-1 activity in live  $\beta$ -cells. Identification of HIF-1 activity and correlation with insulin secretion and viability will allow for more informed implant construction and better prediction of post-transplantational function.

**Methods:** MIN6 cells were infected with the marker virus and rotationally cultured to form clusters. Clusters were encapsulated in PEG hydrogels and incubated in 20%, 2%, or 1%  $O_2$ . Gels were imaged daily for hypoxia marker signaling and for morphological observation. Daily GSIS was quantified by insulin ELSIA and cell viability was assessed by LIVE/DEAD staining.

**Results:** Clusters cultured in 2% and 1%  $O_2$  displayed high levels HIF activity compared to 20%  $O_2$  clusters. 20%  $O_2$  clusters maintained viability and achieved a smooth, islet-like morphology by Day 14. Clusters in 2% and 1%  $O_2$  failed to associate cohesively and showed reduced viability. As a whole, constructs cultured in 20%  $O_2$  exhibited 10-fold higher GSIS than constructs in 2% and 1%  $O_2$ .

**Conclusions:** Our marker is an effective approach for identifying cellular hypoxia in 3D cultures.  $\beta$ -cell clusters in 2% and 1%  $O_2$  are similarly affected by reduced oxygen tension, with HIF-1 activity correlating to reduced GSIS and impaired cell/cluster morphology. Simultaneous aggregative culture and hypoxic conditioning may not be beneficial to  $\beta$ -cell transplantation.

### 3.2 Introduction

Cell-based therapies for treatment of T1DM remain hindered by dramatically-reduced oxygenation of excised and transplanted islets [279 Davalli 1995],[280 Carlsson 2001],[281 Miao 2006]. While alleviating some of the difficulties associated with tissue transplantation, encapsulation can further decrease oxygen tension in the graft [186 de Groot 2003],[282 Cornolti 2009]. To reduce hypoxia-related loss of function, methods such as hypoxic preconditioning [283 Semenza 2011b],[284 Lo 2012] and islet dissociation/re-association (to produce smaller, more  $\beta$ -cell dense clusters) have been suggested [191 Cavallari 2007],[285 Schuit 2001]. Still, further advancement in islet transplantation will depend upon quick and accurate detection of the hypoxic state, an understanding of the cellular impact of and response to hypoxia, and an ability to remediate the hypoxic condition or avoid it in the first place.

Most cells exhibit substantial changes in gene expression as an adaptive response to oxygenation below 5 or 6%. A majority of these changes involve upregulation of genes by activity of HIF-1, a heterodimeric bHLH-PAS family transcription factor whose presence in the cell is tightly regulated by oxygen. Specifically, the HIF-1 $\alpha$  subunit is subject to rapid degradation under normoxic conditions, but is exponentially stabilized as oxygen becomes limited [105 Jiang 1996b]. HIF responses serve to adapt the cell for survival in a low oxygen environment by, among other things, switching the cell to glycolytic metabolism, promoting local angiogenesis, inhibiting apoptosis, and reducing oxygen-intensive cellular activities [286 Cassavaugh 2011]. In the insulin-secreting  $\beta$ -cells of the pancreas, HIF-1-induced

switching to glycolytic metabolism has been shown to decouple glucose sensing from insulin exocytosis resulting in a dramatic impairment of insulin secretion from hypoxic islets [195 Zehetner 2008],[196 Cantley 2009],[197 Puri 2009].

Determining if and when insulin-producing cells become hypoxic is clearly important in predicting their performance. However, identifying hypoxic cells, especially within 3D islet and islet-like cluster cultures, can be difficult. Measuring oxygen partial pressure and modeling oxygen diffusion/consumption may help identify regions of low local oxygen concentration but do not identify any behavioral changes in the cells. A complimentary technique is to identify HIF-1 activity, which represents a behavioral response to hypoxia whatever the specific oxygen concentration. Due to its activity as a transcription factor and its short half-life (in normoxia, 4-8 minutes) [109Moroz 2009],[287 Yu 1998], direct detection of HIF-1 without compromising the cell and/or construct is difficult or impossible. Furthermore, HIF responses are not homogeneous across cell types, with degree of stabilization and upregulated target genes varying between and within tissues [48 Maxwell 1993],[128 Brachen 2006],[129Lendahl 2009]. Therefore we employ a fluorescent reporter gene system which indicates HIF activity in oxygen-stressed cells rather than HIF abundance. We have previously reported the convenience of this approach for identifying hypoxic cells in  $\beta$ -cell clusters and allowing HIF activity to be monitored in the same sample over time [270 Skiles 2011a].

In the present work, we sought to compare HIF activity in aggregated, encapsulated murine  $\beta$ -cells to other cell properties that are impacted by hypoxia, such

as morphology, viability, and GSIS. While atmospheric oxygen concentrations are common in cell culture, they are not representative of an implant microenvironment; therefore, we examined  $\beta$ -cell behavior in normal culture conditions (20% O<sub>2</sub>) as well as a pair of more physiological oxygen concentrations commonly used for hypoxic preconditioning (2% and 1% O<sub>2</sub>). Given the high oxygen requirement of  $\beta$ -cells, elevated HIF activity would be expected to correlate to decreased insulin secretion and possibly loss of viability. Such results would show the utility of the marker to predict functional changes in encapsulated  $\beta$ -cells and to evaluate the consequences of various oxygen conditions.

### 3.3 Materials and Methods

#### 3.3.1 Cell Culture

MIN6 cells were cultured in RPMI 1640 medium (Mediatech, Manassas, VA) supplemented with 10% fetal bovine serum (PAA, Dartmouth, MA), 1% penicillin-streptomycin (Mediatech), 0.5  $\mu$ g/mL amphotericin B (Mediatech), and 7 mM D-(+)-glucose (Sigma-Aldrich, St. Louis, MO). Cultures were maintained in standard incubation conditions at 37 °C, 5% CO<sub>2</sub>, and high humidity. For experimental use, the cells were trypsinized prior to confluence, counted, and seeded into the wells of a 12-well suspension culture plate at a density of 400,000 cells per well in 1.7 mL of media.

#### 3.3.2 Hypoxia Marker

For marker studies, the cells were infected with a hypoxia marker virus prior to encapsulation, as previously described [270 Skiles 2011a]. Briefly, the marker virus was

added to each well of dispersed cells at an MOI of 100 immediately following cell trypsinization and seeding. The marker is a recombinant adenovirus generated by the pAD-Easy-1 system (QBiogene, Montreal, Canada) that introduces a gene coding for a destabilized variant of the red fluorescent protein, Ds-Red-DR under the control of a minimal SV40 promoter and trimer of the HRE sequence. In an infected cell, hypoxia-stabilized HIF-1 binds to the HRE and allows for hypoxia-induced transcription of the Ds-Red-DR gene and subsequent fluorescent signaling.

Following introduction of the virus, dispersed cells were incubated in rotational culture at 100 rpm for up to 36 hours to allow for infection and for formation of islet-like clusters. Clusters were then encapsulated and immediately imaged, and the gels were divided into three groups for rotational culture in either a 20%, 2%, or 1% oxygen environment. Oxygen concentration was controlled through use of Napco Series 8000 incubators (Thermo Fisher, Waltham, MA) with automated nitrogen purging for maintenance of a set oxygen percentage. Following placement in the appropriate incubator, gels were fluorescently imaged daily followed by replacement of media.

As a positive control, cells were infected with a modified marker virus containing a CMV promoter in place of the HRE trimer, allowing for constitutive expression of the marker signal, regardless of oxygen status. As a negative control, uninfected cells were also fluorescently imaged.

We have previously measured dissolved oxygen content of media incubated in 1% O<sub>2</sub> and observed that 24 hour incubation is sufficient to achieve a steady, equilibrated concentration [270 Skiles 2011a]. Therefore, in the present study, low-

glucose media and high-glucose buffer solutions to be added to gels incubated in 2% and 1% O<sub>2</sub> conditions were pre-equilibrated to 2% and 1% O<sub>2</sub>, respectively, for 24 hours prior to use.

### 3.3.3 PEGDM Synthesis and Cell Encapsulation

PEGDM was synthesized from linear, 10 kDa PEG (Sigma-Aldrich) as previously described [270 Skiles 2011a], following a protocol adapted from Lin-Gibson et al. [177 Lin-Gibson 2004]. Briefly, microwave methacrylation of PEG was carried out by irradiating a 10:1 molar ratio solution of methacrylic anhydride (Sigma-Aldrich) and PEG in a standard domestic microwave for 5 minutes to form PEGDM. This was dissolved in excess dichloromethane (Sigma-Aldrich) then precipitated in cold, anhydrous diethyl ether (Sigma-Aldrich) and collected. The precipitate was dissolved in deionized water and dialyzed against the same for 3 days for purification. Purified PEGDM powder was collected by lyophilization.

A photoactive, PEGDM solution was prepared for the formation of hydrogels. PEGDM was dissolved in HBSS (Mediatech) to form a 10 wt% weight solution and Irgacure 2959 (Ciba, Basel, Switzerland) was added to 0.025 wt% as a photoinitiator. The solution was sterile-filtered prior to use.

Cell clusters were encapsulated in a two-step process. First, the bottom half of the hydrogel was formed by pipetting 20  $\mu$ L of photoactive PEGDM solution into a narrow cylindrical tube. The tube was exposed to UV light (365 nm,  $\sim 7$  mW/cm<sup>2</sup>) for 8 minutes to initiate cross-linking. During this time, previously aggregated MIN6 clusters were removed from their wells and centrifuged for 4 minutes at 210 g. The media was

removed and the clusters were gently resuspended in 20  $\mu$ L of photoactive PEGDM solution. This volume was added on top of the first 20  $\mu$ L volume and cross-linking was completed by an additional 8 minute UV exposure. The hydrogels were then ejected, rinsed in HBSS, and placed in a 24-well plate in 1 mL of media for incubation.

#### 3.3.4 Glucose-Stimulated Insulin Secretion

To evaluate GSIS from encapsulated MIN6 clusters, gels were prepared with each containing aggregates formed from a total of 400,000 cells. Freshly-formed gels were divided into three groups and placed in 24-well plates in 1 mL of low-glucose media (2 mM) each. For the first day, all plates were incubated in rotational culture at 20% O<sub>2</sub>. After 24 hours, the media was removed and replaced with a buffered, high-glucose solution (16.7 mM) for one hour. This solution was removed and frozen for future analysis and replaced with 1 mL of low-glucose media. Plates were then placed in rotational culture at 20%, 2% or 1% O<sub>2</sub>. Thereafter, gels were stimulated in the same manner every 24 hours. Insulin concentration in media samples was quantified by mouse insulin ELISA (Merckodia, Winston-Salem, NC) following the manufacturer's protocol.

#### 3.3.5 Viability

To assess viability of encapsulated cells, an esterase activity and plasma membrane permeability assay (LIVE/DEAD, Invitrogen, Grand Island, NY) was performed. MIN6 cells were aggregated and encapsulated as described and placed in 20%, 2% or 1% oxygen incubation in 1 mL of media each. Every 24 hours, one gel from each incubator

was removed and stained with LIVE/DEAD reagent for 30 minutes following the manufacturer's protocol. Media was replaced in the remaining gels and they were returned to incubation. Stained gels were then briefly rinsed with HBSS and fluorescently imaged. Viable cells were indicated by a green cytoplasmic staining and dead cells were indicated by red nuclear staining. For cells incubated in 2% and 1% O<sub>2</sub>, media pre-equilibrated to 2% and 1% O<sub>2</sub>, respectively, was used.

### 3.3.6 Imaging and Statistical Analysis

Fluorescent imaging was performed on a Nikon Eclipse Ti (Nikon Instruments, Melville, NY) inverted, fluorescent microscope. For fluorescent capture, care was taken to ensure that consistent lamp intensity and exposure settings were maintained and that fields were representative of the whole gel. In marker studies, the same gels were tracked over time. Image analysis was performed in NIS-Elements AR 3.0 (Nikon) software. For quantitative GSIS studies, a minimum of three replicate samples were analyzed. Results are reported as mean  $\pm$  standard deviation. Differences between values were assessed by a student's t-test assuming unequal variances with statistical significance occurring when  $p < 0.05$  (indicated in the results with an asterisk, '\*').

## 3.4 Results

### 3.4.1 Encapsulation and Cell Morphology

Clusters of aggregated MIN6 cells were formed by 36 hour rotational culture of 400,000 cells in low-adherence 12-well culture plates. Previous studies indicated that clusters larger than 300  $\mu\text{m}$  experience core hypoxia even at 20% oxygen conditions,

and that few clusters of this size would be formed in rotational culture of 400,000 cells [270 Skiles 2011a]. For each well, all clusters were collected and encapsulated in a single hydrogel, placed in 20%, 2% or 1% oxygen conditions, and periodically imaged over 2 weeks. Hydrogels were cylindrical, approximately 2 mm high and 5 mm in diameter when swollen, with clusters distributed throughout (Figure 3.1).



Figure 3.1 400,000 MIN6 cells aggregated to form islet-like clusters and encapsulated in a 40  $\mu$ L PEGDM hydrogel. Bar = 1 mm.

Initially after formation, the cells were associated into small, irregularly-shaped clusters with individual cells remaining discernable. By 4 days, 20% O<sub>2</sub> clusters were clearly distinguishable from Day 1 clusters, with Day 7 clusters displaying a more regular,

ovoid shape and a smooth surface morphology akin to native islets. Individual cells within the cluster could not be distinguished. In 1% or 2% oxygen, clusters did not achieve a smooth, round morphology by 4, 7 or 14 days and individual cells were still  $\beta$ -cells discernable within the clusters. Clusters in 20% oxygen could be distinguished from those in 1% or 2% oxygen by 4 days, though not sooner. After 2 weeks, clusters incubated in 20% oxygen were large, round and healthy looking with a clear islet-like appearance while clusters incubated in 2% and 1% oxygen appeared unchanged or irregular and necrotic (Figure 3.2).

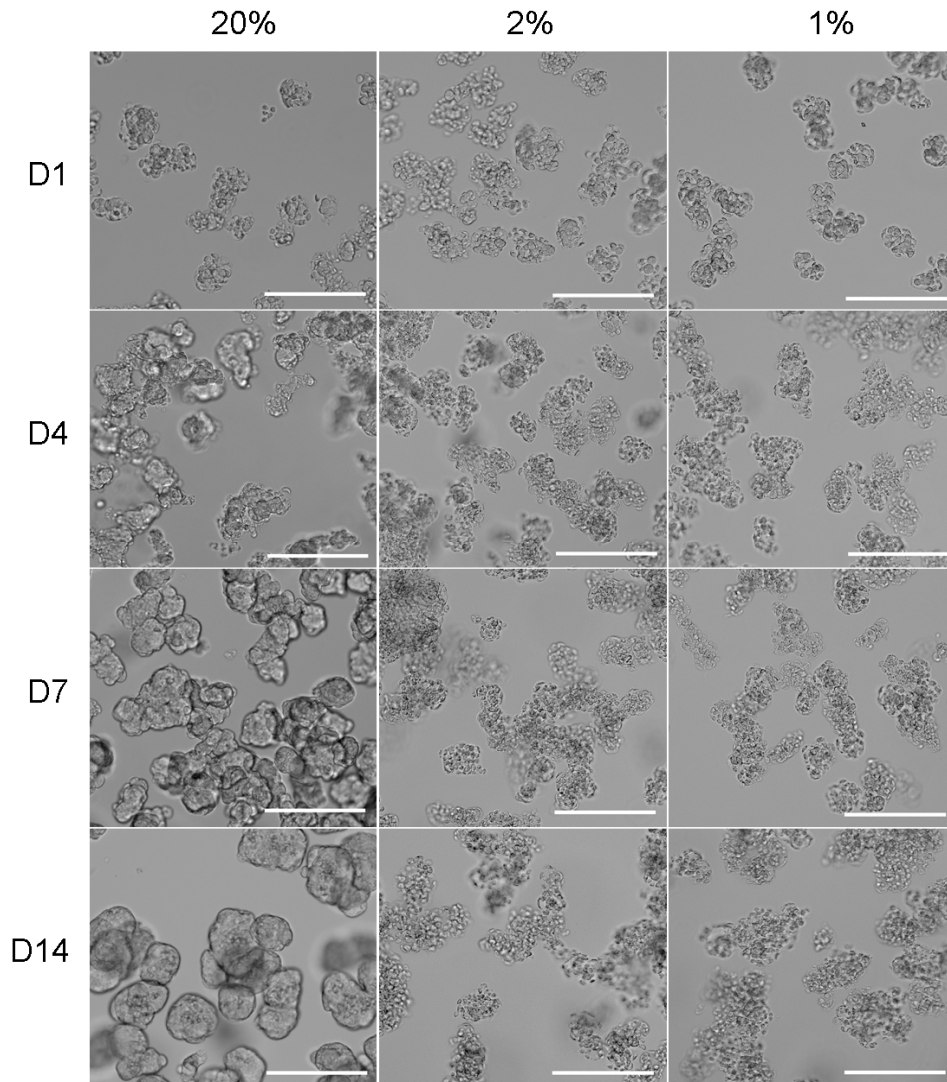


Figure 3.2 Brightfield microscopy images of islet-like clusters for the analysis of morphology over 2 weeks in 20% O<sub>2</sub>, 2% O<sub>2</sub>, or 1% O<sub>2</sub>. Clusters incubated in 20% O<sub>2</sub> attained a morphology similar to that of primary islets by 1 week and retained that morphology thereafter. Clusters incubated in 2% and 1% O<sub>2</sub> never achieved a primary islet-like morphology, with loosely associated cells and irregular aggregate morphology.

### 3.4.2 Hypoxia Marker

To correlate hypoxia with cellular activity of HIF-1, a fluorescent reporter system was employed. Transient infection with the marker virus allowed the cells to produce a red fluorescent protein under the control of active HIF-1. If present, this signal was easily detected by fluorescent microscopy. At the time of encapsulation (Time 0), no cells were observed to display fluorescent signal. At the given capture settings, Clusters incubated in 20% oxygen exhibit few or no cells displaying fluorescent signal at the given capture settings over the course of the study. Clusters incubated in 2% and 1% O<sub>2</sub> showed a dramatic increase in number and intensity of fluorescing cells beginning on Day 1 compared to 20% O<sub>2</sub> clusters (Figure 3.3). Intense signal in 2% O<sub>2</sub> slightly preceded such signal in 1% O<sub>2</sub>. Maximum signal intensity was reached on Day 2 or 3. Signal pervasiveness and intensity appeared similar between 2% and 1% O<sub>2</sub> clusters. Fluorescence was heterogeneous throughout signaling clusters, with signal clearly identifiable in individual cells. Though signaling cells appeared somewhat randomly distributed in the clusters, fluorescence was often observed in central cells of larger clusters. In control studies, all CMV-DsRed-DR infected cells displayed rapid, intense fluorescent signaling indicating efficacy of the system and high rate of infection. Uninfected cells displayed no fluorescence.

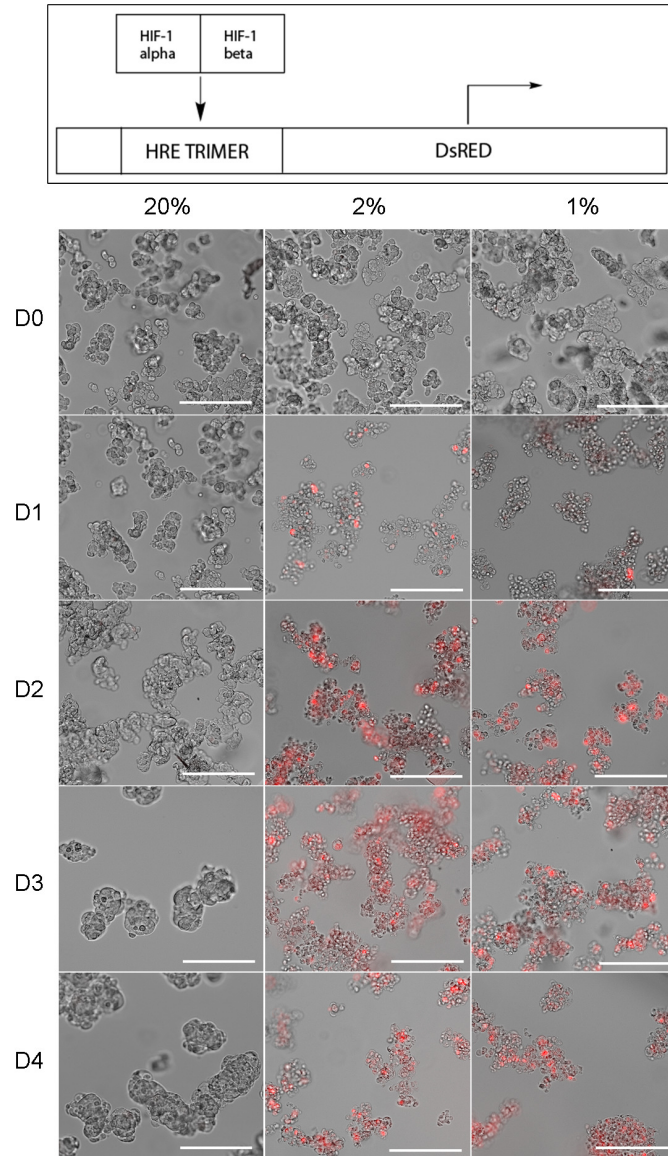


Figure 3.3 (Top) Schematic of HIF-induced cellular fluorescence used to identify HIF activity in this study. At sufficiently low oxygen concentrations, HIF-1 $\alpha$  is stabilized, dimerizes with HIF-1 $\beta$  and binds to the HRE sequence, initiating transcription of the target gene, in this case Ds-Red-DR. (Bottom) Hypoxic signaling in islet-like clusters of MIN6 cells infected with the hypoxia marker virus for HIF-activated fluorescence. Clusters incubated in 20% O<sub>2</sub> displayed little or no fluorescence through the study. Clusters incubated in 2% and 1% O<sub>2</sub> expressed signal by Day 2 with fluorescence located throughout all clusters.

### 3.4.3 Glucose-Stimulated Insulin Secretion

We assessed the secretory activity of MIN6 clusters incubated in 20%, 2%, and 1% O<sub>2</sub> for comparison to HIF-1 activity as indicated by the fluorescent marker. These results are graphically represented in Figure 3.4.

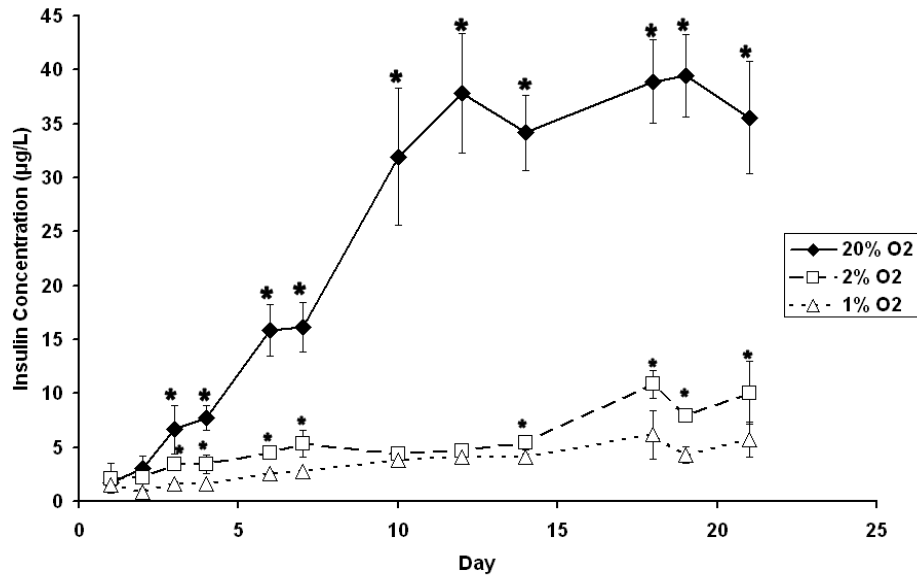


Figure 3.4 GSIS in clusters of MIN6 cells cultured in 20%, 2%, or 1% O<sub>2</sub> (mean  $\pm$  standard deviation, n = 3). Large asterisks indicated significant difference between 20% O<sub>2</sub> and both low-oxygen conditions. Small asterisks indicate significant difference between 2% and 1% O<sub>2</sub> samples ( $p < 0.05$ ).

Consistent with islet-like morphological arrangement and minimal indication of HIF-1 activity, clusters incubated in 20% oxygen displayed high levels of insulin secretion. Continued increase in secretion was observed from Day 1 through Day 12. This correlates well with the timeframe over which primary islet-like size and morphology were achieved. On Day 12 insulin secretion plateaued, with  $37.8 \pm 5.5$   $\mu$ g of insulin secreted during the 1 hour stimulation period. In clusters incubated in 1% and 2% O<sub>2</sub>,

very little increase in secretion from Day 1 was observed over the course of the study. Statistical significance between secretion from 20% clusters and secretion from low-oxygen clusters was seen by Day 3, the time by which hypoxia signaling reached a maximum. Secretion from clusters incubated in 2% O<sub>2</sub> was slightly higher than secretion from clusters incubated in 1% O<sub>2</sub>. On Day 12, one-hour secretion from clusters incubated in 2% and 1% O<sub>2</sub> was measured to be  $4.7 \pm 0.2 \mu\text{g}$  and  $4.1 \pm 0.1 \mu\text{g}$ , respectively, equating to 8 to 9 times less insulin than by clusters in 20% O<sub>2</sub>. As reported, these secretion results represent the overall insulin-producing capability of constructs incubated in their respective oxygen condition.

#### 3.4.4 Viability

The viability of cells within the encapsulated clusters was examined via a Live/Dead esterase activity/plasma membrane integrity assay (Figure 3.5). On Day 1, nearly 100% viability was observed in cells from all three oxygen conditions. Cells incubated in 20% O<sub>2</sub> maintained this level of viability throughout the 14 day study. Loss of viability in a small number of cells was first observed on Day 2 in gels incubated in 1% oxygen and on Day 4 in gels incubated in 2% oxygen. Through the remaining two weeks of the study, the appearance of non-viable cells slowly increased in both of these conditions; however, overall viability appeared to remain high.

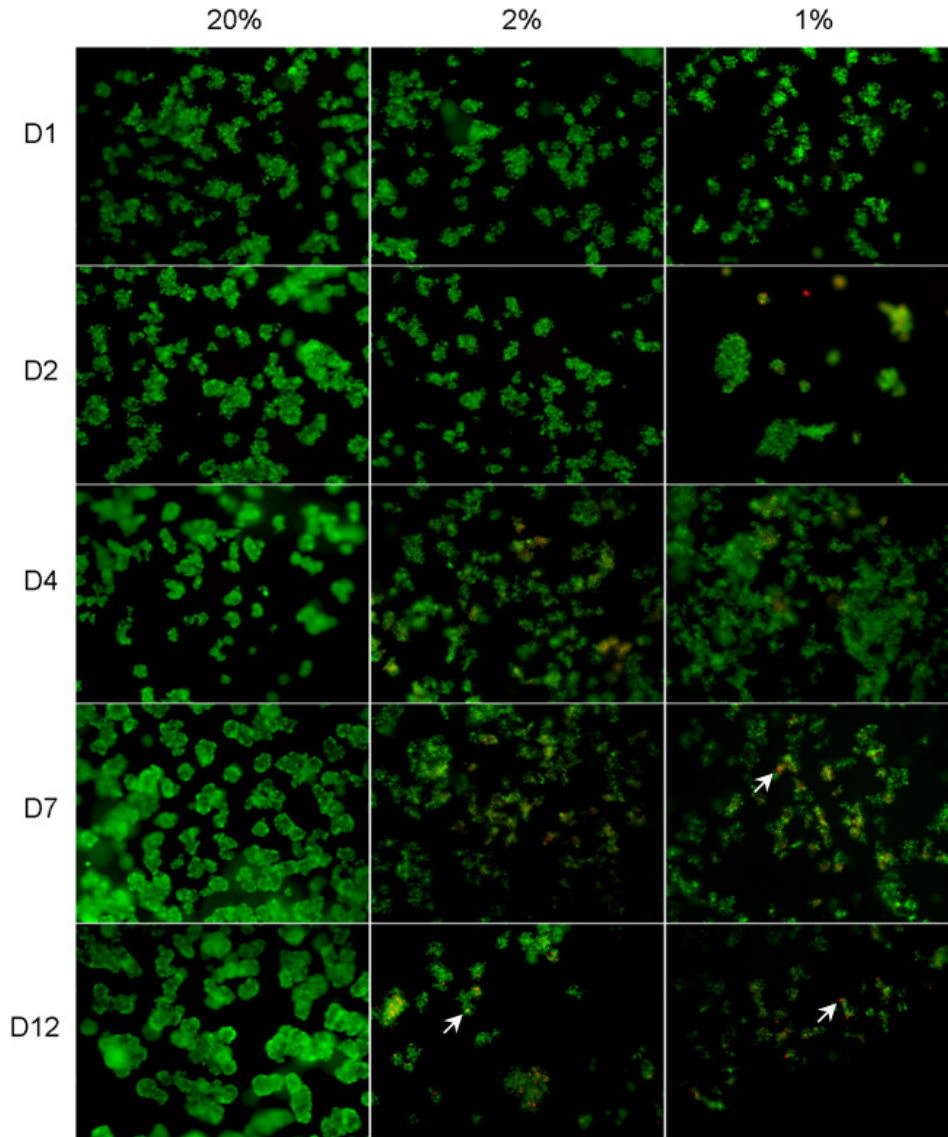


Figure 3.5 Analysis of viability in clusters of MIN6 cells. Cells incubated in 20% O<sub>2</sub> appear completely viable (green staining) over two weeks. Clusters incubated in 2% and 1% O<sub>2</sub> both displayed some cell death (red staining, indicated with white arrows) within clusters by Day 4. Numerous cells appeared to be non-viable in these conditions by Day 14, though total viability was estimated to remain above ~75%.

Consistent with morphological observations, green cytoplasmic staining, indicating viable cells, expanded and intensified in 20% O<sub>2</sub> clusters over the same timeframe in which they adopted a primary islet-like morphology. That these clusters were healthy and functional is supported by their high, sustained GSIS. Alternatively, green cytoplasmic staining in 2% and 1% O<sub>2</sub> clusters was unchanged or increasingly diminished indicating a reduced cytoplasmic volume and reduced esterase activity. This corresponded to both evidence of active HIF-1 and poor GSIS. Representative non-viable cells are indicated by the arrows in the figure. Though useful as an indicator of change in viability between clusters incubated in 20% O<sub>2</sub> and those incubated in hypoxic oxygen conditions, percent viability within the clusters was not able to be accurately quantified due to the 3D nature of the cultures and difficulty in distinguishing neighboring cells.

### 3.5 Discussion

That low oxygen tension has a profoundly negative impact on insulin secretion from pancreatic  $\beta$ -cells, both *in vitro* and *in vivo*, has been widely documented[**184** Dionne 1989],[**185** Dionne 1993],[**186** De Groot 2003],[**280** Carlsson 2001]. However, the difficulty in assessing when a cell becomes hypoxic (i.e. begins to respond to hypoxia) on a cellular level within 3D aggregates has hindered better understanding of whether various physiological/culture conditions will illicit a detrimental hypoxic response. Many common approaches to “identifying” hypoxia involve direct or indirect measurement of oxygen partial pressure or dissolved oxygen concentration. However, these methods suffer from a number of drawbacks, including invasiveness and potential

tissue/construct damage, insufficient resolution for cellular-scale detection, consumption of oxygen in the detection process, requirement for tissue/construct sacrifice, reliance upon expensive equipment, and/or poor precision [288 Springett 2007],[289 Grist 2010]. Furthermore, these methods focus on measurement of oxygen concentration but not cellular activity in response to that concentration.

Alternatively, the method discussed in this work identifies activity of the primary regulator of intracellular response to hypoxia, HIF-1, and in this sense may be considered to truly identify hypoxic status. This method has the added benefit that signaling and detection do not impact viability and that the tissue/construct need not be sacrificed in the detection process, as is required in histological analysis, allowing for the same population to be examined over time. Our marker can be easily applied to monolayer culture, micromass culture, and tissue culture within 3D scaffolds to investigate the potential impact on oxygenation resulting from each of these conditions. Furthermore, because the signal protein is a direct target of HIF-1, this system is ideal for examining the relationship between culture conditions and various other HIF-induced responses.

HIF-activated pathways have been recognized as the primary mechanisms by which low, intracellular, oxygen concentration is translated to a program of transcriptional responses which result in loss of  $\beta$ -cell function. We therefore undertook the current work based on an interest in using identification of intracellular HIF-1 activity as an indicator of activation of these downstream pathways. We employed a previously-developed fluorescent marker system to identify HIF-1 activity

in living cells which we compared to a number of physiological and functional events known to be impacted by hypoxia. We showed that marker signal was induced by hypoxic incubation and that signal corresponded to irregular cell association and morphology, inability of clusters to achieve primary islet-like organization, and dramatic decline in GSIS. Furthermore, hypoxic signal was apparent by Day 2, prior to the time at which a difference in morphology of GSIS was detectable, highlighting the use of this system as a predictor of cell viability and function.

Luther et al. report that unencapsulated clusters of MIN6 cells cultured in 20% oxygen achieve a size and conformation similar to primary islets after 7 days [290 Luther 2005]. In the present study, we report that encapsulated MIN6 clusters achieve primary islet-like size and appearance by Day 7 when cultured at 20% oxygen but not at 2% or 1% oxygen. Alternatively, MIN6 clusters incubated in 1% and 2% oxygen displayed hypoxia marker signal expression, indicative of HIF activity, and failed to achieve the tight, round morphology found in primary islets. Individual cells within the clusters remained more distinguishable suggesting loose cell interactions rather than the tight interactions seen in clusters at 20% oxygen. Proper function of pancreatic  $\beta$ -cells is heavily dependent upon cell-to-cell contact [291 Hauge-Evans 1999],[292 Lin 2011],[293 Luther 2006]. HIF-1-induced repression of cell adhesion proteins such as E-cadherin through upregulation of lysyl oxidase LOX, LOXL2, SIP1 and Snail provides an appealing explanation for this poor association [294 Schietke 2010],[295 Evans 2007].

HIF-1 also impacts insulin secretion directly by hindering metabolic pathways required for insulin exocytosis [283 Semenza 2011b]. Secretion of insulin from

pancreatic  $\beta$ -cells is highly coupled to glucose sensing through aerobic mitochondrial pathways [296 Lee 2008]. In  $\beta$ -cells with active HIF-1, these pathways are switched off resulting in severely blunted GSIS. We found that  $\beta$ -cell clusters incubated in atmospheric oxygen conditions (20%) did not exhibit impaired GSIS, despite the hindrances to oxygen diffusion that encapsulation and 3D tissues provide. However, when cultured in low physiological levels of oxygen, the cells exhibited clear HIF activity and impairment of GSIS in both 2% and 1% O<sub>2</sub>.

Current studies suggest that there may be benefits to dissociating islets and reforming them into islet-like clusters, primarily to reduce cluster diameter and improve oxygen transport [285 Schuit 2001],[191 Cavallari 2007]. Indeed, large diameter clusters can experience internal hypoxic gradients with central cells experiencing significantly different oxygen conditions than peripheral cells. In previous studies, we reported that central cells in clusters larger than approximately 300  $\mu$ m displayed increased HIF activity via the reporter gene, even in 20% O<sub>2</sub> [270 Skiles 2011a]. Clusters smaller than this size did not exhibit the increase in 20% O<sub>2</sub> and exhibited more uniform HIF activity in 2% and 1% O<sub>2</sub>. Thus it is likely that severe oxygen gradients are not developed in clusters of the size examined in the current study. Another approach to improve post-transplantational function of  $\beta$ -cells is hypoxic preconditioning prior to implantation in order to prime them for the reduced oxygenation of the implant site [283 Semenza 2011b],[284 Lo 2012]. Our results suggest that simultaneous aggregation and hypoxic conditioning do not result in maintenance of islet-like morphology or GSIS and that the two techniques should be applied individually or sequentially.

### 3.6 Conclusions

It is clear that identifying cellular hypoxia will be beneficial to the advancement of cell-based diabetes therapies. Our marker, indicating HIF-1 activity, represents an ideal means of making such an identification. With this tool, we hope to establish correlations between  $\beta$ -cell oxygenation in 3D systems and  $\beta$ -cell function. Having shown its usefulness in a model system, we intend to apply this marker to future studies in isolated mouse islets. Here, we will be able to make predictions about implant function at various implantation sites with differing degrees of oxygenation. We will also examine the correlations between HIF-1 activity, cell binding protein production during re-aggregation, and GSIS in 3D culture systems. We feel that our marker system represents a convenient, non-invasive method of indicating intracellular HIF-1 activity that can serve as a much-needed tool for identifying hypoxia and examining its effects in current and future cell-based delivery endeavors.

#### Acknowledgements:

We thank the lab of Dr. Melissa Moss of the Chemical Engineering Department at the University of South Carolina, Columbia for shared use of equipment and the Medical University of South Carolina Instrument Resource Facility for assistance with histology. Special thanks to Dr. Kristi Anseth at the University of Colorado, Boulder for the generous donation of the MIN6 cell line.

This research was funded through grants from the National Science Foundation (EPS 0903795) and the National Institutes of Health (P20 RR-016461).

## Chapter 4

Use of Culture Geometry to Control Hypoxia-Induced VEGF Secretion from

ADSCs: Optimizing a Cell-Based Approach to Drive Vascular Growth<sup>3</sup>

---

<sup>3</sup>M.L. Skiles, S. Sahai, L. Rucker, J.O. Blanchette. Use of culture geometry to control hypoxia-induced VEGF secretion from ADSCs: optimizing a cell-based approach to drive vascular growth. *Tissue Eng Part A* (submitted, in revision)

#### 4.1 Abstract

ADSCs possess potent angiogenic properties and represent a source for cell-based approaches to delivery of bioactive factors to drive vascularization of tissues. Hypoxic signaling appears to be largely responsible for triggering release of these angiogenic cytokines, including VEGF. 3D culture may promote activation of hypoxia-induced pathways, and has furthermore been shown to enhance cell survival by promoting cell-cell interactions while increasing angiogenic potential. However, the development of hypoxia within ADSC spheroids is difficult to characterize. In the present study we investigated the impact of spheroid size on HIF-1 activity in spheroid cultures under atmospheric and physiological oxygen conditions using a fluorescent marker. Hypoxia could be induced and modulated by controlling the size of the spheroid; HIF-1 activity increased with spheroid size and with decreasing external oxygen concentration. Furthermore, VEGF secretion was impacted by the hypoxic status of the culture, increasing with elevated HIF-1 activity, up to the point at which viability was compromised. Together, these results suggest the ability to use 3D culture geometry as a means to control output of angiogenic factors from ADSCs, and imply that at a particular environmental oxygen concentration an optimal culture size for cytokine production exists. Consideration of culture geometry and microenvironmental conditions at the implantation site will be important for successful realization of ADSCs as a pro-angiogenic therapy.

## 4.2 Introduction

Therapies that stimulate regeneration of damaged tissues in the body or restore deficient tissues with bioengineered replacements represent an appealing and emerging technology. Such therapies often involve the implantation of cells or tissue into an ischemic wound environment, necessitating rapid vascularization for survival and integration of the implant. Indeed, diffusional mass transfer limitations restrict the potential size of engineered tissues and remain one of the biggest challenges to their clinical success [201 Lovett 2009],[203 Novosel 2011]. New strategies to enhance angiogenesis are required to overcome these hurdles.

Strategies that harness the angiogenic potential of cells have shown promising results in recent studies. Fibroblasts [297 Levenberg 2005],[298 Kunz-Schughart 2006] and mesenchymal stem cells (MSCs) [232 Kim 2007],[299 Blasi 2011],[300 Halfon 2011] can significantly contribute to endothelial network formation and maintenance of microvasculature. Dispersed mesenchymal stromal cells implanted in dermal wounds [252 Lee 2009],[301 Nie 2011] and ischemic tissue [302 Kang 2010],[303 Bhang 2011] increased local levels of angiogenic cytokines and promoted increased capillary density. Of the potential cell candidates to be utilized for cell-based delivery, ADSCs appear particularly well suited for use in regenerative medicine due to their relative abundance and ease of culture as well as their ability to differentiate into relevant cell types in musculoskeletal tissue engineering (e.g., osteoblasts, chondrocytes, vascular smooth muscle cells).

The manner of cell transplantation to an injury site can impact transplant performance. Cells injected as a dispersion have reduced cell-cell and cell-matrix interactions which are important in sustaining pro-survival pathways and suppressing apoptosis [265 Bates 2000],[303 Bhang 2011]. Alternatively, 3D cultures retain these interactions, while also providing reduced oxygen tension within the cell mass which may prime the cells for the ischemic implantation site [267 Bhang 2012a],[268 Saleh 2011],[269 Baraniak 2012], enhancing therapeutic effect. For example, cord blood MSCs implanted as 3D spheroids upregulated expression of anti-apoptotic and angiogenic proteins, downregulated expression of proapoptotic proteins, and showed superior integration into newly forming vessels in ischemic mouse hind limbs compared to dispersed cells [267 Bhang 2012a].

Oxygen gradients that form within 3D tissues are not necessarily detrimental. In particular, hypoxia is responsible for initiating angiogenesis *in vivo* [304 Shweiki 1992],[305 Germain 2010] through activation of HIFs and subsequent upregulation of bioactive factors such as VEGF [256 Forsythe 1996],[306 Maxwell 2002],[307 Fong 2009],[308 Rey 2010]. HIF proteins are dimeric transcription factors of the bHLH-PAS family each composed of an  $\alpha$  and  $\beta$  subunit [52 Wang 1995]. The  $\alpha$  subunit undergoes oxygen-dependent hydroxylation, marking it for proteosomal degradation. When local oxygen concentrations are not adequate for hydroxylation to occur, the subunit is stabilized, pairs with a  $\beta$  subunit, and is free to bind to HREs found in the promoter region of a number of genes involved in adapting the cell for survival in low oxygen.

Thus, oxygen tension in 3D cell masses can contribute to activation of HIF-regulated pathways which benefit the cells. For instance, stabilization of HIF and VEGF upregulation in growing avascular tumors is well known to promote tumor vascularization [309 Brahim-Horn 2001],[310 Semenza 2012b]. Similarly, endothelial cells cultured as spheroids were found to express higher levels of HIF-1 $\alpha$  mRNA than those cultured as a monolayer under the same oxygen conditions [311 Bhang 2012b]. Additionally, hypoxia is known to play a role in regulating cell differentiation. During formation of vascularized endochondral bone, regional hypoxia leads to HIF activation and VEGF upregulation and is integral for the formation of a cartilage template and synchronization of ossification with angiogenesis [312 Zelzer 2004],[313 Araldi 2010]. Thus it is clear that identifying approaches to regulate desirable, HIF-activated signaling in ADSCs could provide new avenues towards creation of vascularized tissue and repair of critical size defects in bone.

The present study investigates the ability to control VEGF secretion from ADSCs by regulating hypoxic status. The effects of culture dimensions and incubator oxygen tension (atmospheric conditions as well as a pair of hypoxic levels) on angiogenic potential of ADSC spheroids are examined. HIF activity within the spheroids, identified using a previously-described fluorescent marker system [270 Skiles 2011a], was compared to levels of VEGF secretion from the cells. The impact of pelleting and hypoxia on cell viability and morphology were examined by staining and histological analysis. Results from this study provide insight into the nature of hypoxia in 3D

cultures and may suggest a relevant approach for tailoring the release of angiogenic factors from ADSCs for improved vascularization of engineered tissues.

### 4.3 Materials and Methods

#### 4.3.1 Cell Culture

Passage 1 human ADSCs isolated from lipoaspirates were purchased from Invitrogen (Carlsbad, CA) and cultured in Complete MesenPRO RS™ reduced-serum medium supplemented with a penicillin-streptomycin solution (Mediatech, Manassas, VA; final concentration: 115 IU/mL penicillin, 115 µg/mL streptomycin). This medium was also used throughout all experiments. For passaging, cells were kept in a humidified atmosphere of 95% air and 5% carbon dioxide at 37°C. Medium was changed three times a week. At approximately 80% confluence, the cells were trypsinized and sub-cultured at a ratio of 1:4 until reaching passage 6, as recommended by the supplier. All data included in these studies were obtained from cells between passages 3 and 6. Maintenance of ADSC stemness was verified by cell-surface staining and flow cytometry. Purchased, P1 cells were > 95% positive for stem cell surface markers CD44 and CD105. Fluorescent antibody labeling for each (CD44: eBioscience, San Diego, CA; CD105: Biolegend, San Diego, CA) revealed > 95% staining for both markers at P6 (Figure 4.1).

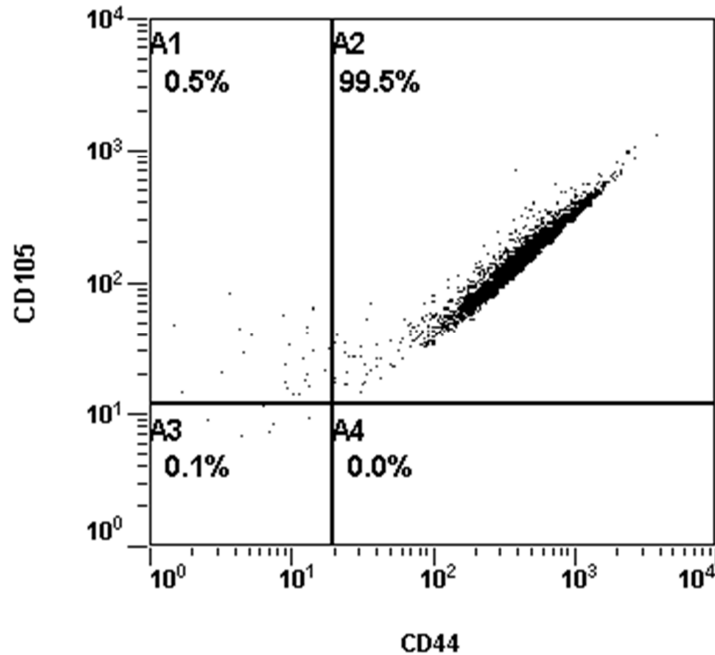


Figure 4.1 Flow cytometry analysis of cell surface markers CD44 and CD105 in P6 ADSCs. The cells were still >95% positive for both markers at passage 6, indicating maintenance of stemness.

Nitrogen-purged, programmable incubators (Napco Series 8000, Thermo Electron, Waltham, Massachusetts) were used to maintain low oxygen levels for hypoxic culture studies. For 2% and 1% oxygen studies, all media, buffers, and fixatives to be used with the cells were kept in vented tubes in the corresponding incubator overnight prior to use to equilibrate the solutions to the appropriate oxygen concentration.

#### 4.3.2 Hypoxia Marker Virus

We have previously described the recombinant adenovirus used in this study to identify HIF activity [270 Skiles 2011a]. Briefly, the virus was generated using the pAdEasy-1 system (QBiogene, Montreal, Canada) by inserting into the vector a

destabilized variant of the red fluorescent protein, DsRed, (termed DsRed-DR) under the control of a minimal SV40 promoter and an HRE trimer. Previous ADSC studies have indicated approximately 100% infection efficacy using an MOI of 80 (data not shown), which was utilized in these studies.

#### 4.3.3 ADSC Infection and 3D Culture Formation

At approximately 80% confluence, ADSCs were trypsinized, centrifuged, resuspended in growth medium and counted. For HIF activity tracking studies, hypoxia marker virus was added to suspended cells and gently mixed for 30 minutes. ADSC spheroids of four different sizes were prepared by centrifugal pelleting. Five thousand (5k), 10,000 (10k), 20,000 (20k), or 60,000 (60k) cells were pipetted into 0.5 mL, screw-cap microcentrifuge tubes and centrifuged at 500 rcf for 2 minutes. Spontaneous aggregation of the pelleted cells into cohesive spheroids occurred during overnight incubation at 37°C. Spheroids of each size were then divided into three groups for incubation in 20%, 2%, or 1% O<sub>2</sub>. While in incubation, the tube caps were loosened slightly to allow for gas transfer. Medium was changed daily.

Spheroids for HIF activity tracking studies were encapsulated in polyethylene glycol (PEG) by methods identical to those that have been published previously [270 Skiles 2011a]. For reference, a video demonstration of this method by the authors is suggested [314 Skiles 2011b].

#### 4.3.4 Quantification of Secreted VEGF

For secretion studies, spheroids were cultured in a volume of media based on cell number. 60k, 20k, 10k, and 5k spheroids were cultured in 900 $\mu$ L, 300 $\mu$ L, 150 $\mu$ L, and 75 $\mu$ L of medium, respectively. 60,000 cells grown in monolayer were also cultured at each oxygen concentration in 1mL of medium. Every 24 hours, the medium was removed from each sample and replaced with fresh medium. Media samples were stored at -80°C prior to analysis. Levels of VEGF in media samples were determined by ELISA (Abcam, Cambridge, MA) following the manufacturer's instructions. For each group, 6 independent samples were analyzed.

#### 4.3.5 Analysis of Cell Viability and Morphology

Cell viability in ADSC spheroids was examined using a LIVE/DEAD cytotoxicity/viability assay (Invitrogen) and by histological examination. The LIVE/DEAD kit was used according to the manufacturer's instructions to identify esterase activity in live cells and loss of plasma membrane integrity in dead cells. For histological analysis of morphology, spheroids were first fixed overnight in a 4% paraformaldehyde solution. The spheroids were then embedded in 2% agar, paraffin processed, and cut into 5 $\mu$ m sections. Sections were stained with hematoxylin and eosin and imaged.

#### 4.3.6 Fluorescent Cell Imaging and Image Analysis

Imaging for spheroid size determination and fluorescent detection of the hypoxia marker was performed on a Nikon Eclipse Ti inverted fluorescent microscope (Nikon Instruments, Melville, NY) and image processing and analysis was performed in NIS-

Elements software (Nikon Instruments). Identical camera and microscope settings were used for each capture within a study. Spheroids were imaged immediately following encapsulation and then every 24 hours thereafter. Histological sections were imaged on a Nikon Optiphot-2 microscope (Nikon) fitted with a Zeiss AxioCam MRc camera (Carl Zeiss, Oberkochen, Germany).

For determination of spheroid sizes, the cross-sectional area of spheroids was measured in the software from representative, central-plane images of spheroids from each size group and the diameter of a circle with an equivalent area was calculated. Results are reported as the mean  $\pm$  standard deviation of 6 independent samples. To roughly quantify hypoxia marker signal, a fluorescent signal threshold intensity was applied to representative images from each group. The area of signal meeting or exceeding the threshold value was compared to the total spheroid area as calculated from the image. The threshold value was chosen such that no signal was detected in monolayer cells incubated in 20% O<sub>2</sub>, as levels of HIF-1 $\alpha$  in these cultures were below detectable limits by western blotting in previous studies [315 Sahai 2012].

#### 4.3.7 Statistical Analysis

All values are reported as mean  $\pm$  standard deviation of replicate samples. Statistical significance of differences between samples was determined by a two-tailed student's t-test assuming unequal variances (“\*\*\*” indicates statistical significance at  $p \leq 0.01$ , “\*” indicates statistical significance at  $p \leq 0.05$ ).

## 5.4 Results

### 4.4.1 Pelleted ADSCs form Spherical, 3D Cultures of Reproducible Size

Following centrifugation, ADSCs formed a small plaque at the tip of each microcentrifuge tube. After overnight incubation, the cells had spontaneously condensed into round spheroids with a diameter dependent upon the initial number of cells. Figure 4.2A shows representative spheroids of each size at Time 0. ADSC spheroids were cohesive and consistently sized within each group. In Figure 4.2B the average diameter for spheroids from each study group at Time 0 (white bar) and at Day 4 (black bar) is shown. Minimum spheroid diameter was achieved by Day 4 with no further condensation observed thereafter. 5k, 10k, 20k and 60k spheroids were  $362 \pm 10 \mu\text{m}$ ,  $454 \pm 21 \mu\text{m}$ ,  $557 \pm 20 \mu\text{m}$ , and  $811 \pm 37 \mu\text{m}$  in diameter, respectively, immediately after formation. Spheroids diameters on Day 4 were  $282 \pm 6 \mu\text{m}$ ,  $379 \pm 8 \mu\text{m}$ ,  $469 \pm 16 \mu\text{m}$ , and  $714 \pm 15 \mu\text{m}$ , respectively. The ratio of spheroid size on Day 4 to initial spheroid size was similar for all size groups, ranging from approximately 78% for 5k spheroids to 88% for 60k spheroids. Differences in culture oxygen concentration did not appear to have an effect on spheroid condensation.

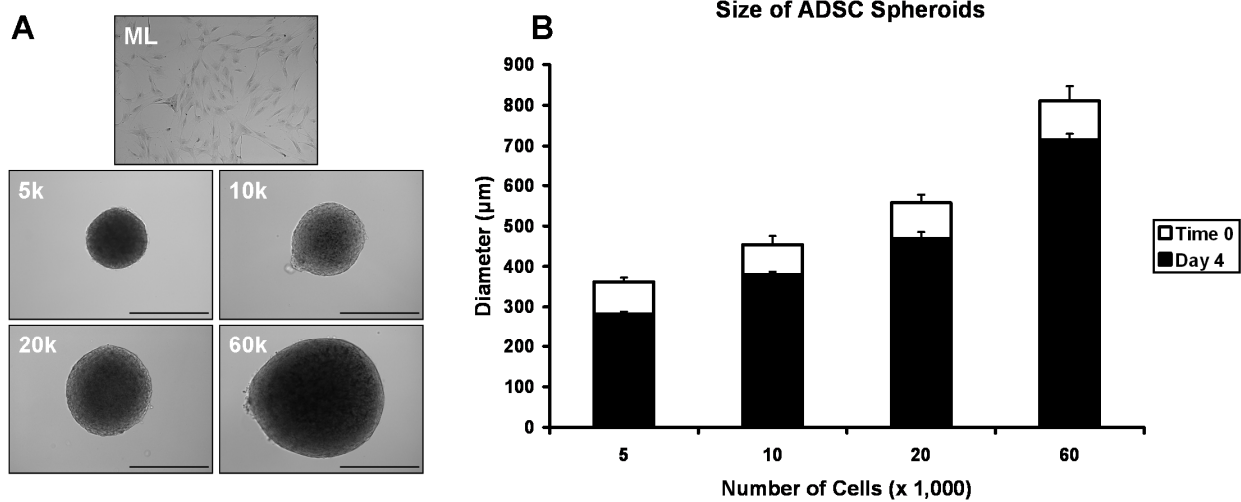


Figure 4.2 Diameter of spheroids formed by centrifugally pelleting different numbers of ADSCs. Initial spheroid size could be reliably controlled by adjusting the number of cells pelleted (white bars). Spheroids continued to condense for several days following initial formation before reaching a final minimal diameter by Day 4 (black bars). Bar = 500µm.

#### 4.4.2 Spheroid Size and External O<sub>2</sub> Concentration Affect Regional Hypoxic Signaling

The degree of HIF activity in ADSC spheroids as indicated by red fluorescent signaling of the HIF marker is shown in Figure 4.3. In spheroids of all sizes, HIF activity increased as incubator oxygen concentration decreased. With decreasing oxygen, signal onset was more rapid and signal area and intensity were increased. Signal also increased with spheroid size. 5k spheroids incubated in 20% O<sub>2</sub> displayed little or no signal over 5 days. Increasingly more signal was seen in 20% O<sub>2</sub> spheroids as spheroid diameter increased. For each oxygen concentration, signal onset was more rapid and signal area and intensity were higher as spheroid diameter increased. In general, signal was first observed in central regions of the spheroids and remained most intense there.

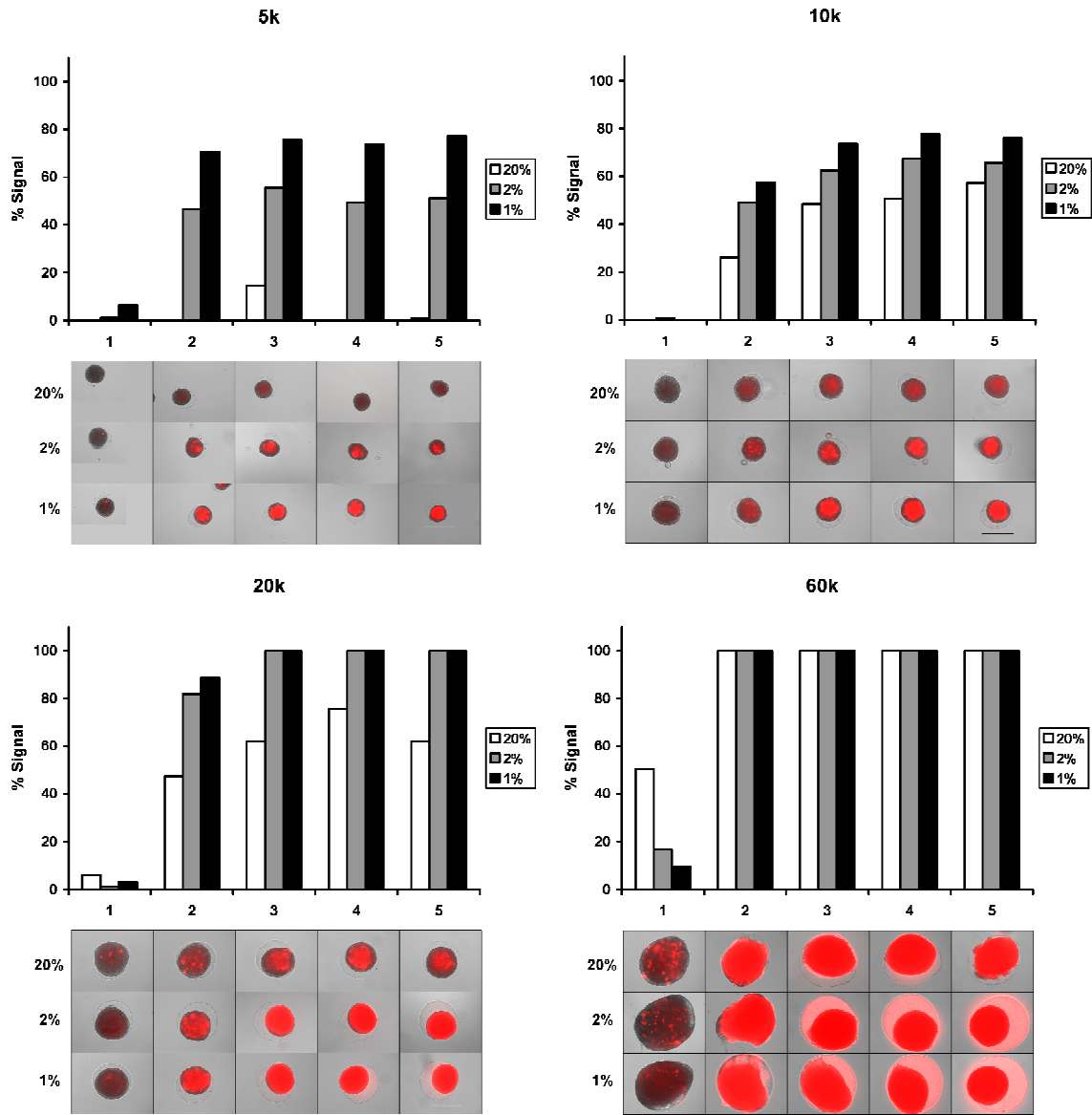


Figure 4.3 Fluorescent DsRed signaling as an indicator of HIF activity in 5k (top left), 10k (top right), 20k (bottom left), and 60k (bottom right) ADSC spheroids incubated in 20%, 2% or 1% O<sub>2</sub>. The relative extent of signaling is quantified in the graph above each set of figures by applying a signal intensity threshold value. The voided region caused by spheroid condensation can be seen as a ring in the hydrogel around the culture in some images. Bar = 500µm.

To roughly quantify the prevalence of HIF activity throughout the spheroids, the intensity threshold was applied to each image to identify regions exceeding it. The areas of these regions were compared to the total spheroid cross-sectional area as determined in the software (graphs in Figure 4.3).

The capture settings used in Figure 4.3 resulted in some spheroids with high levels of HIF activity being overexposed. In this case, differences in signal intensity between overexposed spheroids could be resolved by reducing the camera exposure time (Figure 4.4). Though useful in identifying differences in HIF activity in spheroids that exceeded the dynamic range of capture at the given settings, apparent signal intensities measured from those images cannot be compared to intensities in Figure 4.3.

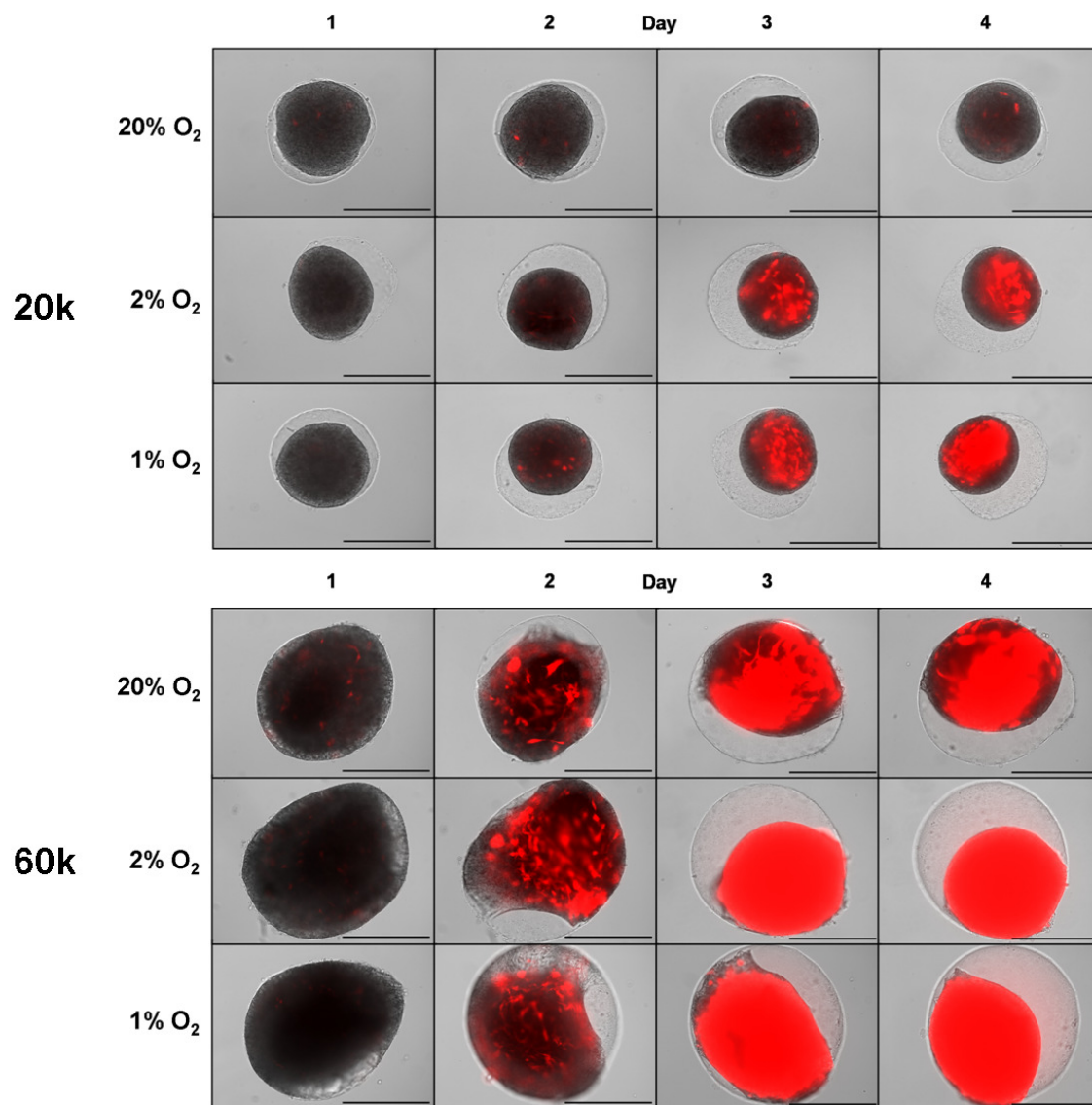


Figure 4.4 Fluorescent HIF reporter signal displayed at 1/5 the exposure length as in Figure 4.3 for 20k and 60k spheroids. Differences in signal intensity between samples that were lost due to over-saturation are better resolved at the lower exposure. Overexposure is still observed in 60k Day 3 and 4 spheroids. Bar = 500 $\mu$ m.

#### 4.4.3 Degree of Hypoxia Impacts VEGF Secretion Profile

Figure 4.5 displays per-cell VEGF secretion from ADSCs in monolayers and spheroids cultured under different oxygen concentrations. The calculated mean values and standard deviations are reported in Table 4.1.

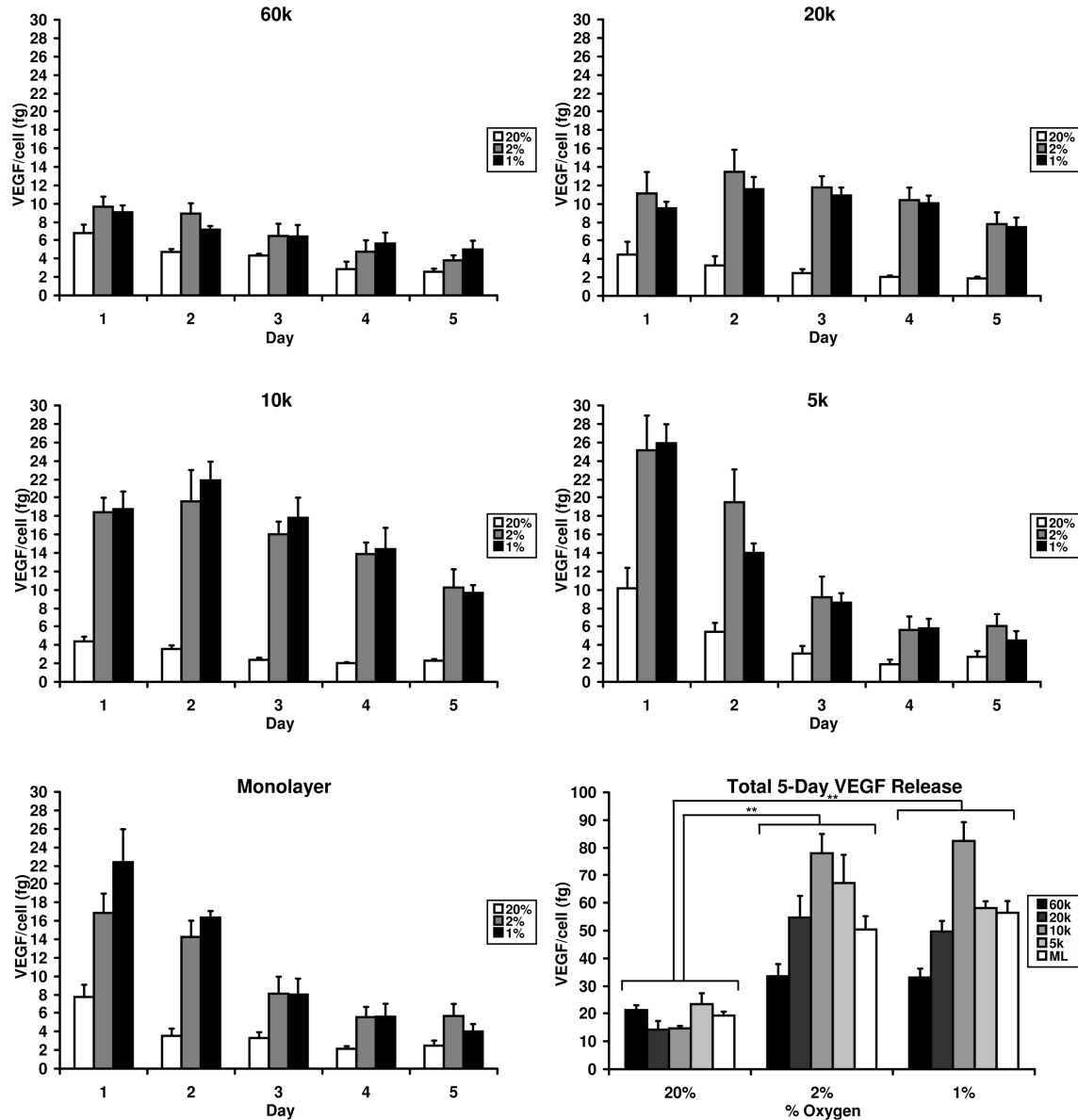


Figure 4.5 Levels of daily and total per-cell VEGF release from ADSC monolayers and 5k, 10k, 20k, and 60k spheroids incubated for 5 days in 20%, 2%, or 1% O<sub>2</sub>.

**VEGF (fg)**

%O <sub>2</sub>	Size	Day					Total
		1	2	3	4	5	
20%	ML	7.8 ± 1.3	3.5 ± 0.8	3.3 ± 0.6	1.9 ± 0.3	2.3 ± 0.5	18.8 ± 1.4
2%		16.8 ± 2.1	14.2 ± 1.7	8.1 ± 1.8	5.1 ± 1.0	5.2 ± 1.2	49.5 ± 4.6
1%		22.1 ± 3.5	16.4 ± 0.7	8.0 ± 1.7	5.1 ± 1.3	3.2 ± 0.6	54.8 ± 4.1
20%	5k	10.2 ± 2.2	5.4 ± 1.0	3.1 ± 0.8	1.9 ± 0.5	2.7 ± 0.6	23.2 ± 4.3
2%		25.2 ± 3.7	19.5 ± 3.6	9.2 ± 2.2	5.6 ± 1.4	6.0 ± 1.4	63.9 ± 7.7
1%		25.9 ± 2.0	14.0 ± 1.0	8.6 ± 1.0	5.8 ± 1.0	4.5 ± 1.0	58.9 ± 1.6
20%	10k	4.4 ± 0.5	3.5 ± 0.4	2.4 ± 0.2	2.0 ± 0.1	2.3 ± 0.2	14.6 ± 0.9
2%		18.4 ± 1.6	19.6 ± 3.5	16.0 ± 1.4	13.9 ± 1.2	10.3 ± 2.0	78.1 ± 6.9
1%		18.7 ± 1.9	21.9 ± 2.0	17.8 ± 2.2	14.4 ± 2.3	9.7 ± 0.8	82.5 ± 6.8
20%	20k	4.5 ± 1.4	3.3 ± 1.0	2.5 ± 0.4	2.0 ± 0.1	1.9 ± 0.2	14.1 ± 3.1
2%		11.1 ± 2.3	13.5 ± 2.4	11.8 ± 1.2	10.4 ± 1.4	7.8 ± 1.3	54.7 ± 7.8
1%		9.5 ± 0.7	11.6 ± 1.3	10.9 ± 0.8	10.1 ± 0.8	7.5 ± 1.0	49.7 ± 3.8
20%	60k	6.7 ± 1.0	4.7 ± 0.3	4.3 ± 0.2	2.8 ± 0.8	2.5 ± 0.3	20.6 ± 1.2
2%		9.7 ± 1.1	8.9 ± 1.1	6.4 ± 1.4	4.7 ± 1.2	3.8 ± 0.5	34.0 ± 4.8
1%		9.1 ± 0.7	7.1 ± 0.5	6.4 ± 1.3	5.6 ± 1.2	5.0 ± 0.9	33.9 ± 2.9

Table 4.1 Mean values and standard deviation of VEGF release from ADSC cultures. Statistical significance of differences between groups is indicated in Table 4.2.

Released VEGF values represent total release over the 24 hours prior to the stated time point. For each culture size, cells secreted significantly more VEGF when cultured in 2% or 1% O<sub>2</sub> than in 20% O<sub>2</sub>, while little significant difference was observed between 2% and 1% O<sub>2</sub>. In 2% and 1% O<sub>2</sub> culture, monolayers and 5k spheroids displayed significantly elevated VEGF secretion on Day 1 followed by a sharp decline through Day 5. Under the same conditions, 10k and 20k spheroids displayed a much more sustained elevation in VEGF secretion over 5 days, with peak secretion occurring on Day 2. 60k spheroids showed minor elevation of VEGF secretion on Day 1 which decreased over the remaining days. Total 5-day secretion was similar in 2% and 1% O<sub>2</sub> culture, which were both significantly higher than 20% O<sub>2</sub> culture. Total per-cell VEGF

release increased from monolayers to 5k spheroids and from 5k to 10k spheroids then decreased from 10k to 20k spheroids and from 20k to 60k spheroids. Statistical significance of differences in VEGF release between the different study groups can be found in Table 4.2.

**Statistical Significance**

vs.		5k				10k				20k				60k				vs.														
		Day																														
%O <sub>2</sub>	Size	1	2	3	4	5	1	2	3	4	5	1	2	3	4	5	1	2	3	4	5	%O <sub>2</sub>	1	2	3	4	5					
20% 2% 1%	ML	*	**				**		*			**		*			**	**	*			**	**	*			20% v. 2%	**	**	**	**	**
		**	*					*	**	**	**	**		**	**	**	**	**	**	**	**	*					20% v. 1%	**	**	**	**	*
			**			*	**	**	**	**	**	**	**	**	**	**	**	**	**	**	**	**	**			**	2% v. 1%	*	*			**
20% 2% 1%	5k						**	**				**	**			*	**	*	*	*	*	**	*	*	*	*	20% v. 2%	**	**	**	**	**
							**		*	*	*	**	**		*	*	**	**	*	*	*	*				**	20% v. 1%	**	**	**	**	**
							**	**	**	**	**	**	*	**	**	**	**	**	*	*	*	*	*			*	2% v. 1%		*			
20% 2% 1%	10k															**	**	**	**	**	*	**	**	**	**	**	20% v. 2%	**	**	**	**	**
												**	**	**	**	*	**	**	**	**	**	**	**	**	**	**	20% v. 1%	**	**	**	**	**
												**	**	**	**	**	**	**	**	**	**	**	**	**	**	**	2% v. 1%					
20% 2% 1%	20k																**	*	**		**	**	*	**		**	20% v. 2%	**	**	**	**	**
																	**	**	**	**	**	**	**	**	**	**	20% v. 1%	**	**	**	**	**
																	**	**	*	*	**	**	**	*	*	**	2% v. 1%					
20% 2% 1%	60k																					**	**	*	*	**	20% v. 2%	**	**	*	*	**
																						**	**	*	**	**	20% v. 1%	**	**	*	**	**
																						**	**			*	2% v. 1%		**			*

\*\* = p ≤ 0.01  
\* = p ≤ 0.05

Total	20%					2%					1%					vs.					
	60	20	10	5	k	60	20	10	5	k	60	20	10	5	k	%O <sub>2</sub>	60	20	10	5	ML
ML	*	*	**	*		**		**	*		**		**			20% v. 2%	**	**	**	**	**
5		**	**			**		*			**	*	**			20% v. 1%	**	**	**	**	**
10	**					**	**				**	**				2% v. 1%					
20	**					**					**										
k																					

Table 4.2 Table indicating statistical significance of differences in mean VEGF release from the cultures under study. “\*\*” indicates statistical significance at p ≤ 0.01. “\*” indicates statistical significance at p ≤ 0.05.

#### 5.4.4 Impact of Hypoxia on Morphology and Viability

The morphology of stained spheroid sections is shown in Figure 4.6a-h. On Day 1, all spheroids appeared cellular and cohesive throughout (a-c). After 5 days of culture in 20% O<sub>2</sub>, little morphological change was observed in most spheroids, though 60k spheroids did display a small central region of cells exhibiting cytoplasmic swelling (h). In 2% O<sub>2</sub>, the region with cytoplasmic swelling in 60k spheroids was much larger and some cellular discontinuity was observed (g). In 1% O<sub>2</sub>, the 60k spheroids exhibited noticeable central tissue loss and a discontinuous core. Cells that did inhabit the central region all expressed cytoplasmic swelling (f). The 10k and 20k spheroids cultured in 2% and 1% O<sub>2</sub> for 5 days exhibited only minor morphological changes in some central cells but little or no loss of tissue. These spheroids cultured in 1% O<sub>2</sub> are shown in Figures 4d and 4e.

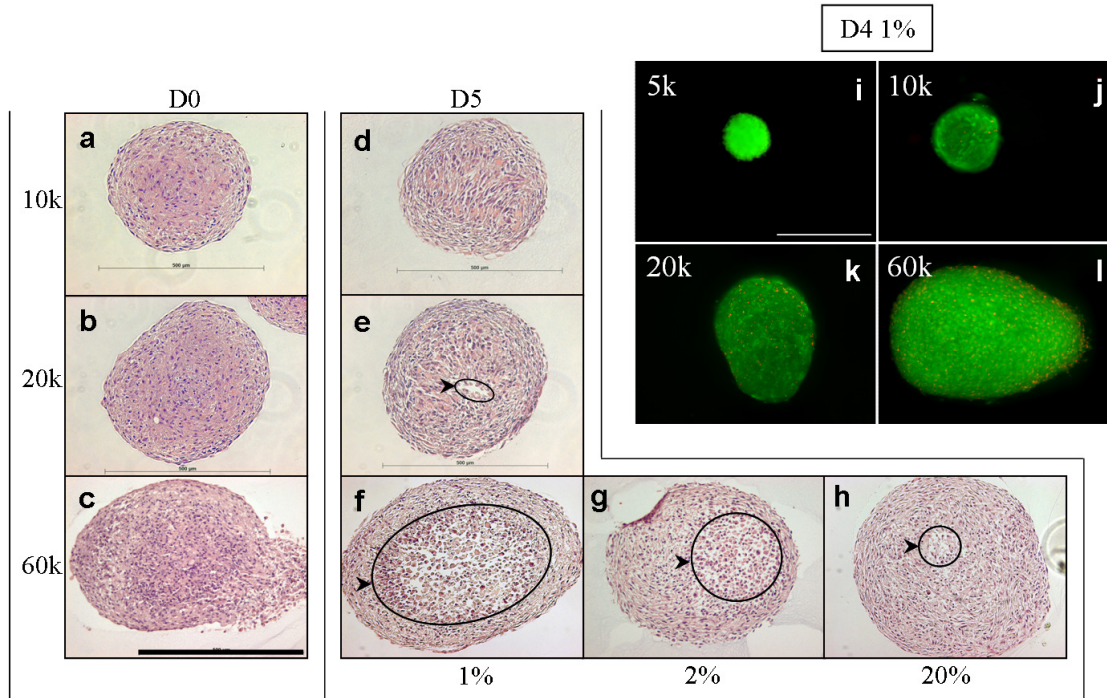


Figure 4.6 a-h) H&E staining of ADSC spheroid sections. Immediately following formation, spheroids showed high cellularity and cohesion (a-c). Cytoplasmic swelling and loss of cellular cohesion (circled regions) of central cells increased significantly with decreasing culture oxygenation in 60k spheroids (f-h). 10k and 20k spheroids incubated in 1%  $O_2$  for 5 days showed little morphological change, though cellular discontinuity was seen in a small central region of some 20k spheroids (d & e). Inset: i-l) Live/Dead viability assessment of ADSCs in 5k (i), 10k (j), 20k (k), and 60k (l) spheroids cultured at 1%  $O_2$  for 4 days. Green fluorescence indicates a viable cell while red, nuclear fluorescence indicates a non-viable cell. Bar = 500 $\mu$ m.

A LIVE/DEAD viability stain showed that on Day 1, no dead cells were observed in 5k, 10k, and 20k spheroids and only a small number were observed in 60k spheroids. As seen in Figure 4i-l, on Day 4 no dead cells were observed in 5k spheroids and only a small number of dead cells were observed in 10k spheroids. 20k and 60k spheroids displayed relatively more non-viable cells, though these still appeared to represent a small percentage of overall cells. All dead cells were located in peripheral regions of the spheroids.

## 4.5 Discussion

In this work, we examined the degree of HIF activity in ADSCs cultured as spheroids of different sizes in atmospheric and reduced-oxygen conditions. We found that HIF activity increased in spheroids in a size-dependent manner and with decreasing culture oxygenation. As a well-defined HIF target, we expected VEGF to be secreted at levels that increased correspondingly with HIF activity. VEGF release profiles could be altered by changing the spheroid size, with 10k spheroids cultured in 2% or 1% O<sub>2</sub> secreting most efficiently. That spheroids larger than 10k secreted VEGF less efficiently despite having greater HIF activity may be due in part to loss of cell viability as hypoxic severity increases, as is supported by the histology. Our results indicate that culture geometry can be used as a means to control cell function and stress the need to carefully consider tissue size and expected oxygen concentration at the implant site when engineering a therapeutic graft in order to maximize the benefits of HIF-activated pathways.

The majority of studies in 3D stem cell cultures are carried out in atmospheric oxygenation or under a single “hypoxic” oxygen level (often 1% or 5% O<sub>2</sub>) and examine only a single culture size. We suspected that differences in culture size and external oxygen concentration (even within the hypoxic range) would significantly impact culture oxygenation and in turn affect cellular function. To test this, we prepared ADSC spheroids in a range of sizes and cultured them in three different oxygen concentrations. Centrifugal pelleting resulted in rapid formation of cohesive and spherical cultures while providing a high degree of control over spheroid size. Additionally, a wide range of sizes

could be produced (including spheroids both larger and smaller than those reported in this study). Culture size was highly reproducible and only dependent on the number of cells in the initial suspension.

HIF activity was monitored within the spheroids over 5 days. As the master regulator of transcriptional responses to low oxygen conditions, HIF activation may be the most meaningful indicator of cellular hypoxia [48 Maxwell 1993]. Tracking HIF activity rather than oxygen concentration/distribution, as in other techniques [316 Revsbech 1983],[317 Krihak 1996],[318 Acosta 2007], provides evidence of a behavioral response. This is useful, as the oxygen concentration required to trigger a behavioral effect can vary between cells or even within the same cell under different microenvironmental conditions [126 Chi 2006],[319 Gibbs 2012]. With our HIF marker, image capture settings could be adjusted to match observed signal with quantified HIF-1 levels. Furthermore, it allowed for non-invasive identification and localization of hypoxia in cells within the 3D cultures and could follow HIF activity in the same sample over time without requiring its sacrifice. Hydrogel encapsulation facilitated consistency in repeated imaging of the same sample. While the hydrogel capsule can alter oxygen diffusion to some degree, the nature of qualitative trends observed between spheroids of different sizes were not affected. We saw that reduced oxygenation resulted in increased transcriptional activity of HIF-1 in spheroids and that increasing spheroid size amplified this effect. Quicker onset and increased intensity of fluorescent signaling was observed as culture size increased and external oxygen concentration decreased.

These results are in line with other studies: HIF-1 was shown to be exponentially stabilized in monolayer cultures as oxygen concentration decreased from 6 to 0.5% [105 Jiang 1996b], and higher protein levels of HIF-1 $\alpha$  were observed in ischemic mouse limb buds implanted with spheroid cultures rather than dispersed HUVECs [311 Bhang 2012b]. Similarly, small ADSC clusters (100-200 $\mu$ m) were shown to contain higher protein levels of HIF-1 $\alpha$  than monolayer ADSCs in both 20% and 1% O<sub>2</sub> [303 Bhang 2011]. Our studies provided evidence on transcriptional activity of HIF-1 and examined a range of larger spheroid sizes (350 - 800  $\mu$ m) that better represent the size of cultures commonly prepared in osteochondral tissue engineering.

Because of the potential for a capsule to impact diffusion, spheroids for VEGF secretion studies were not encapsulated. Our results indicated that VEGF release is impacted by both external oxygenation and spheroid size, with VEGF profiles differing as these two parameters were altered. In 1% and 2% O<sub>2</sub>, 10k spheroids appeared to provide optimal secretion. Compared to cultures incubated in 20% O<sub>2</sub>, 60k, 20k, 10k, and 5k spheroids and monolayers incubated in hypoxic conditions O<sub>2</sub> showed an approximate 1.5, 3.5, 5.5, 2.5, and 2.5-fold increase in VEGF production per cell, respectively. However, in our HIF tracking studies, 20k and 60k spheroids displayed greater HIF activity than 10k spheroids. We suspect that this is due to the severity of hypoxia occurring within these spheroids, especially in the spheroid core. Severe hypoxia is known to result in a rapid and dramatic reduction in protein turnover, inhibiting protein translation and transduction [28 Hochachka 1996],[320 Pettersen 1986],[321 Koumenis 2002]. Additionally, sudden, severe hypoxia can trigger apoptotic

pathways or even result in cellular necrosis [322 Greijer 2004],[323 Kiang 2006],[324 Burton 2009]. Results from our nuclear dye exclusion assay indicated few non-viable cells, even in 60k spheroids cultured at 1% O<sub>2</sub>. However, histological examination revealed significant acellularity and evidence of necrosis in these spheroids. This interior cell death indicates severe central hypoxia and offers an explanation for the lower than anticipated VEGF secretion from 60k and 20k spheroids.

Taken together, our data suggests that the profile of VEGF release from a 3D ADSC spheroid is the result of a balance between two opposing effects of hypoxia: 1) Decreased oxygen tension resulting from cellular oxygen utilization and diffusional limitations stabilizes HIF-1 and induces upregulation of VEGF. 2) Excessive hypoxic tension, such as increasingly occurs in the interior of spheroids as size is increased, can lead to global protein down-regulation and cell death. ADSCs have demonstrated pro-angiogenic potential and may represent a preferential source for cell-based delivery in tissue engineering and regenerative medicine. Furthermore, the benefits of 3D culture are recognized. Considering culture geometry and expected environmental oxygen concentration allow for optimization of angiogenic function of 3D ADSC cultures and will be essential to balancing the beneficial and detrimental effects of hypoxia to achieve their successful utilization in tissue engineering and regenerative medicine.

#### Acknowledgements

The authors would like to thank Dr. Melissa Moss and the Instrument Resource Facility and the University of South Carolina School of Medicine for the generous use of equipment and assistance with histology. The authors would also like to acknowledge

support for this work provided by a grant from the National Institutes of Health (RO3AR062816).

## Chapter 5

### Conclusion

Although oxygen tension is a potent signaling stimulus in cells, it often remains unconsidered in experiments carried out under standard culture conditions. However, to drive restorative function of transplant tissues *in vivo*, proper *in vitro* application of physiological cues that contribute to regulating cell behavior will be needed. In particular, physiological oxygen concentrations are well below the atmospheric concentration, in a range that is often viewed as hypoxic in relation to standard culture practices. Within this range, HIFs govern cellular responses to local reductions in oxygen concentration. These responses can result in down-regulation of typical cell functions and programmed cell death, or alternatively, stimulation of adaptive behaviors involved in beneficial processes such as growth, differentiation, and repair. However, surprisingly few cell transplantation and tissue engineering efforts consider the role of HIF activity in tissue function, even though the intended therapeutic site is a physiological environment within the body. Due to its ability to regulate cell behavior, cell therapies may benefit from a view that treats oxygen as similar to other paracrine factors: a biomolecule that must be presented to cells at the proper concentration in order to illicit the intended response. However, because specific responses to a particular oxygen concentration can be cell-type and context dependent,

HIF activity may represent a more reliable indicator of microenvironmental oxygen conditions that affect cell behavior. In the present work, a fluorescent reporter system was used to identify HIF activity in cells and demonstrate how an understanding of HIF activity can be used to instruct decisions that affect the therapeutic potential of different cell transplantation strategies.

HIF activity was characterized in encapsulated, 3D  $\beta$ -cell clusters and in 3D ADSC spheroids. Transplantation of encapsulated  $\beta$ -cells is a regenerative medicine therapy aimed at restoring normoglycemia in patients with T1DM through secretion of insulin from the transplanted tissue which is protected from immune destruction by the encapsulating material. To maintain important cell-to-cell contacts which contribute to  $\beta$ -cell survival and secretory function,  $\beta$ -cells are often transplanted as native, 3D islets or as reaggregated islet-like clusters. Lack of vascularization, low oxygenation at the implant site, and oxygen gradients resulting from the 3D nature of the tissues and the protective capsule have all been suggested to contribute to hypoxia-induced loss of function in such therapies. ADSCs have been applied in regenerative medicine therapies to help restore ischemic tissue injuries. ADSCs have potent angiogenic properties that are upregulated under hypoxic conditions. 3D, spheroid culture of ADSCs may modulate their hypoxic status and contribute to their survival through cell-cell interaction. Inclusion of ADSC spheroids in *in vitro* engineered tissues or *in vivo* regenerating tissues may contribute to the formation of a pro-angiogenic niche within the tissue which could help drive rapid vascularization and assist tissue integration and survival. Both of these therapies offer the promise of improved outcomes in patient. Each also demonstrates a

role for hypoxia in the success of the therapy. In  $\beta$ -cell encapsulation and transplantation, cellular hypoxia should be avoided in order to prevent HIF-regulated loss of insulin secretion, while when using ADSCs to drive angiogenesis, promotion of hypoxia can contribute to upregulation of HIF-regulated, pro-angiogenic behaviors. The ability to identify HIF activity within cells in each of these systems can guide culturing and engineering decisions in order to optimize their therapeutic potential.

The use of a fluorescent reporter system to identify HIF activity in  $\beta$ -cells or ADSCs has not been reported previously. The present studies indicate that the reporter is a viable and useful tool for determining the hypoxic status of cells used in regenerative therapies.  $\beta$ -cells and ADSCs cultured in 1% and 2%  $O_2$ , conditions under which HIF should be stable, exhibited fluorescent signaling indicating HIF transcriptional activity. Cells cultured as monolayers in 20%  $O_2$ , conditions under which HIF should not be stable, did not exhibit fluorescence. Compared with other methods commonly used to identify HIF, such as Western blotting and immunostaining, the reporter technique was favorable because it allowed for repeated observation of HIF activity over time. Additionally, the fluorescent signal could be observed through PEGDM matrices, meaning that encapsulated cells did not need to be removed from the capsule in order for HIF activity to be examined.

HIF activity, indicated by the reporter, correlated well to differences in behavior between signaling and non-signaling tissues. HIF activity in  $\beta$ -cell clusters corresponded to much lower GSIS than in clusters that did not display HIF activity. Recently-aggregated  $\beta$ -cell clusters that displayed fluorescent signaling also failed to achieve a

cohesive, islet-like morphology over time, while non-signaling clusters gradually became smooth and round, much like native islets. Surprisingly, HIF activity did not appear to correspond to a substantial drop in viability in  $\beta$ -cell clusters over 2 weeks. In ADSC spheroids, increased HIF activity corresponded to an increase in VEGF secretion, although spheroid size also appeared to indirectly effect VEGF secretion by affecting regional cell survival. Intense fluorescent signaling corresponded to the appearance of pre-apoptotic or necrotic morphologies in large spheroids.

Using the HIF reporter system in 3D tissue cultures also provided information about how tissue size affects the formation of oxygen gradients within the tissue, and allowed for regional identification of heterogeneous HIF activity.  $\beta$ -cell clusters incubated in 20%  $O_2$  that were smaller than 250-300 $\mu$ m did not display fluorescent signaling. However, larger clusters displayed HIF activity in their central region in 20%  $O_2$ , which increased in size as cluster size increased to maintain a signal-free peripheral region of consistent thickness. Likewise, onset of fluorescent signaling in ADSC spheroids occurred in central regions.

Finally, results from the present studies offer instructive suggestions about the design decisions for  $\beta$ -cell and ADSC transplantation therapies. In  $\beta$ -cells, large clusters displayed central regional HIF activity. Thus, it may be beneficial to utilize clusters that are smaller than 250 $\mu$ m in order to avoid hypoxia-induced loss of function. Additionally, 1%  $O_2$  culture induced strong HIF activity and reduced GSIS which was not remediated by an increase in oxygen concentration within the hypoxic range to 2%  $O_2$ . Therefore strategies to ensure implant-site oxygenation of >2% could be beneficial to the success

of  $\beta$ -cell therapies. Finally, incubation in low oxygen conditions did not allow for normal morphological arrangement of recently-aggregated  $\beta$ -cell clusters. This suggests that reaggregation and hypoxic preconditioning techniques should not be employed simultaneously in  $\beta$ -cells. In ADSC, external oxygen concentration and culture size were both shown to contribute to pervasiveness of HIF activity in spheroids. Increasing spheroid size and decreasing external oxygenation could both be used to augment HIF activity. Moderate elevation of HIF activity was shown to correlate to an increase in VEGF secretion per cell, however, very high levels of HIF activity correlated to increased cell death which reduced secretion efficiency. This suggests that for a desired application, optimal cell function can be driven by careful selection of culture parameters to effect hypoxic status. In the study, 400 $\mu$ m spheroids were shown to produce VEGF most efficiently. This is the first report to show that tissue size can be used to optimize cell-based delivery of angiogenic factors from ADSCs. Overall, then, the studies reported in this work point to the important ways in which oxygen tension can affect cell behavior in cell transplantation therapies and highlights the usefulness of the fluorescent HIF reporter system. Conclusions from these studies, and others which may utilize HIF tracking, should be instructive in guiding the use of appropriate physiological stimuli in tissue engineering and regenerative therapies to drive optimal restorative function.

## References

- 1) Duursma E.K., Boisson M.P.R.M. Global oceanic and atmospheric oxygen stability considered in relation to the carbon cycle and to different time scales. *Oceanologica Acta* 1994, 17(2);117-141.
- 2) Castresana J., Saraste M. Evolution of energetic metabolism – the respiration-early hypothesis. *Trends Biochem Sci* 1995, 20(11);443-448.
- 3) Dismukes G.C., Klimov V.V., Baranov S.V., Kozlov Yu.N., DasGupta J., Tyryshkin A. The origin of atmospheric oxygen on Earth: The innovation of oxygenic photosynthesis. *Proc Natl Acad Sci USA* 2001, 98(5);2170-2175.
- 4) Kump L.R. The rise of atmospheric oxygen. *Nature* 2008, 451(7176);277-278.
- 5) Stamati K., Mudera V, Cheema U. Evolution of oxygen utilization in multicellular organisms and implications for cell signaling in tissue. *J of Tissue Eng* 2011, 2(1);1-12.
- 6) Whitney E., Rolfes S. *Understanding Nutrition*, 10th ed, 2005;6. Thomson-Wadsworth.
- 7) Solaini G., Baracca A., Lenaz G., Sgarbi G. Hypoxia and mitochondrial oxidative metabolism. *Biochim Biophys Acta* 2010, 1797(6-7);1171-1177.
- 8) Brunori M., Antonini G., Malatesta F., Sarti P., Wilson M.T. Cytochrome-c oxidase. *Eur J Biochem* 1987, 169;1-8.
- 9) Bergamini C.M., Gambetti S., Dondi A., Cervellati C. Oxygen, reactive oxygen species and tissue damage. *Curr Pharm Des* 2004, 10(14);1611-1626.
- 10) Raymond J., Sergrè D. The effect of oxygen on biochemical networks and the evolution of complex life. *Science* 2006, 311(5768);1764-1767.
- 11) Summons R.E., Bradley A.S., Jahnke L.L., Waldbauer J.R. Steroids, triterpenoids and molecular oxygen. *Philos Trans R Soc Lond B Biol Sci* 2006, 361(1470);951-968.

- 12) Jiang Y.Y., Kong D.X., Qin T., Zhang H.Y. How does oxygen rise drive evolution? Clues from oxygen-dependent biosynthesis of nuclear receptor ligands. *Biochem Biophys Res Commun* 2010, 391(2);1158-1160.
- 13) Thannickal V.J. Oxygen in the evolution of complex life and the price we pay. *Am J Respir Cell Mol Biol* 2009, 40(5);507-510.
- 14) Andreyev A.Y., Kushnareva Y.E., Starkov A.A. Mitochondrial metabolism of reactive oxygen species. *Biochemistry (Moscow)* 2005, 70(2);200-214.
- 15) Gibson J.S., Milner P.I., White R., Fairfax T.P., Wilkins R.J. Oxygen and reactive oxygen species in articular cartilage: modulators of ionic homeostasis. *Pflügers Arch* 2008, 455(4);563-573.
- 16) Chance B., Williams B.R. Respiratory enzymes in oxidative phosphorylation. *J Biol Chem* 1955, 217(1);383-451.
- 17) Priestley J. Observations on different kinds of air. *Philosophical Transactions* 1772, 62;147.
- 18) Lavoisier, A. *Traité Élémentaire de Chimie. Présenté dans un Ordre Nouveau et d'après Découvertes Modernes*. Paris: Cuchet, 1789.
- 19) Hochscheid S., Bentivegna F., Hays G.C. First records of dive durations for a hibernating sea turtle. *Biol Lett* 2005, 1(1);82-86.
- 20) Watkins W.A., Daher M.A., DiMarzio N.A. Sperm whale dives tracked by radio tag telemetry. *Marine Mammal Sci* 2002, 18(1);55-68.
- 21) Irving L. Respiration in diving mammals. *Physiol Rev* 1939, 19(1);112-134.
- 22) Leach R.M., Treacher D.F. Oxygen transport – 2. Tissue hypoxia. *BMJ* 1998, 317(7169);1370-1373.
- 23) Carreau A., El Hafny-Rahbi B., Matejuk A., Grillon C., Kieda C. Why is the partial oxygen pressure of human tissue a crucial parameter? Small molecules and hypoxia. *J Cell Mol Med* 2011, 15(6);1239-1253.
- 24) Fermor B., Christensen S.E., Youn I., Cernanec J.M., Davies C.M., Weinberg J.B. Oxygen, nitric oxide, and articular cartilage. *Eur Cell Mater* 2007, 13;5-65.
- 25) Ivanovic Z. Hypoxia or in situ normoxia: The stem cell paradigm. *J Cell Physiol* 2009, 219(2);271-275.

- 26) Simon M.C., Keith B. The role of oxygen availability in embryonic development and stem cell function. *Nat Rev Cell Biol* 2008, 9(4);285-296.
- 27) Semenza G.L. Hypoxia-inducible factors in physiology and medicine. *Cell* 2012a, 148(3);399-408.
- 28) Hochachka P.W., Buck L.T., Doll C.J., Land S.C. Unifying theory of hypoxia tolerance: Molecular/metabolic defense and rescue mechanisms for surviving oxygen lack. *Proc Natl Acad Sci USA* 1996, 93;9493-9498.
- 29) Shimizu S., Eguchi Y., Kamiike W., Itoh Y., Hasegawa J., Yamabe K., Otsuki Y., Matsuda H., Tsujimoto Y. Induction of apoptosis as well as necrosis by hypoxia and predominant prevention of apoptosis by bcl-2 and bcl-x<sub>L</sub>. *Cancer Res* 1996, 56(9);2161-2166.
- 30) Zhang H., Bosch-Marce M., Shimoda L.A., Tan Y.S., Baek J.H., Wesley J.B., Gonzalez F.J., Semenza G.L. Mitochondrial autophagy is an HIF-1-dependent adaptive metabolic response to hypoxia. *J Biol Chem* 2008, 283(16);10892-10903.
- 31) Azad M.B., Chen Y., Henson E.S., Cizeau J., McMillan-Ward E., Israels S.J., Gibson S.B. Hypoxia induces autophagic cell death in apoptosis-competent cells through a mechanism involving BNIP3. *Autophagy* 2008, 4(2);195-204.
- 32) Kumar V., Abbas A.K., Fausto N., Aster J.C., Perkins J.A. Robbins and Cotran pathologic basis of disease, 8<sup>th</sup> ed. Saunders Elsevier 2010, Philadelphia, PA, USA.
- 33) Wilson D.F., Ercińska M., Drown C., Silver I.A. The oxygen dependence of cellular energy metabolism. *Arch Biochem Biophys* 1979, 195(2);485-493.
- 34) Ercińska M., Wilson D.F. Regulation of cellular energy metabolism. *J Membr Biol* 1982, 70(1);1-14.
- 35) Rumsey W.L., Schlosser C., Nuutinen E.M., Robiolio M., Wilson D.F. Cellular energetics and the oxygen dependence of respiration in cardiac myocytes isolated from adult rat. *J Biol Chem* 1990, 265(26);15392-15402.
- 36) Schumaker P.T., Chandel N., Agusti A.G. Oxygen conformance of cellular respiration in hepatocytes. *Am J Physiol* 1993, 265(4);L395-L402.
- 37) Budinger G.R., Chandel N., Shao Z.H., Li C.Q., Melmed A., Becker L.B., Schumacker P.T. Cellular energy utilization and supply during hypoxia in embryonic cardiac myocytes. *Am J Physiol* 1996, 270(1);L44-L53.

- 38) Chandel N.S., Budinger G.R., Choe S.H., Schumacker P.T. Cellular respiration during hypoxia. Role of cytochrome oxidase as the oxygen sensor in hepatocytes. *J Biol Chem* 1997, 272(30);18808-18816.
- 39) Budinger G.R., Duranteau J., Chandel N.S., Schumacker P.T. Hibernation during hypoxia in cardiomyocytes. Role of mitochondria as the O<sub>2</sub> sensor. *J Biol Chem* 1998, 273(6);3320-3326.
- 40) Brown G.C., Hafner R.P., Brand M.D. A 'top-down' approach to the determination of control coefficients in metabolic control theory. *Eur J Biochem* 1990a, 188(2);321-325.
- 41) Brown G.C., Lakin-Thomas P.L., Brand M.D. Control of respiration and oxidative phosphorylation in isolated rat liver cells. *Eur J Biochem* 1990b, 192(2);355-362.
- 42) Eguchi Y., Shimizu S., Tsujimoto Y. Intracellular ATP levels determine cell death fate by apoptosis or necrosis. *Cancer Res* 1997, 57(10);1835-1840.
- 43) López-Barneo J., López-López J.R., Ureña J., González C. Chemotransduction in the carotid body: K<sup>+</sup> current modulated by pO<sub>2</sub> in type I chemoreceptor cells. *Science* 1988, 241(4865);580-582.
- 44) Bondurant M.C., Koury M.J. Anemia induces accumulation of erythropoietin mRNA in the kidney and liver. *Molec Cell Biol* 1986, 6(7);2731-2733.
- 45) Schuster S.J., Badiavas E.V., Costa-Giomi P., Weinmann R., Erslev A.J., Caro J. Stimulation of erythropoietin gene transcription during hypoxia and cobalt exposure. *Blood* 1989, 73(1);13-16.
- 46) Semenza G.L., Wang G.L. A nuclear factor induced by hypoxia via de novo protein synthesis binds to the human erythropoietin gene enhancer at a site required for transcriptional activation. *Mol Cell Biol* 1992, 12(12);5447-5454.
- 47) Semenza G.L., Nejfelt M.N., Chi S.M., Antonarakis S.E. Hypoxia-inducible nuclear factors bind to an enhancer element located 3' to the human erythropoietin gene. *Proc Natl Acad Sci USA* 1991, 88(13);5680-5684.
- 48) Maxwell P.H., Pugh C.W., Ratcliffe P.J. Inducible operation of the erythropoietin 3' enhancer in multiple cell lines: Evidence for a widespread oxygen-sensing mechanism. *Proc Natl Acad Sci USA* 1993, 90(6);2423-2427.
- 49) Wang G.L., Semenza G.L. General involvement of hypoxia-inducible factor 1 in transcriptional response to hypoxia. *Proc Natl Acad Sci USA* 1993a, 90(9);4304-4308.

- 50) Wiener C.M., Booth G., Semenza G.L. *In vivo* expression of mRNAs encoding hypoxia-inducible factor 1. *Biochem Biophys Res Comm* 1996, 225(2);485-488.
- 51) Rytönen K.T., Williams T.A., Renshaw G.M., Primmer C.R., Nikinmaa M. Molecular evolution of the metazoan PHD-HIF oxygen-sensing system. *Mol Biol Evol* 2011, 28(6);1913-1926.
- 52) Wang G.L., Jiang B.H., Rue E.A., Semenza G.L. Hypoxia-inducible factor 1 is a basic-helix-loop-helix-PAS heterodimer regulated by cellular O<sub>2</sub> tension. *Proc Natl Acad Sci USA* 1995, 92(12);5510-5514.
- 53) Kewley R.J., Whitelaw M.L., Chapman-Smith A. The mammalian basic helix-loop-helix/PAS family of transcriptional regulators. *Int J Biochem Cell Biol* 2004, 36(2);189-204.
- 54) Semenza G.L., Jiang B.H., Leung S.W., Passantino R., Concordet J.P., Maire P., Giallongo A. Hypoxia response elements in the aldolase A, enolase 1, and lactate dehydrogenase A gene promoters contain essential binding sites for hypoxia-inducible factor 1. *J Biol Chem* 1996, 271(51); 32529–37.
- 55) Taylor B.L., Zhulin I.B. PAS domains: internal sensors of oxygen, redox potential, and light. *Microbiol Mol Biol Rev* 1999, 63(2);479-506.
- 56) Murre C., McCaw P.S., Vaessin H., Caudy M., Jan L.Y., Jan Y.N., Cabrera C.V., Buskin J.N., Hauschka S.D., Lassar A.B., Weintraub H., Baltimore D. Interactions between heterologous helix-loop-helix proteins generate complexes that bind specifically to a common DNA sequence. *Cell* 1989, 58(3);537-544.
- 57) Reisz-Porszasz S., Probst M.R., Fukunaga B.N., Hankinson O. Identification of functional domains of the aryl hydrocarbon receptor nuclear translocator protein (ARNT). *Mol Cell Biol* 1994, 14(9);6075-86.
- 58) Ema M., Morita M., Ikawa S., Tanaka M., Matsuda Y., Gotoh O., Saijoh Y., Fujii H., Hamada H., Kikuchi Y., Fujii-Kuriyama Y. Two new members of the murine Sim gene family are transcriptional repressors and show different expression patterns during mouse embryogenesis. *Mol Cell Biol* 1996, 16(10);5865-5875.
- 59) Jiang B.H., Rue E., Wang G.L., Roe R., Semenza G.L. Dimerization, DNA binding, and transactivation properties of hypoxia-inducible factor 1. *J Biol Chem* 1996a, 271(30);17771-17778.
- 60) Kobayashi A., Numayama-Tsuruta K., Sogawa K., Fujii-Kuriyama Y. CBP/p300 functions as a possible transcriptional coactivator of Ah receptor nuclear translocator (Arnt). *J Biochem* 1997, 122(4);703-710.

- 61) Ferré-D'Amaré A.R., Prendergast G.C., Ziff E.B., Burley S.K. Recognition by Max of its cognate DNA through a dimeric b/HLH/Z domain. *Nature* 1993, 363(6424);38-45.
- 62) Pongratz I., Antonsson C., Whitelaw M.L., Poellinger L. Role of the PAS domain in regulation of dimerization and DNA binding specificity of the dioxin receptor. *Molec Cell Biol* 1998, 18(7);4079-4088.
- 63) Crews S.T. Control of cell lineage-specific development and transcription by bHLH-PAS proteins. *Genes Dev* 1998, 12(5);607-620.
- 64) Jiang B.H., Zheng J.Z., Leung S.W., Roe R., Semenza G.L. Transactivation and inhibitory domains of hypoxia-inducible factor 1 alpha. Modulation of transcriptional activity by oxygen tension. *J Biol Chem* 1997, 272(31);19253-19260.
- 65) Huang L.E., Schau M., Bunn H.F. Regulation of hypoxia inducible factor 1alpha is mediated by an O<sub>2</sub>-dependent degradation domain via the ubiquitin-proteasome pathway. *Proc Natl Acad Sci USA* 1998, 95(14);7987-7992.
- 66) Ema M., Hirota K., Mimura J., Abe H., Yodoi J., Sogawa K., Poellinger L., Fujii-Kuriyama Y. Molecular mechanisms of transcription activation by HLF and HIF1alpha in response to hypoxia: their stabilization and redox signal-induced interaction with CBP/p300. *EMBO J* 1999, 18(7);1905-1914.
- 67) O'Rourke J.F., Tian Y.M., Ratcliffe P.J., Pugh C.W. Oxygen-regulated and transactivating domains in endothelial PAS protein 1: comparison with hypoxia-inducible factor -1 alpha. *J Biol Chem* 1999, 274(4);2060-2071.
- 68) Maynard M.A., Oi H., Chung J., Lee E.H., Kondo Y., Hara S., Conaway R.C., Conaway J.W., Ohh M. Multiple splice variants of the human HIF-3 alpha locus are targets of the con Hippel-Lindau E3 ubiquitin ligase complex. *J Biol Chem* 2003, 278(13);11032-11040.
- 69) Makino Y., Kanopka A., Wilson W.J., Tanaka H., Poellinger L. Inhibitory PAS domain protein (IPAS) is a hypoxia-inducible splicing variant of the hypoxia-inducible factor-3alpha locus. *J Biol Chem* 2002, 277(36);32405-32408.
- 70) Chilov D., Camenisch G., Kvietikova I., Ziegler U., Gassmann M., Wenger R.H. Induction and nuclear translocation of hypoxia-inducible factor-1 (HIF-1): heterodimerization with ARNT is not necessary for nuclear accumulation of HIF-1alpha. *J Cell Sci* 1999, 112(8);1203-1212.

- 71) Brière J.J., Favier J., Bénit P., El Chouzzi V., Lorenzato A., Rabier D., Di Renzo M.F., Gimenez-Rogueplo A.P., Rustin P. Mitochondrial succinate is instrumental for HIF1 $\alpha$  nuclear translocation in SDHA-mutant fibroblasts under normoxic conditions. *Hum Mol Genet* 2005, 14(21);3263-3269.
- 72) Arany Z., Huang L.E., Eckner R., Bhattacharya S., Jiang C., Goldberg M.A., Bunn H.F., Livingston D.M. An essential role for p300/CBP in the cellular response to hypoxia. *Proc Natl Acad Sci USA* 1996, 93(23);12969-12973.
- 73) Brunelle J.K., Bell E.L., Quesada N.M., Vercauteren K., Tiranti V., Zeviani M., Scarpulla R.C., Chandel N.S. Oxygen sensing requires mitochondrial ROS but not oxidative phosphorylation. *Cell Metab* 2005, 1(6);409-414.
- 74) Epstein A.C.R., Gleadle J.M., McNeill L.A., Hewitson K.S., O'Rourke J., Mole D.R., Mukherji M., Metzen E., Wilson M.I., Dhanda A., Tian Y.M., Masson N., Hamilton D.L., Jaakkola P., Barstead R., Hodgkin J., Maxwell P.H., Pugh C.W., Schofield C.J., Ratcliffe P.J. *C. elegans* EGL-9 and mammalian homologs define a family of dioxygenases that regulate HIF by prolyl hydroxylation. *Cell* 2001, 107(1);43-54.
- 75) Bruick R.K., McKnight S.L. A conserved family of prolyl-4-hydroxylases that modify HIF. *Science* 2001, 294(5545);1337-1340.
- 76) Berra E., Benizri E., Ginouvès A., Volmat V., Roux D., Pouyssegur J. HIF prolyl-hydroxylase 2 is the key oxygen sensor setting low steady-state levels of HIF-1 $\alpha$  in normoxia. *EMBO J* 2003, 22(16);4082-4090.
- 77) Huang L.E., Arany Z., Livingston D.M., Bunn H.F. Activation of hypoxia-inducible transcription factor depends primarily upon redox-sensitive stabilization of its  $\alpha$  subunit. *J Biol Chem* 1996, 271(50);32253-32259.
- 78) Ratcliffe P.J., O'Rourke J.F., Maxwell P.H., Pugh C.W. Oxygen sensing, hypoxia-inducible factor-1 and the regulation of mammalian gene expression. *J Exp Biol* 1998, 201(8);1153-1162.
- 79) Ivan M., Kondo K., Yang H., Kim W., Valiando J., Ohh M., Salic A., Asara J.M., Lane W.S., Kaelin W.G. Jr. HIF $\alpha$  targeted for VHL-mediated destruction by proline hydroxylation: Implications for O<sub>2</sub> sensing. *Science* 2001, 292(5516);464-468.
- 80) Masson N., Willam C., Maxwell P.H., Pugh C.W., Ratcliffe P.J. Independent function of two destruction domains in hypoxia-inducible factor- $\alpha$  chains activated by prolyl hydroxylation. *EMBO J* 2001, 20(18);5197-5206.
- 81) Schofield C.J., Ratcliffe P.J. Oxygen sensing by HIF hydroxylases. *Nat Rev Mol Cell Biol* 2004, 5(5);343-354.

- 82) Baek J.H., Mahon P.C., Oh J., Kelly B., Krishnamachary B., Pearson M., Chan D.A., Giaccia A.J., Semenza G.L. OS-9 interacts with hypoxia-inducible factor 1 $\alpha$  and prolyl hydroxylase to promote oxygen-dependent degradation of HIF-1 $\alpha$ . *Mol Cell* 2005, 17(4);503-512.
- 83) Maxwell P.H., Wiesener M.S., Chang G.W., Clifford S.C., Vaux E.C., Cockman M.E., Wykoff C.C., Pugh C.W., Maher E.R., Ratcliffe P.J. The tumour suppressor protein VHL targets hypoxia-inducible factors for oxygen dependent proteolysis. *Nature* 1999, 399(6733);271-275.
- 84) Ohh M., Park C.W., Ivan M., Hoffman M.A., Kim T.Y., Huang E., Pavletich N., Chau V., Kaelin W.G. Ubiquitination of hypoxia-inducible factor requires direct binding to the  $\beta$ -domain of the von Hippel-Lindau protein. *Nat Cell Biol* 2000, 2(7);423-427.
- 85) Baek J.H., Liu Y.V., McDonald K.R., Wesley J.B., Hubbi M.E., Byun H., Semenza G.L. Spermidine/spermine-N1-acetyltransferase 2 is an essential component of the ubiquitin ligase complex that regulates hypoxia-inducible factor 1. *J Biol Chem* 2007, 282(32);23572-23580.
- 86) Kallio P.J., Okamoto K., O'Brien S., Carrero P., Makino Y., Tanaka H., Poellinger L. Signal transduction in hypoxic cells: inducible nuclear translocation and recruitment of the CBP/p300 coactivator by the hypoxia-inducible factor-1 $\alpha$ . *EMBO J* 1998, 17(22);6573-6586.
- 87) Lando D., Peet D.J., Whelan D.A., Gorman J.J., Whitelaw M.L. Asparagine hydroxylation of the HIF transactivation domain: A hypoxia switch. *Science* 2002a, 295(5556);858-861.
- 88) Lando D., Peet D.J., Gorman J.J., Whelan D.A., Whitelaw M.L., Bruick R.K. FIH-1 is an asparaginyl hydroxylase enzyme that regulates the transcriptional activity of hypoxia-inducible factor. *Genes Dev* 2002b, 16(12);1466-1471.
- 89) Koivunen P., Hirsila M., Gunzler V., Kivirikko K.I., Myllyharju J. Catalytic properties of the asparaginyl hydroxylase (FIH) in the oxygen sensing pathway are distinct from those of its prolyl 4-hydroxylases. *J Biol Chem* 2004, 279(11);9899-9904.
- 90) Taguchi A., Yanagisawa K., Tanaka M., Cao K., Matsuyama Y., Goto H., Takahashi T. Identification of hypoxia-inducible factor-1  $\alpha$  as a novel target for miR-17-92 microRNA cluster. *Cancer Res* 2008, 68(14);5540-5545.
- 91) Bruning U., Cerone L., Neufeld Z., Fitzpatrick S.F., Cheong A., Scholz C.C., Simpson D.A., Leonard M.O., Tambuwala M.M., Cummins E.P., Taylor C.T. MicroRNA-155

- promotes resolution of hypoxia-inducible factor 1 $\alpha$  activity during prolonged hypoxia. *Mol Cell Biol* 2011, 31(19); 4087–4096.
- 92) Chamboredon S., Ciais D., Desroches-Castan A., Savi P., Bono F., Feige J.J., Cherradi N. Hypoxia-inducible factor-1 $\alpha$  mRNA: a new target for destabilization by tristetraprolin in endothelial cells. *Mol Biol Cell* 2011, 22(18); 3366–3378.
- 93) Liu Y.V., Baek J.H., Zhang H., Diez R., Cole R.N., Semenza G.L. RACK1 competes with HSP90 for binding to HIF-1 $\alpha$  and is required for O<sub>2</sub>-independent and HSP90 inhibitor-induced degradation of HIF-1 $\alpha$ . *Mol Cell* 2007, 25(2);207–217.
- 94) Pan Y., Mansfield K.D., Bertozzi C.C., Rudenko V., Chan D.A., Giaccia A.J., Simon M.C. Multiple factors affecting cellular redox status and energy metabolism modulate hypoxia-inducible factor prolyl hydroxylase activity in vivo and in vitro. *Mol Cell Biol* 2007, 27(3);912–925.
- 95) Finley L.W., Carracedo A., Lee J., Souza A., Egia A., Zhang J., Teruya-Feldstein J., Moreira P.I., Cardoso S.M., Clish C.B., Pandolfi P.P., Haigis M.C. SIRT3 opposes reprogramming of cancer cell metabolism through HIF1 $\alpha$  destabilization. *Cancer Cell* 2011, 19(3);416–428.
- 96) Kaelin Jr.W.G., Ratcliffe P.J. Oxygen sensing by metazoans: the central role of the HIF hydroxylase pathway. *Mol Cell* 2008, 30(4);393–402.
- 97) Luo W., Hu H., Chang R., Zhong J., Knabel M., O’Meally R., Cole R.N., Pandey A., Semenza G.L. Pyruvate kinase M<sup>2</sup> is a PHD3-stimulated coactivator for hypoxia-inducible factor 1. *Cell* 2001, 145(5);732-744.
- 98) Semenza G.L. Targeting HIF-1 for cancer therapy. *Nat Rev Cancer* 2003, 3(10);721-732.
- 99) Land S.C., Tee A.R. Hypoxia-inducible factor 1 $\alpha$  is regulated by the mammalian target of rapamycin (mTOR) via an mTOR signaling motif. *J Biol Chem* 2007, 282(28);20534-20543.
- 100) Tanimoto K., Tsuchihara K., Kanai A., Arauchi T., Esumi H., Suzuki Y., Sugano S. Genome-wide identification and annotation of HIF-1 $\alpha$  binding sites in two cell lines using massively parallel sequencing. *Hugo J* 2010, 4(1-4);35-48.
- 101) Mimura I., Tanaka T., Wada Y., Kodoma T., Nangaku M. Pathophysiological response to hypoxia - from the molecular mechanisms of malady to drug discovery: epigenetic regulation of the hypoxia response via hypoxia-inducible factor and histone modifying enzymes. *J Pharmacol Sci* 2011, 115(4);453-458.

- 102) Xu J., Wang B., Xu Y., Sun L., Tian W., Shukla D., Barod R., Grillari J., Grillari-Voglauer R., Maxwell P.H., Esteban M.A. Epigenetic regulation of HIF-1 $\alpha$ /2 $\alpha$  binding to a reverse hypoxia-response element. *Oncogene* 2012, 31(8);1065-1072.
- 103) Vanharanta S., Shu W., Brenet F., Hakimi A.A., Heguy A., Viale A., Reuter V.E., Hsieh J.J., Scandura J.M., Massagué J. Epigenetic expansion of VHL-HIF signal output drives mutliorgan metastasis in renal cancer. *Nat Med* 2013, 19(1);50-56.
- 104) Nguyen M.P., Lee S., Lee Y.M. Epigenetic regulation of hypoxia inducible factor in disease and therapeutics. *Arch Pharm Res* 2013 [in press].
- 105) Jiang B.H., Semenza G.L., Bauer C., Marti H.H. Hypoxia-inducible factor 1 levels vary exponentially over a physiologically relevant range of O<sub>2</sub> tension. *Am J Physiol* 1996b, 271(4);1172-1180.
- 106) Bracken C.P., Fedele A.O., Linke S., Balrak W., Lisy K., Whitelaw M.L., Peet D.J. Cell-specific regulation of hypoxia-inducible factor (HIF)-1 $\alpha$  and HIF-2 $\alpha$  stabilization and transactivation in a graded oxygen environment. *Journal Biol Chem* 2006, 281(32);22575-22585.
- 107) Jaakkola P., Mole D.R., Tian Y.M., Wilson M.I., Gielbert J., Gaskell S.J., von Kriegsheim A., Hebestreit H.F., Mukherju M., Schofield C.J. Targeting of HIF-alpha to the von Hippel-Lindau ubiquitylation complex by O<sub>2</sub>-regulated prolyl hydroxylation. *Science* 2001, 292(5516);468-472.
- 108) Jeong J.W., Bae M.K., Ahn M.Y., Kim S.H., Sohn T.K., Bae M.H., Yoo M.A., Song E.J., Lee K.J., Kim K.W. Regulation and destabilization of HIF-1 $\alpha$  by ARD1-mediated acetylation. *Cell* 2002, 111(5);709-720.
- 109) Moroz E., Carlin S., Dyomina K., Burke S., Thaler H.T., Blasberg R., Serganova I. Real-time imaging of HIF-1 $\alpha$  stabilization and degradation. *PLoS One* 2009, 4(4);e5077.
- 110) Hirsila M., Koivunen P., Günzler V., Kivirikko K.I., Myllyharju J. Characterization of the human prolyl 4-hydroxylases that modify the hypoxia-inducible factor. *J Biol Chem* 2003, 278(33);30772-30780.
- 111) Wang G.L. Semenza G.L. Characterization of hypoxia-inducible factor 1 and regulation of DNA binding activity by hypoxia. *J Biol Chem* 1993b, 268(29);21513-21518.
- 112) Jewell U.R., Kvietikova I., Scheid A., Bauer C., Wenger R.H., Gassmann M. Induction of HIF-1 $\alpha$  in response to hypoxia is instantaneous. *FASEB J* 2001, 15(7);1312-1314.

- 113) Maltepe E., Schmidt J.V., Baunoch D., Bradfield C.A., Simon M.C. Abnormal angiogenesis and response to glucose and oxygen deprivation in mice lacking the protein ARNT. *Nature* 1997, 386(6623);403-407.
- 114) Iyer N.V., Kotch L.E., Agani F., Leung S.W., Laughner E., Wenger R.H., Gassmann M., Gearhart J.D., Lawler A.M., Yu A.Y., Semenza G.L. Cellular and developmental control of O<sub>2</sub> homeostasis by hypoxia-inducible factor 1a. *Genes Dev* 1998, 12(2);149– 162.
- 115) Ryan H.E., Lo J., Johnson R.S. HIF-1a is required for solid tumor formation and embryonic vascularization. *EMBO J* 1998, 17(11);3005–3015.
- 116) Melillo G., Musso T., Sica A., Taylor L.S., Cox G.W., Varesio L. A hypoxia-responsive element mediates a novel pathway of activation of the inducible nitric oxide synthase promoter. *J Exp Med* 1995, 182(6);1683–1693.
- 117) Loboda A., Jozkowicz A., Dulak J. HIF-1 and HIF-2 transcription factors – similar but not identical. *Mol Cells* 2010, 29(5);435-442.
- 118) Semenza G.L. HIF-1: mediator of physiological and pathophysiological response to hypoxia. *J Appl Physiol* 2000, 88(4);1474-1480.
- 119) Ke Q., Costa M. Hypoxia-Inducible Factor-1 (HIF-1). *Molec Pharmacol* 2006, 70(6);1469-1480.
- 120) Manola D.J., Rowan A., Lavoie T., Natarajan L., Kelly B.D., Ye S.Q., Garcia J.G., Semenza G.L. Transcriptional regulation of vascular endothelial cell response to hypoxia by HIF-1. *Blood* 2005, 105(2);659-669.
- 121) Goda N., Ryan H.E., Khadivi B., McNulty W., Rickert R.C., Johnson R.S. Hypoxia-inducible factor 1 $\alpha$  is essential for cell cycle arrest during hypoxia. *Mol Cell Biol* 2003, 23(1);359-369.
- 122) Mole D.R., Blancher C., Copley R.R., Pollard P.J., Gleadle J.M., Ragoussis J., Ratcliffe P.J. Genome-wide association of hypoxia-inducible factor (HIF)-1 $\alpha$  and HIF-2 $\alpha$  DNA binding with expression profiling of hypoxia-inducible transcripts. *J Biol Chem* 2009, 284(25);16767-16775.
- 123) Schödel J., Oikonomopoulos S., Ragoussis J., Pugh C.W., Ratcliffe P.J., Mole D.R. High-resolution genome-wide mapping of HIF-binding sites by ChIP-seq. *Blood* 2011, 117(23);e207-e217.
- 124) Ortiz-Barahona A., Villar D., Pescador N., Amigo J., del Peso L. Genome-wide identification of hypoxia-inducible factor binding sites and target genes by a

- probabilistic model integrating transcription-profiling data and in silico binding site prediction. *Nucleic Acids Res* 2010, 38(7);2332-2345.
- 125) Stroka D.M., Burkhardt T., Desbaillets I., Wenger R.H., Neil D.A., Bauer C., Gassmann M., Candinas D. HIF-1 is expressed in normoxic tissue and displays an organ-specific regulation under systemic hypoxia. *FASEB J* 2001, 15(13);2445-2453.
  - 126) Chi J.T., Wang Z., Nuyten D.S., Rodriguez E.H., Schaner M.E., Salim A., Wang Y., Kristensen G.B., Helland A., Børresen- Dale A.L., Giaccia A., Longaker M.T., Hastie T., Yang G.P., van de Vijver M.J., Brown P.O. Gene expression programs in response to hypoxia: cell type specificity and prognostic significance in human cancers. *PLoS Med* 2006, 3(3);e47.
  - 127) Gardner L.B., Corn P.G. Hypoxic regulation of mRNA expression. *Cell Cycle* 2008, 7(13);1916–1924.
  - 128) Brachen C.P., Fedele A.O., Linke S., Balrak W., Lisy K., Whitelaw M.L., Peet D.J. Cell-specific regulation of hypoxia-inducible factor (HIF)-1 $\alpha$  and HIF-2 $\alpha$  stabilization and transactivation in a graded oxygen environment. *J Biological Chem* 2006, 281(32);22575-22585.
  - 129) Lendahl U., Lee K.L., Yang H., Poellinger L. Generating specificity and diversity in the transcriptional response to hypoxia. *Nature Rev Genet* 2009, 10(12);821-832.
  - 130) Benita Y., Kikuchi H., Smith A.D., Zhang M.Q., Chung D.C., Xavier R.J. An integrative genomics approach identifies Hypoxia Inducible Factor-1 (HIF-1)-target genes that form the core response to hypoxia. *Nucleic Acids Res* 2009, 37(14);4587-4602.
  - 131) Semenza G.L. Oxygen sensing, homeostasis, and disease. *N Engl J Med* 2011a, 365(6);537-547.
  - 132) Kenneth N.S., Rocha S. Regulation of gene expression by hypoxia. *Biochem J* 2008, 414(1);19-29.
  - 133) Hu C.J., Wang L.Y., Chodosh L.A., M B.K., Simon C. Differential roles of hypoxia-inducible factor 1 $\alpha$  (HIF-1 $\alpha$ ) and HIF-2 $\alpha$  in hypoxic gene regulation. *Mol Cell Biol* 2003, 23(24);9361-9374.
  - 134) Raval R.R., Lau K.W., Tran M.G., Sowter H.M., Mandriota S.J., Li J.L., Pugh C.W., Maxwell P.H., Harris A.L., Ratcliffe P.J. Contrasting properties of hypoxia-inducible factor 1 (HIF-1) and HIF-2 in von Hippel-Lindau-associated renal cell carcinoma. *Mol Cell Biol* 2005, 25(13);5675-5686.

- 135) Covello K.L., Kehler J., Yu H., Gordan J.D., Arsham A.M., Hu C.J., Labosky P.A., Simon M.C., Keith B. HIF-2 $\alpha$  regulates Oct-4: effects of hypoxia on stem cell function, embryonic development, and tumor growth. *Genes Dev* 2006, 20(5);557-570.
- 136) Makino Y., Cao R., Svensson K., Bertilsson G., Asman M., Tanaka H., Cao Y., Berkenstam A., Poellinger L. Inhibitory PAS domain protein is a negative regulator of hypoxia-inducible gene expression. *Nature* 2001, 414(6863); 550–554.
- 137) Krohn K.A., Link J.M., Mason R.P. Molecular imaging of hypoxia. *J Nucl Med* 2008, Suppl 2;129S-148S.
- 138) Kim Y.R., Huang I.J., Lee S.R., Tejima E., Mandeville J.B., van Meer M.P., Dai G., Choi Y.W., Dijkhuizen R.M., Lo E.H., Rosen B.R. Measurements of BOLD/CBV ratio show altered fMRI hemodynamics during stroke recovery in rats. *J Cereb Blood Flow Metab* 2005, 25(7);820–829.
- 139) Leontiev O., Buxton R.B. Reproducibility of BOLD, perfusion, and CMRO<sub>2</sub> measurements with calibrated-BOLD fMRI. *Neuroimage* 2007, 35(1);175–184.
- 140) Mason R.P., Shukla H.P., Antich P.P. In vivo oxygen tension and temperature: simultaneous determination using <sup>19</sup>F NMR spectroscopy of perfluorocarbon. *Magn Reson Med* 1993, 29:296–302.
- 141) Zhao D., Jiang L., Mason R.P. Measuring changes in tumor oxygenation. *Methods Enzymol* 2004, 386;378–418.
- 142) Vaupel P., Schlenger K., Knoop C., Hockel M. Oxygenation of human tumors: evaluation of tissue oxygen distribution in breast cancers by computerized O<sub>2</sub> tension measurements. *Cancer Res* 1991, 51(12);3316–3322.
- 143) Collingridge D.R., Piepmeier J.M., Rockwell S., Knisely J.P. Polargraphic measurements of oxygen tension in human glioma and surrounding peritumoural brain tissue. *Radiother Oncol* 1999, 53(2);127-131.
- 144) Kim J.G., Song Y., Zhao D., Constantinescu A., Mason R.P., Liu H. Interplay of tumor vascular oxygenation and tumor pO<sub>2</sub> observed using near-infrared spectroscopy, an oxygen needle electrode, and <sup>19</sup>F MR pO<sub>2</sub> mapping. *J Biomed Opt* 2003, 8(1);53-62.
- 145) Mason R.P., Hunjan S., Constantinescu A., Song Y., Zhao D., Hahn E.W., Antich P.P., Peschke P. Tumor oximetry: comparison of <sup>19</sup>F MR EPI and electrodes. *Adv Exp Med Biol* 2003, 530;19–27.

- 146) Jorge P.A., Mayeh M., Benrashid R., Caldas P., Santos J.L., Farahi F. Applications of quantum dots in optical fiber luminescent oxygen sensors. *Appl Opt* 2006, 45(16);3760-3767.
- 147) Adamsen T.C.H., Grierson J.R., Krohn K.A. A new synthesis of the labeling precursor for [18F]-fluoromisonidazole. *J Labelled Comp Radiopharm* 2005, 48;923–927.
- 148) Varia M.A., Calkins-Adams D.P., Rinker L.H., Kennedy A.S., Novotny D.B., Fowler W.C. Jr., Raleigh J.A. Pimonidazole: a novel hypoxia marker for complementary study of tumor hypoxia and cell proliferation in cervical carcinoma. *Gynecol Oncol* 1998, 71(2);270-277.
- 149) Olive P.L., Durand R.E., Raleigh J.A., Luo C., Aquin-Parsons C. Comparison between the comet assay and pimonidazole binding for measuring tumour hypoxia. *Br J Cancer* 2000, 83(11);1525-1531.
- 150) Nordmark M., Loncaster J., Aquino-Parsons C., Chou S.C., Ladekarl M., Havsteen H., Lindegaard J.C., Davidson S.E., Varia M., West C., Hunter R., Overgaard J., Raleigh J.A. Measurements of hypoxia using pimonidazole and polarographic oxygen-sensitive electrodes in human cervix carcinomas. *Radiother Oncol* 2003, 67(1);35-44.
- 151) Gross J.D., Constantinidis I., Sambanis A. Modeling of encapsulated cell systems. *J Theor Biol* 2007, 244(3);500-510.
- 152) Cheema U., Brown R.A., Alp B., MacRobert A.J. Spatially defined oxygen gradients and vascular endothelial growth factor expression in an engineered 3D cell model. *Cell Mol Life Sci* 2008, 65(1);177-186.
- 153) Buchwald P. FEM-based oxygen consumption and cell viability models for avascular pancreatic islets. *Theor Biol Med Model* 2009, 6;5.
- 154) Shibata T., Giaccia A.J., Brown J.M. Development of a hypoxia-responsive vector for tumor-specific gene therapy. *Gene Ther* 2000, 7(6);493–498.
- 155) Payen E., Bettan M., Henri A., Tomkiewicz E., Houque A., Kuzniak I., Zuber J., Scherman D., Beuzard Y. Oxygen tension and a pharmacological switch in the regulation of transgene expression for gene therapy. *J Gene Med* 2001, 3(5);498–504.
- 156) Koshikawa N., Takenaga K., Tagawa M., Sakiyama S. Therapeutic efficacy of the suicide gene driven by the promoter of vascular endothelial growth factor gene against hypoxic tumor cells. *Cancer Res* 2000, 60(11);2936–2941.

- 157) Harada H., Kizaka-Kondoh S., Hiraoka M. Optical imaging of tumor hypoxia and evaluation of efficacy of a hypoxia-targeting drug in living animals. *Mol Imaging* 2005, 4(3);82–193.
- 158) Vordermark D., Shibata T., Brown J.M. Green fluorescent protein is a suitable reporter of tumor hypoxia despite an oxygen requirement for chromophore formation. *Neoplasia* 2001, 3(6);527–534.
- 159) Serganova I., Doubrovin M., Vider J., Ponomarev V., Soghomonyan S., Beresten T., Ageyeva L., Serganov A., Cai S., Balatoni J., Blasberg R., Gelovani J. Molecular imaging of temporal dynamics and spatial heterogeneity of hypoxia-inducible factor-1 signal transduction activity in tumors in living mice. *Cancer Res* 2004, 64(17);6101–6108.
- 160) Laschke M.W., Harder Y., Amon M., Martin I., Farhadi J., Ring A., Torio-Padron N., Schramm R., Rücker M., Junker D., Häufel J.M., Carvalho C., Heberer M., Germann G., Vollmar B., Menger M.D. Angiogenesis in tissue engineering: breathing life into constructed tissue substitutes. *Tissue Eng* 2006, 12(8);2093–2104.
- 161) Langer R., Vacanti J.P. Tissue engineering. *Science* 1993, 260(5110);920–926.
- 162) Mason C., Dunnill P. A brief definition of regenerative medicine. *Regen Med* 2008, 3(1);1–5.
- 163) Kelly W.D., Lillehei R.C., Merkel F.K., Idezuki Y., Goetz F.C. Allotransplantation of the pancreas and duodenum along with the kidney in diabetic nephropathy. *Surgery* 1967, 61(6);827–837.
- 164) Lim F., Sun A.M. Microencapsulated islets as bioartificial endocrine pancreas. *Science* 1980, 210(4472);908–910.
- 165) Dufrane D., Goebbels R.M., Saliez A., Guiot Y., Gianello P. Six-month survival of microencapsulated pig islets and alginate biocompatibility in primates: Proof of concept. *Transplantation* 2006a, 81(9);1345–1353.
- 166) Abalovich A.G., Bacqué M.C., Grana D., Milei J. Pig pancreatic islet transplantation into spontaneously diabetic dogs. *Transplant Proc* 2009, 41(1);328–330.
- 167) Elliott R.B., Escobar L., Tan P.L.J., Muzina M., Zwain S., Buchanan C. Live encapsulated porcine islets from a type 1 diabetic patient 9.5 yr after xenotransplantation. *Xenotransplantation* 2007, 14(2);157–161.

- 168) Tuch B.E., Foster J.L., Keogh G.W., Vaithilingam V., Williams L.J., Philips R., Wu W. Safety and viability of microencapsulated human islets transplanted into diabetic humans. *Diabetes Care* 2009, 32(10);1887-1889.
- 169) Langlois G., Dusseault J., Bilodeau S., Tam S.K., Magassouba D., Hallé J.P. Direct effect of alginate purification on the survival of islets immobilized in alginate-based microcapsules. *Acta Biomaterialia* 2009, 5(9);3433-3440.
- 170) Liu X.Y., Nothias J.M., Scavone A., Garfinkel M., Millis J.M. Biocompatibility investigation of polyethylene glycol and alginate-poly-L-lysine for islet encapsulation. *ASAIO J* 2010, 56(3);241-245.
- 171) Bryant S.J., Anseth K.S. Hydrogel properties influence ECM production by chondrocytes photoencapsulated in poly(ethylene glycol) hydrogels. *J Biomed Mater Res* 2002, 59(1);63-72.
- 172) Rice M.A., Anseth K.S. Encapsulating chondrocytes in copolymer gels: Bimodal degradation kinetics influence cell phenotype and extracellular matrix development. *J Biomed Mater Res A* 2004, 70(4);560-568.
- 173) Burdick J.A., Anseth K.S. Photoencapsulation of osteoblasts in injectable RGD-modified hydrogels for bone tissue engineering. *Biomaterials* 2002, 23(22);4315-4323.
- 174) Benton J.A., Fairbanks B.D., Anseth K.S. Characterization of valvular interstitial cell function in three dimensional matrix metalloproteinase degradable PEG hydrogels. *Biomaterials* 2009, 30(34);6593-6603.
- 175) Nuttelman C.R., Tripodi M.C., Anseth K.S. *In vitro* osteogenic differentiation of human mesenchymal stem cells photoencapsulated in PEG hydrogels. *J Biomed Mater Res A* 2004, 68(4);773-782.
- 176) Cruise G.M., Scharp D.S., Hubbell J.A. Characterization of permeability and network structure of interfacially photopolymerized poly(ethylene glycol) diacrylate hydrogels. *Biomaterials* 1998, 19(14);1287-1294.
- 177) Lin-Gibson S., Bencherif S., Cooper J.A., Wetzel S.J., Antonucci J.M., Vogel B.M., Horkay F., Washburn N.R. Synthesis and characterization of PEG dimethacrylates and their hydrogels. *Biomacromolecules* 2004, 5(4);1280-1287.
- 178) Weber L.M., Lopez C.G., Anseth K.S. Effects of PEG hydrogel crosslinking density on protein diffusion and encapsulated islet survival and function. *J Biomed Mater Res A* 2009, 90(3);720-729.

- 179) Weber L.M., He J., Bradley B., Haskins K., Anseth K.S. PEG-based hydrogels as an *in vitro* encapsulation platform for testing controlled  $\beta$ -cell microenvironments. *Acta Biomater* 2006, 2(1);1-8.
- 180) Bryant S.J., Nuttelman C.R., Anseth K.S. Cytocompatibility of UV and visible light photoinitiating systems on cultured NIH/3T3 fibroblasts *in vitro*. *J Biomater Sci Polym Ed* 2000, 11(5);439-457.
- 181) De Vos P., De Haan B.J., Wolters G.H.J., Strubbe J.H., Van Schilfgaarde R. Improved biocompatibility but limited graft survival after purification of alginate for microencapsulation of pancreatic islets. *Diabetologia* 1997, 40(3);262-270.
- 182) Suzuki K., Bonner-Wier S., Trivedi N., Yoon K.H., Hollister-Lock J., Colton C.K., Weir G.C. Function and survival of macroencapsulated syngeneic islets transplanted into streptozocin-diabetic mice. *Transplantation* 1998, 66(1);21-28.
- 183) De Vos P., Van Straaten J.F.M., Nieuwenhuizen A.G., de Groot M., Ploeg R.J., De Haan B.J., Van Schilfgaarde R. Why do microencapsulated islet grafts fail in the absence of fibrotic overgrowth? *Diabetes* 1999, 48(7);1381-1388.
- 184) Dionne K.E., Colton C.K., Yarmush M.L. Effect of oxygen on isolated pancreatic tissue. *ASAIO Trans* 1989, 35(3);739-741.
- 185) Dionne K.E., Colton C.K., Yarmush M.L. Effect of oxygen on insulin secretion by isolated rat and canine islets of Langerhans. *Diabetes* 1993, 42(1);12-21.
- 186) de Groot M., Schuurs T.A., Keizer P.P.M., Fekken S., Leuvenink H.G.D., Van Schilfgaarde R. Response of encapsulated rat pancreatic islets to hypoxia. *Cell Transplant* 2003, 12(8);867-875.
- 187) Shapiro A.M.J., Lakey J.R.T., Ryan E.A., Korbitt G.S., Toth E., Warnock G., Kneteman N.M., Rajotte R.V. Islet transplantation in seven patients with type 1 diabetes mellitus using a glucocorticoid-free immunosuppressive regimen. *New Engl J Med* 2000, 343(4);230-238.
- 188) Shapiro J.A.M., Ricordi C., Hering B.J., Auchincloss H., Lindblad R., Robertson R.P., Secchi A., Brendel M.D., Berney T., Brennan D.C., Cagliero E., Alejandro R., Ryan E.A., DiMercurio B., Morel P., Polonsky K.S., Reems J., Bretzel R.G., Bertuzzi F., Froud T., Kandaswamy R., Sutherland D.E.R., Eisenbarth G., Segal M., Preiksaitis J., Korbitt G.S., Barton F.B., Viviano L., Seyfert-Margolis V., Bluestone J., Lakey J.R.T. International trial of the Edmonton Protocol for islet transplantation. *New Engl J Med* 2006, 355(13);1318-1330.

- 189) Schrezenmeir J., Kirchgessner J., Gerö L., Kunz L.A., Beyer J., Mueller-Klieser W. Effect of microencapsulation on oxygen distribution in islet organs. *Transplantation* 1994, 57(9);1308-1314.
- 190) Lehmann R., Zuellig R.A., Kugelmeier P., Baenninger P.B., Moritz W., Perren A., Clavien P.A., Weber M., Spinaz G.A. Superiority of small islets in human islet transplantation. *Diabetes* 2007, 56(3);594-603.
- 191) Cavallari G., Zuellig R.A., Lehmann R., Weber M., Moritz W. Rat pancreatic islet size standardization by the "Hanging Drop" technique. *Transplant Proc* 2007, 39(6);2018-2020.
- 192) Sweet I.R., Khalil G., Wallen A.R., Steedman M., Schenkman K.A., Reems J.A., Kahn S.E., Callis J.B. Continuous measurement of oxygen consumption by pancreatic islets. *Diabetes Technol Ther* 2002, 4(5);661-672.
- 193) Wang W., Upshaw L., Strong D.M., Robertson R.P., Reems J.A. Increased oxygen consumption rates in response to high glucose detected by a novel oxygen biosensor system in non-human primate and human islets. *J Endocrinol* 2005, 185(3);445-455.
- 194) Dufrane D., van Steenberghe M., Goebbels R.M., Saliez A., Guiot Y., Gianello P. The influence of implantation site on the biocompatibility and survival of alginate encapsulated pig islets in rats. *Biomaterials* 2006b, 27(17);3201-3208.
- 195) Zehetner J, Danzer C., Collins S., Eckhardt K., Gerber P.A., Ballschmieter P., Galvanovskis J., Shimomura K., Ashcroft F.M., Thorens B., Rorsman P., Krek W. PVHL is a regulator of glucose metabolism and insulin secretion in pancreatic  $\beta$  cells. *Genes Dev* 2008, 22(22);3135-3146.
- 196) Cantley J., Selman C., Shukla D., Abramov A.Y., Forstreuter F., Esteban M.A., Claret M., Lingard S.J., Clements M., Harten S.K., Asare-Anane H., Batterham R.L., Herrera P.L., Persaud S.J., Duchon M.R., Maxwell P.H., Withers D.J. Depletion of the von Hippel-Lindau gene in pancreatic  $\beta$  cells impairs glucose homeostasis in mice. *J Clin Invest* 2009, 119(1);125-135.
- 197) Puri S., Cano D.A., Hebrok M. A role for von Hippel-Lindau protein in pancreatic  $\beta$ -cell function. *Diabetes* 2009, 58(2);433-441.
- 198) Griffith L.G., Naughton G. Tissue engineering — current challenges and expanding opportunities. *Science* 2002, 295(5557);1009–1014.
- 199) Ikada Y. Challenges in tissue engineering. *J R Soc Interface* 2006, 2(10);589–601.

- 200) Rouwkema J., Rivron N.C., van Blitterswijk C.A. Vascularization in tissue engineering. *Trends Biotechnol* 2008, 26(8);434-441.
- 201) Lovett M., Lee K., Edwards A., Kaplan D.L. Vascularization strategies for tissue engineering. *Tissue Eng Part B Rev* 2009, 15(3);353-370.
- 202) Santos M.I., Reis R.L. Vascularization in bone tissue engineering: physiology, current strategies, major hurdles and future challenges. *Macromol Biosci* 2010, 10(1);12-27.
- 203) Novosel E.C., Kleinhans C., Kluger P.J. Vascularization is the key challenge in tissue engineering. *Adv Drug Deliv Rev* 2011, 63(4-5);300-311.
- 204) Horch R.E., Kneser U., Polykandriotis E., Schmidt V.J., Sun J., Arkudas A. Tissue engineering and regenerative medicine—where do we stand? *J Cell Mol Med* 2012, 16(6);1157-1165.
- 205) Laschke M.W., Menger M.D. Vascularization in tissue engineering: angiogenesis versus inosculation. *Eur Surg Res* 2012, 48(2);85-92.
- 206) Folkman J., Hochberg M. Self-regulation of growth in three dimensions. *J Exp Med* 1973, 138(4);745-753.
- 207) Colton C.K. Implantable biohybrid artificial organs. *Cell Transplant* 1995, 4(4);415-436.
- 208) Carmeliet P., Jain R.K. Molecular mechanisms and clinical applications of angiogenesis. *Nature* 2001, 413(6862);397-402.
- 209) Carmeliet P. Mechanisms of angiogenesis and arteriogenesis. *Nat Med* 2000, 6(4);389-395.
- 210) Hirschi K.K., Skalak T.C., Peirce S.M., Little C.D. Vascular assembly in natural and engineered tissues. *Ann N Y Acad Sci* 2002, 961;223-242.
- 211) Zisch A.H., Lutolf M.P., Hubbell J.A. Biopolymeric delivery matrices for angiogenic growth factors. *Cardiovasc Pathol* 2003, 12(6);295-310.
- 212) Sokolsky-Papkov M., Agashi K., Olaye A., Shakesheff K., Domb A.J. Polymer carriers for drug delivery in tissue engineering. *Adv Drug Deliv Rev* 2007, 59(4-5);187-206.

- 213) Übersax L., Merkle H.P., Meinel L. Biopolymer-based growth factor delivery for tissue repair: from natural concepts to engineered systems. *Tissue Eng Part B Rev* 2009, 15(3);263-289.
- 214) Fu Y., Kao W.J. Drug release kinetics and transport mechanisms of non-degradable and degradable polymeric delivery systems. *Expert Opin Drug Deliv* 2010, 7(4);429-444.
- 215) Helm C.L., Fleury M.E., Zisch A.H., Boschetti F., Swartz M.A. Synergy between interstitial flow and VEGF directs capillary morphogenesis in vitro through a gradient amplification mechanism. *Proc Natl Acad Sci USA* 2005, 102(44);15779-15784.
- 216) Mizuno H. Adipose-derived stem cells for tissue repair and regeneration: ten years of research and a literature review. *J Nippon Med Sch* 2009, 76(2);56-66.
- 217) Kilroy G.E., Foster S.J., Wu X., Ruiz J., Sherwood S., Heifetz A., Ludlow J.W., Stricker D.M., Potiny S., Green P., Halvorsen Y.D., Cheatham B., Storms R.W., Gimble J.M. Cytokine profile of human adipose-derived stem cells: expression of angiogenic, hematopoietic, and pro-inflammatory factors. *J Cell Physiol* 2007, 212(3);702-709.
- 218) Hong S.J., Traktuev D.O., March K.L. Therapeutic potential of adipose-derived stem cells in vascular growth and tissue repair. *Curr Opin Organ Transplant* 2010, 15(1);86-91.
- 219) Rasmussen J.G., Frøbert O., Pilgaard L., Kastrup J., Simonsen U., Zachar V., Fink T. Prolonged hypoxic culture and trypsinization increase the pro-angiogenic potential of human adipose tissue-derived stem cells. *Cytotherapy* 2011, 13(3);318-328.
- 220) Planat-Benard V., Silvestre J.S., Cousin B., André M., Nibbelink M., Tamarat R., Clergue M., Manneville C., Saillan-Barreau C., Duriez M., Tedgui A., Levy B., Pénicaud L., Casteilla L. Plasticity of human adipose lineage cells toward endothelial cells: physiological and therapeutic perspectives. *Circulation* 2004, 109(5);656-663.
- 221) Miranville A., Heeschen C., Sengenès C., Curat C.A., Busse R., Bouloumié A. Improvement of postnatal neovascularization by human adipose tissue-derived stem cells. *Circulation* 2004, 110(3);349-355.
- 222) Cao Y., Sun Z., Liao L., Meng Y., Han Q., Zhao R.C. Human adipose tissue-derived stem cells differentiate into endothelial cells in vitro and improve postnatal neovascularization in vivo. *Biochem Biophys Res Commun* 2005, 332(2);370-379.

- 223) Colazzo F., Chester A.H., Taylor P.M., Yacoub M.H. Induction of mesenchymal to endothelial transformation of adipose-derived stem cells. *J Heart Valve Dis* 2010, 19(6);736-744.
- 224) Keerl S., Gehmert S., Gehmert S., Song Y.H., Alt E. PEGF and bFGF modulate tube formation in adipose tissue-derived stem cells. *Ann Plast Surg* 2010, 64(4);487-490.
- 225) Shi Z., Neoh K.G., Kang E.T., Poh C.K., Wang W. Enhanced endothelial differentiation of adipose-derived stem cells by substrate nanotography. *J Tissue Eng Regen Med* 2012, [in press].
- 226) Kim W.S., Park B.S., Sung J.H., Yang J.M., Park S.B., Kwak S.J., Park J.S. Wound healing effect of adipose-derived stem cells: a critical role of secretory factors on human dermal fibroblasts. *J Dermatol Sci* 2007, 48(1);15-24.
- 227) Lu F., Mizuno H., Uysal C.A., Cai X., Ogawa R., Hyakusoku H. Improved viability of random pattern skin flaps through the use of adipose-derived stem cells. *Plast Reconstr Surg* 2008, 121(1);50-58.
- 228) Kim W.S., Park B.S., Sung J.H. The wound-healing and antioxidant effects of adipose-derived stem cells. *Expert Opin Biol Ther* 2009, 9(7);879-887.
- 229) Nambu M., Kishimoto S., Nakamura S., Mizuno H., Yanagibayashi S., Yamamoto N., Azuma R., Nakamura S., Kiyosawa T., Ishihara M., Kanatani Y. Accelerated wound healing in healing-impaired *db/db* mice by autologous adipose tissue-derived stromal cells combined with atelocollagen matrix. *Ann Plast Surg* 2009, 62(3);317-321.
- 230) Nakagami H., Maeda K., Morishita R., Iguchi S., Nishikawa T., Takami Y., Kikuchi Y., Saito Y., Tamai K., Ogihara T., Kaneda Y. Novel autologous cell therapy in ischemic limb disease through growth factor secretion by cultured adipose tissue-derived stromal cells. *Arterioscler Thromb Vasc Biol* 2005, 25(12);2542-2547.
- 231) Moon M.H., Kim S.Y., Kim Y.J., Kim S.J., Lee J.B., Bae Y.C., Sung S.M., Jung J.S. Human adipose tissue-derived mesenchymal stem cells improve postnatal neovascularization in a mouse model of hindlimb ischemia. *Cell Physiol Biochem* 2006, 17(5-6);279-290.
- 232) Kim Y., Kim H., Cho H., Bae Y., Suh K., Jung J. Direct comparison of human mesenchymal stem cells derived from adipose tissues and bone marrow in mediating neovascularization in response to vascular ischemia. *Cell Physiol Biochem* 2007, 20(6);867-876.

- 233) Miyahara Y., Nagaya N., Kataoka M., Yanagawa B., Tanaka K., Hao H., Ishino K., Ishida H., Shimizu T., Kangawa K., Sano S., Okano T., Kitamura S., Mori H. Monolayered mesenchymal stem cells repair scarred myocardium after myocardial infarction. *Nat Med* 2006, 12(4);459-465.
- 234) Valina C., Pinkernell K., Song Y.H., Bai X., Sadat S., Campeau R.J., Le Jemtel T.H., Alt E. Intracoronary administration of autologous adipose tissue-derived stem cells improves left ventricular function, perfusion, and remodelling after acute myocardial infarction. *Eur Heart J* 2007, 28(21);2667-2677.
- 235) Cai L., Johnstone B.H., Cook T.G., Tan J., Fishbein M.C., Chen P.S., March K.L. IFATS collection: Human adipose tissue-derived stem cells induce angiogenesis and nerve sprouting following myocardial infarction, in conjunction with potent preservation of cardiac function. *Stem Cells* 2009, 27(1);230-237.
- 236) Schenke-Layland K., Strem B.M., Jordan M.C., Deemedio M.T., Hedrick M.H., Roos K.P., Fraser J.K., Maclellan W.R. Adipose tissue-derived cells improve cardiac function following myocardial infarction. *J Surg Res* 2009, 153(2);217-223.
- 237) Wang L., Deng J., Tian W., Xiang B., Yang T., Li G., Wang J., Gruwel M., Kashour T., Rendell J., Glogowski M., Tomanek B., Freed D., Deslauriers R., Arora R.C., Tian G. Adipose-derived stem cells are an effective cell candidate for treatment of heart failure: an MR imaging study of rat hearts. *Am J Physiol Heart Circ Physiol* 2009, 297(3);H1020-H1031.
- 238) Takahashi T., Kalka C., Masuda H., Chen D., Silver M., Kearney M., Magner M., Isner J.M., Asahara T. Ischemia- and cytokine-induced mobilization of bone marrow-derived endothelial progenitor cells for neovascularization. *Nat Med* 1999, 5(4);434-438.
- 239) Crosby J.R., Kaminski W.E., Schatteman G., Martin P.J., Raines E.W., Seifert R.A., Bowen-Pope D.F. Endothelial cells of hematopoietic origin make a significant contribution to adult blood vessel formation. *Circ Res* 2000, 87(9);728-730.
- 240) Ceradini D.J., Gurtner G.C. Homing to hypoxia: HIF-1 as a mediator of progenitor cell recruitment to injured tissue. *Trends Cardiovasc Med* 2005, 15(2);57-63.
- 241) Nakao N., Nakayama T., Yahata T., Muguruma Y., Saito S., Miyata Y., Yamamoto K., Naoe T. Adipose tissue-derived mesenchymal stem cells facilitate hematopoiesis in vitro and in vivo: advantages over bone marrow-derived mesenchymal stem cells. *Am J Pathol* 2010, 177(2);547-554.

- 242) Askari A.T., Unzek S., Popovic Z.B., Goldman C.K., Forudi F., Kiedrowski M., Rovner A., Ellis S.G., Thomas J.D., DiCorleto P.E., Topol E.J., Penn M.S. Effect of stromal-cell-derived factor 1 on stem-cell homing and tissue regeneration in ischaemic cardiomyopathy. *Lancet* 2003, 362(9385);697-703.
- 243) Ceradini D.J., Kulkarni A.R., Callaghan M.J., Tepper O.M., Bastidas N., Kleinman M.E., Capla J.M., Galiano R.D., Levine J.P., Gurtner G.C. Progenitor cell trafficking is regulated by hypoxic gradients through HIF-1 induction of SDF-1. *Nat Med.* 2004, 10(8);858-864.
- 244) Traktuev D.O., Merfeld-Clauss S., Li J., Kolonin M., Arap W., Pasqualini R., Johnstone B.H., March K.L. A population of multipotent CD34- positive adipose stromal cells share pericyte and mesenchymal surface markers, reside in a periendothelial location, and stabilize endothelial networks. *Circ Res* 2008, 102(1);77–85.
- 245) Traktuev D.O., Prater D.N., Merfeld-Clauss S., Sanieevaiah A.R., Saadatzadeh M.R., Murphy M., Johnstone B.H., Ingram D.A., March K.L. Robust functional vascular network formation in vivo by cooperation of adipose progenitor and endothelial cells. *Circ Res* 2009, 104(12);1410–1420.
- 246) Gimble J.M., Katz A.J., Bunnell B.A. Adipose-derived stem cells for regenerative medicine. *Circ Res* 2007, 100(9);149-1260.
- 247) Matsumoto A., Matsumoto S., Sowers A.L., Koscielniak J.W., Trigg N.J., Kuppusamy P., Mitchell J.B., Subramanian S., Krishna M.C., Matsumoto K. Absolute oxygen tension (pO<sub>2</sub>) in murine fatty and muscle tissue as determined by EPR. *Magn Reson Med* 2005, 54(6);1530-1535.
- 248) Pasarica M., Sereda O.R., Redman L.M., Alberado D.C., Hymel D.T., Roan L.E., Rood J.C., Burk DH, Smith SR. Reduced adipose tissue oxygenation in human obesity: evidence for rarefaction, macrophage chemotaxis, and inflammation without an angiogenic response. *Diabetes* 2009, 58(3);718-715.
- 249) Mohyeldin A., Garzón-Muvdi T., Quiñones-Hinojosa A. Oxygen in stem cell biology: a critical component of the stem cell niche. *Cell Stem Cell* 2010, 7(2);150-161.
- 250) Rehman J., Traktuev D., Li J., Merfeld-Clauss S., Temm-Grove C.J., Bovenkerk J.E., Pell C.L., Johnstone B.H., Considine R.V., March K.L. Secretion of angiogenic and antiapoptotic factors by human adipose stromal cells. *Circulation* 2004, 109(10);1292-1298.

- 251) Rosová I., Dao M., Capoccia B., Link D., Nolte J.A. Hypoxic preconditioning results in increased motility and improved therapeutic potential of human mesenchymal stem cells. *Stem Cells* 2008, 26(8);2173-2182.
- 252) Lee E.Y., Xia Y., Kim W.S., Kim M.H., Kim T.H., Kim K.J., Park B.S., Sung J.H. Hypoxia-enhanced wound-healing function of adipose-derived stem cells: increase in stem cell proliferation and up-regulation of VEGF and bFGF. *Wound Repair Regen* 2009, 17(4);540-547.
- 253) Liu L., Gao J., Yuan Y., Chang Q., Liao Y., Lu F. Hypoxia preconditioned human adipose derived mesenchymal stem cells enhance angiogenic potential via secretion of increased VEGF and bFGF. *Cell Biol Int* 2013, (in press).
- 254) Levy A.P., Levy N.S., Wegner S., Goldberg M.A. Transcriptional regulation of the rat vascular endothelial growth factor gene by hypoxia. *J Biol Chem* 1995, 270(22);13333-13340.
- 255) Liu Y., Cox S.R., Morita T., Kourembanas S. Hypoxia regulates vascular endothelial growth factor gene expression in endothelial cells. Identification of a 5' enhancer. *Circ Res* 1995, 77(3);638-643.
- 256) Forsythe J.A., Jiang B.H., Iyer N.V., Agani F., Leung S.W., Koos R.D., Semenza G.L. Activation of vascular endothelial growth factor gene transcription by hypoxia-inducible factor 1. *Mol Cell Biol* 1996, 16(9);4604-4613.
- 257) Tang Y.L., Zhu W., Cheng M., Chen L., Zhang J., Sun T., Kishore R., Phillips M.I., Losordo D.W., Qin G. Hypoxic preconditioning enhances the benefit of cardiac progenitor cell therapy for treatment of myocardial infarction by inducing CXCR4 expression. *Circ Res* 2009, 104(10);1209–1216.
- 258) Yue Y., Zhang P., Liu D., Yang J.F., Nie C., Yang D. Hypoxia preconditioning enhances the viability of ADSCs to increase the survival rate of ischemic skin flaps in rats. *Aesthetic Plast Surg* 2013, 37(1);159-170.
- 259) Chacko S.M., Ahmed S., Selvendiran K., Kuppusamy M.L., Khan M., Kuppusamy P. Hypoxic preconditioning induces the expression of pro-survival and pro-angiogenic markers in mesenchymal stem cells. *Am J Physiol Cell Physiol* 2010, 299(6), C1562–C1570.
- 260) Abdollahi H., Harris L.J., Zhang P., McIlhenny S., Srinivas V., Tulenko T., Dimuzio P.J., Dimuzio P.J. The role of hypoxia in stem cell differentiation and therapeutics. *J Surg Res* 2010, 165(1);112-117.

- 261) Zachar V, Duroux M, Emmersen J, Rasmussen JG, Pennisi CP, Yang S, Fink T. Hypoxia and adipose-derived stem cell-based tissue regeneration and engineering. *Expert Opin Biol Ther* 2011, 11(6);775-786.
- 262) Geiger F., Lorenz H., Xu W., Szalay K., Kasten P., Claes L., Augat P., Richter W. VEGF producing bone marrow stromal cells (BMSC) enhance vascularization and resorption of a natural coral bone substitute. *Bone* 2007, 41(4);516-522.
- 263) Baraniak P.R., McDevitt T.C. Stem cell paracrine actions and tissue regeneration. *Regen Med* 2010, 5(1);121-143.
- 264) Shweiki, D., Neeman, M., Itin, A., Keshet, E. Induction of vascular endothelial growth factor expression by hypoxia and by glucose deficiency in multicell spheroids: implications for tumor angiogenesis. *Proc Natl Acad Sci USA* 1995, 92(3);768-772.
- 265) Bates R.C., Edwards N.S., Yates, J.D. Spheroids and cell survival. *Crit Rev Oncol Hematol* 2000, 36(2-3);61-74.
- 266) Gaedtke L., Thoenes L., Culmsee C., Mayer B., Wagner E. Proteomic analysis reveals differences in protein expression in spheroid versus monolayer cultures of lowpassage colon carcinoma cells. *J Proteome Res* 2007, 6(11);4111-4118.
- 267) Bhang S.H., Lee S., Shin J.Y., Lee T.J., Kim B.S. Transplantation of cord blood mesenchymal stem cells as spheroids enhances vascularization. *Tissue Eng Part A* 2012a, 18(19-20);2138-47.
- 268) Saleh F.A., Genever P.G. Turning round: multipotent stromal cells, a three-dimensional revolution? *Cytotherapy* 2011, 13(8);903-912.
- 269) Baraniak P.R., McDevitt T.C. Scaffold-free culture of mesenchymal stem cell spheroids in suspension preserves multilineage potential. *Cell Tissue Res* 2012, 347(3);701-11.
- 270) Skiles M.L., Fancy R., Topiwala P., Sahai S., Blanchette J.O. Correlating hypoxia with insulin secretion using a fluorescent hypoxia detection system. *J Biomed Mater Res B Appl Biomater* 2011a, 97(1);148-55.
- 271) Semenza G.L. HIF-1 and mechanisms of hypoxia sensing. *Curr Opin Cell Biol* 2001, 13(2);167-171.
- 272) Matta S.G., Wobken J.D., Williams F.G., Bauer G.E. Pancreatic islet cell reaggregation systems: efficiency of cell reassociation and endocrine cell topography of rat islet-like aggregates. *Pancreas* 1994, 9(4);439-449.

- 273) Carlsson P.O., Liss P., Andersson A., Jansson L. Measurements of oxygen tension in native and transplanted rat pancreatic islets. *Diabetes* 1998, 47(7);1027-1032.
- 274) Dulong J.L., Legallais C. A theoretical study of oxygen transfer including cell necrosis for the design of a bioartificial pancreas. *Biotechnol Bioeng* 2007, 96(5);990-998.
- 275) Moritz W., Meier F., Stroka D., Giuliani M., Kugelmeier P., Nett PhC., Lehmann R., Candinas D., Gassmann M., Weber M. Apoptosis in hypoxic human pancreatic islets correlates with HIF-1 $\alpha$  expression. *FASEB J* 2002, 16(7);745-747.
- 276) Ma T., Grayson W.L., Frölich M., Vunjak-Novakovic G. Hypoxia and stem cell-based engineering of mesenchymal tissues. *Biotechnol Prog* 2009, 25(1);32-42.
- 277) He J., Genetos D.C., Yellowley C.E., Leach J.K. Oxygen tension differentially influences osteogenic differentiation of human adipose stem cells in 2D and 3D cultures. *J Cell Biochem* 2010, 110(1);87-96.
- 278) Skiles M.L., Wilder N.B., Sahai S., Blanchette J.O. Identifying HIF activity in three-dimensional cultures of islet-like clusters. *Int J Artif Organs* 2013, 36(3);175-183.
- 279) Davalli A.M., Ogawa Y., Ricordi C., Scharp D.W., Bonner-Weir S., Weir G.C. A selective decrease in the beta cell mass of human islets transplanted into diabetic nude mice. *Transplantation* 1995, 59(6);817-820.
- 280) Carlsson P.O., Palm F., Andersson A., Liss P. Markedly decreased oxygen tension in transplanted rat pancreatic islets irrespective of the implantation site. *Diabetes* 2001, 50(3);489-495.
- 281) Miao G., Ostrowski R.P., Mace J., Hough J., Hopper A., Peverini R., Chinnock R., Zhang J., Hathout E. Dynamic production of hypoxia-inducible factor-1 $\alpha$  in early transplanted islets. *Am J Transplant* 2006, 6(11);2636-2643.
- 282) .259. Cornolti R., Figliuzzi M., Remuzzi A. Effect of micro- and macroencapsulation on oxygen consumption by pancreatic islets. *Cell Transplant* 2009, 18(2);195-201.
- 283) Semenza G.L. Hypoxia-inducible factor 1: regulator of mitochondrial metabolism and mediator of ischemic preconditioning. *Biochim Biophys Acta* 2011b, 1813(7);1263-1268.
- 284) Lo J.F., Wang Y., Blake A., Yu G., Harvat T.A., Jeon H., Oberholzer J., Eddington D.T. Islet preconditioning via multimodal microfluidic modulation of intermittent hypoxia. *Anal Chem* 2012, 84(4);1987-1993.

- 285) Schuit F.C., Huypens P., Heimberg H., Pipeleers D.G. Glucose sensing in pancreatic  $\beta$ -cells a model for the study of other glucose-related cells in gut, pancreas, and hypothalamus. *Diabetes* 2001, 50(1);1-11.
- 286) Cassavaugh J., Lounsbury K.M. Hypoxia-mediated biological control. *J Cell Biochem* 2011, 112(3);735-744.
- 287) Yu A.Y., Frid M.G., Shimoda L.A., Wiener C.M., Stenmark K., Semenza G.L. Temporal, spatial, and oxygen-related expression of hypoxia-inducible factor-1 in the lung. *Am J Physiol* 1998, 275(4 pt 1);L818-L826.
- 288) Springett R., Swartz H.M. Measurements of oxygen *in vivo*: overview and perspectives on methods to measure oxygen within cells and tissues. *Antioxid Redox Sign* 2007, 9(8);1295-1301.
- 289) Grist S.M., Chrostowski L., Cheung K.C. Optical oxygen sensors for applications in microfluidic cell culture. *Sensors* 2010, 10(10);9286-9316.
- 290) Luther M.J., Davies E., Muller D., Harrison M., Bone A.J., Persaud S.J., Jones P.M. Cell-to-cell contact influences proliferative marker expression and apoptosis in MIN6 cells grown in islet-like structures. *Am J Endocrinol Metab* 2005, 288(3);E502-E509.
- 291) Hauge-Evans A.C., Squires P.E., Persaud S.J., Jones P.M. Pancreatic  $\beta$ -cell- $\beta$ -cell interactions are required for integrated responses to nutrient stimuli. *Diabetes* 1999, 48(7);1402-1408.
- 292) Lin C.C., Anseth K. Cell-cell communication mimicry with poly(ethylene glycol) hydrogels for enhancing  $\beta$ -cell function. *Proc Natl Acad Sci USA* 2011, 108(16);6380-6385.
- 293) Luther M.J., Hauge-Evans A., Souza K.L.A., Jörns A., Lenzen S., Persaud S.J., Jones P.M. MIN6  $\beta$ -cell- $\beta$ -cell interactions influence insulin secretory responses to nutrients and non-nutrients. *Biochem Biophys Res Commun* 2006, 343(1);99-104.
- 294) Schietke R., Warnecke C., Wacker I., Schödel J., Mole D.R., Campean V., Amann K., Goppelt-Struebe M., Behrens J., Eckardt K.U., Wiesener M.S. The lysyl oxidases LOX and LOXL2 are necessary and sufficient to repress E-cadherin in hypoxia. *J Biologic Chem* 2010, 285(9);6658-6669.
- 295) Evans A.J., Russel R.C., Roche O., Burry T.N., Fish J.E., Chow V.W., Kim W.Y., Saravanan A., Maynard M.A., Gervais M.L., Sufan R.I., Roberts A.M., Wilson L.A., Betten M., Vandewalle C., Berx G., Marsden P.A., Irwin M.S., The B.T., Jewett

- M.A. Ohh M. VHL promotes E2 box-dependent E-cadherin transcription by HIF-mediated regulation of SIP1 and Snail. *Molec Cell Biol* 2007, 27(1);157-169.
- 296) Lee D.Y., Park S.J., Nam J.H., Byun Y. Optimal aggregation of dissociated islet cells for functional islet-like cluster. *J Biomater Sci Polym Ed* 2008, 19(4);441-452
- 297) Levenberg S., Rouwkema J., Macdonald M., Garfein E.S., Kohane D.S., Darland D.C., Marini R., Van Blitterswijk C.A., Mulligan R.C., D'Amore P.A., Langer R. Engineering vascularized skeletal muscle tissue. *Nat Biotechnol* 2005, 23(7);879-884.
- 298) Kunz-Schughart L.A., Schroeder J.A., Wondrak M., van Rey F., Lehle K., Hofstaedter F., Wheatley D.N. Potential of fibroblasts to regulate the formation of three-dimensional vessel-like structures from endothelial cells *in vitro*. *Am J Physiol Cell Physiol* 2006, 290(5);C1385-1398.
- 299) Blasi A., Martino C., Balducci L., Saldarelli M., Soletti A., Navone S.E., Canzi L., Cristini S., Invernici G., Parati E.A., Alessandri G. Dermal fibroblasts display similar phenotypic and differentiation capacity to fat-derived mesenchymal stem cells, but differ in anti-inflammatory and angiogenic potential. *Vasc Cell* 2011, 3(1);5.
- 300) Halfon S., Abramov N., Grinblat B., Ginis I. Markers distinguishing mesenchymal stem cells from fibroblasts are downregulated with passaging. *Stem Cells Dev* 2011, 20(1);53-66.
- 301) Nie C., Yang D., Xu J., Si Z., Jin X., Zhang J. Locally administered adipose-derived stem cells accelerate wound healing through differentiation and vasculogenesis. *Cell Transplant* 2011, 20(2);205-216.
- 302) Kang Y., Park C., Kim D., Seong C.M., Kwon K., Choi C. Unsorted human adipose tissue-derived stem cells promote angiogenesis and myogenesis in murine ischemic hindlimb model. *Microvasc Res* 2010, 80(3);310-316.
- 303) Bhang S.H., Cho S.W., La W.G., Lee T.J., Yang H.S., Sun A.Y., Baek S.H., Rhie J.W., Kim B.S. Angiogenesis in ischemic tissue produced by spheroid grafting of human adipose-derived stromal cells. *Biomaterials* 2011, 32(11);2734-2747.
- 304) Shweiki D., Itin A., Soffer D., Keshet E. Vascular endothelial growth factor induced by hypoxia may mediate hypoxia-induced angiogenesis. *Nature* 1992, 359(6398);843-845.
- 305) Germain S., Monnot C., Muller L., Eichmann A. Hypoxia-driven angiogenesis: role of tip cells and extracellular matrix scaffolding. *Curr Opin Hematol* 2010, 17(3);245-251.

- 306) Maxwell P.H., Ratcliffe P. Oxygen sensors and angiogenesis. *Semin Cell Dev Biol* 2002, 13(1);29-37.
- 307) Fong G.H. Regulation of angiogenesis by oxygen sensing mechanisms. *J Mol Med* 2009, 87(6);549-560.
- 308) Rey S., Semenza G.L. Hypoxia-inducible factor-1-dependent mechanisms of vascularization and vascular remodelling. *Cardiovasc Res* 2010, 86(2);236-242.
- 309) Brahimi-Horn C., Berra E., Pouyssegur J. Hypoxia: the tumor's gateway to progression along the angiogenic pathway. *Trends Cell Biol* 2001, 11(11);S32-S36.
- 310) Semenza G.L. Hypoxia-inducible factors: mediators of cancer progression and targets for cancer therapy. *Trends Pharmacol Sci* 2012b, 33(4);207-214.
- 311) Bhang S.H., Lee S., Lee T.J., La W.G., Yang H.S., Cho S.W., Kim B.S. Three-dimensional cell grafting enhances the angiogenic efficacy of human umbilical vein endothelial cells. *Tissue Eng Part A* 2012b, 18(3-4);310-319.
- 312) Zelzer E., Mamluk R., Ferrara N., Johnson R.S., Schipani E., Olsen B.R. VEGFA is necessary for chondrocyte survival during bone development. *Development* 2004, 131(9);2161-2171.
- 313) Araldi E., Schipani E. Hypoxia, HIFs and bone development. *Bone* 2010, 47(2);190-196.
- 314) Skiles M.L., Sahai S., Blanchette J.O. Tracking hypoxic signaling within encapsulated cell aggregates. *J Vis Exp* 2011b, 16(58);3521.
- 315) Sahai S., McFarland R., Skiles M.L., Sullivan D., Williams A., Blanchette J.O. Tracking hypoxic signaling in encapsulated stem cells. *Tissue Eng Part C Methods* 2012, 18(7);557-565.
- 316) Revsbech N.P., Ward D.M. Oxygen microelectrode that is insensitive to medium chemical composition: use in an acid microbial mat dominated by cyanidium caldarium. *Appl Environ Microbiol* 1983, 45(3);755-759.
- 317) Krihak M.K., Shahriari M.R. Highly sensitive, all solid state fiber optic sensor based on the sol-gel coating technique. *Electron Lett* 1996, 32(3);240-242.
- 318) Acosta M.A., Leki P.Y., Kostov Y.V., Leach J.B. Fluorescent microparticles for sensing cell microenvironment oxygen levels within 3D scaffolds. *Biomaterials* 2007, 30(17);3068-3074.

- 319) Gibbs B.F., Yasinska I.M., Pchejetski D., Wyszynski R.W., Sumbayev V.V. Differential control of hypoxia-inducible factor 1 activity during pro-inflammatory reactions of human haematopoietic cells of myeloid lineage. *Int J Biochem Cell Biol* 2012, 44(11);1739-1749.
- 320) Pettersen E.O., Juul N.O., Rønning O.W. Regulation of protein metabolism of human cells during and after acute hypoxia. *Cancer Res* 1986, 46(9);4346-4351.
- 321) Koumenis C., Naczki C., Koritzinsky M., Rastani S., Diehl A., Sonenberg N., Koromilas A., Wouters B.G. Regulation of protein synthesis by hypoxia via activation of the endoplasmic reticulum kinase PERK and phosphorylation of the translation initiation factor eIF $\alpha$ . *Mol Cell Biol* 2002, 22(21);7405-7416.
- 322) Greijer A.E., van der Wall E. The role of hypoxia inducible factor 1 (HIF-1) in hypoxia induced apoptosis. *J Clin Pathol* 2004, 57(10);1009-1014.
- 323) Kiang J.G., Tsen K.T. Biology of hypoxia. *Chin J Physiol* 2006, 49(5);223-233.
- 324) Burton T.R., Gibson S.B. The role of bcl-2 family member BNIP3 in cell death and disease: NIPing at the heels of death. *Cell Death Differ* 2009, 16(4);515-523.

## JOHN WILEY AND SONS LICENSE TERMS AND CONDITIONS

Apr 17, 2013

---

---

This is a License Agreement between Matthew L Skiles ("You") and John Wiley and Sons ("John Wiley and Sons") provided by Copyright Clearance Center ("CCC"). The license consists of your order details, the terms and conditions provided by John Wiley and Sons, and the payment terms and conditions.

**All payments must be made in full to CCC. For payment instructions, please see information listed at the bottom of this form.**

License Number	3131480979680
License date	Apr 17, 2013
Licensed content publisher	John Wiley and Sons
Licensed content publication	Journal of Biomedical Materials Research
Licensed content title	Correlating hypoxia with insulin secretion using a fluorescent hypoxia detection system
Licensed copyright line	Copyright © 2011 Wiley Periodicals, Inc.
Licensed content author	Matthew L. Skiles,Romone Fancy,Pritesh Topiwala,Suchit Sahai,James O. Blanchette
Licensed content date	Feb 2, 2011
Start page	148
End page	155
Type of use	Dissertation/Thesis
Requestor type	Author of this Wiley article
Format	Print and electronic
Portion	Full article
Will you be translating?	No
Total	0.00 USD
Terms and Conditions	

## TERMS AND CONDITIONS

This copyrighted material is owned by or exclusively licensed to John Wiley & Sons, Inc. or one of its group companies (each a "Wiley Company") or a society for whom a Wiley Company has exclusive publishing rights in relation to a particular journal (collectively **WILEY**). By clicking "accept" in connection with completing this licensing transaction, you agree that the following terms and conditions apply to this transaction (along with the billing and payment terms and conditions established by the Copyright Clearance Center Inc., ("CCC's Billing and Payment terms and conditions"), at the time that you opened your RightsLink account (these are available at any time at <http://myaccount.copyright.com>).

### Terms and Conditions

1. The materials you have requested permission to reproduce (the "Materials") are protected by copyright.
2. You are hereby granted a personal, non-exclusive, non-sublicensable, non-transferable, worldwide, limited license to reproduce the Materials for the purpose specified in the licensing process. This license is for a one-time use only with a maximum distribution equal to the number that you identified in the licensing process. Any form of republication granted by this license must be completed within two years of the date of the grant of this license (although copies prepared before may be distributed thereafter). The Materials shall not be used in any other manner or for any other purpose. Permission is granted subject to an appropriate acknowledgement given to the author, title of the material/book/journal and the publisher. You shall also duplicate the copyright notice that appears in the Wiley publication in your use of the Material. Permission is also granted on the understanding that nowhere in the text is a previously published source acknowledged for all or part of this Material. Any third party material is expressly excluded from this permission.
3. With respect to the Materials, all rights are reserved. Except as expressly granted by the terms of the license, no part of the Materials may be copied, modified, adapted (except for minor reformatting required by the new Publication), translated, reproduced, transferred or distributed, in any form or by any means, and no derivative works may be made based on the Materials without the prior permission of the respective copyright owner. You may not alter, remove or suppress in any manner any copyright, trademark or other notices displayed by the Materials. You may not license, rent, sell, loan, lease, pledge, offer as security, transfer or assign the Materials, or any of the rights granted to you hereunder to any other person.
4. The Materials and all of the intellectual property rights therein shall at all times remain the exclusive property of John Wiley & Sons Inc or one of its related companies (WILEY) or their respective licensors, and your interest therein is only that of having possession of

and the right to reproduce the Materials pursuant to Section 2 herein during the continuance of this Agreement. You agree that you own no right, title or interest in or to the Materials or any of the intellectual property rights therein. You shall have no rights hereunder other than the license as provided for above in Section 2. No right, license or interest to any trademark, trade name, service mark or other branding ("Marks") of WILEY or its licensors is granted hereunder, and you agree that you shall not assert any such right, license or interest with respect thereto.

5. NEITHER WILEY NOR ITS LICENSORS MAKES ANY WARRANTY OR REPRESENTATION OF ANY KIND TO YOU OR ANY THIRD PARTY, EXPRESS, IMPLIED OR STATUTORY, WITH RESPECT TO THE MATERIALS OR THE ACCURACY OF ANY INFORMATION CONTAINED IN THE MATERIALS, INCLUDING, WITHOUT LIMITATION, ANY IMPLIED WARRANTY OF MERCHANTABILITY, ACCURACY, SATISFACTORY QUALITY, FITNESS FOR A PARTICULAR PURPOSE, USABILITY, INTEGRATION OR NON-INFRINGEMENT AND ALL SUCH WARRANTIES ARE HEREBY EXCLUDED BY WILEY AND ITS LICENSORS AND WAIVED BY YOU.

6. WILEY shall have the right to terminate this Agreement immediately upon breach of this Agreement by you.

7. You shall indemnify, defend and hold harmless WILEY, its Licensors and their respective directors, officers, agents and employees, from and against any actual or threatened claims, demands, causes of action or proceedings arising from any breach of this Agreement by you.

8. IN NO EVENT SHALL WILEY OR ITS LICENSORS BE LIABLE TO YOU OR ANY OTHER PARTY OR ANY OTHER PERSON OR ENTITY FOR ANY SPECIAL, CONSEQUENTIAL, INCIDENTAL, INDIRECT, EXEMPLARY OR PUNITIVE DAMAGES, HOWEVER CAUSED, ARISING OUT OF OR IN CONNECTION WITH THE DOWNLOADING, PROVISIONING, VIEWING OR USE OF THE MATERIALS REGARDLESS OF THE FORM OF ACTION, WHETHER FOR BREACH OF CONTRACT, BREACH OF WARRANTY, TORT, NEGLIGENCE, INFRINGEMENT OR OTHERWISE (INCLUDING, WITHOUT LIMITATION, DAMAGES BASED ON LOSS OF PROFITS, DATA, FILES, USE, BUSINESS OPPORTUNITY OR CLAIMS OF THIRD PARTIES), AND WHETHER OR NOT THE PARTY HAS BEEN ADVISED OF THE POSSIBILITY OF SUCH DAMAGES. THIS LIMITATION SHALL APPLY NOTWITHSTANDING ANY FAILURE OF ESSENTIAL PURPOSE OF ANY LIMITED REMEDY PROVIDED HEREIN.

9. Should any provision of this Agreement be held by a court of competent jurisdiction to be illegal, invalid, or unenforceable, that provision shall be deemed amended to achieve as nearly as possible the same economic effect as the original provision, and the legality, validity and enforceability of the remaining provisions of this Agreement shall not be affected or impaired thereby.

10. The failure of either party to enforce any term or condition of this Agreement shall not constitute a waiver of either party's right to enforce each and every term and condition of this Agreement. No breach under this agreement shall be deemed waived or excused by either party unless such waiver or consent is in writing signed by the party granting such waiver or consent. The waiver by or consent of a party to a breach of any provision of this Agreement shall not operate or be construed as a waiver of or consent to any other or subsequent breach by such other party.

11. This Agreement may not be assigned (including by operation of law or otherwise) by you without WILEY's prior written consent.

12. Any fee required for this permission shall be non-refundable after thirty (30) days from receipt

13. These terms and conditions together with CCC's Billing and Payment terms and conditions (which are incorporated herein) form the entire agreement between you and WILEY concerning this licensing transaction and (in the absence of fraud) supersedes all prior agreements and representations of the parties, oral or written. This Agreement may not be amended except in writing signed by both parties. This Agreement shall be binding upon and inure to the benefit of the parties' successors, legal representatives, and authorized assigns.

14. In the event of any conflict between your obligations established by these terms and conditions and those established by CCC's Billing and Payment terms and conditions, these terms and conditions shall prevail.

15. WILEY expressly reserves all rights not specifically granted in the combination of (i) the license details provided by you and accepted in the course of this licensing transaction, (ii) these terms and conditions and (iii) CCC's Billing and Payment terms and conditions.

16. This Agreement will be void if the Type of Use, Format, Circulation, or Requestor Type was misrepresented during the licensing process.

17. This Agreement shall be governed by and construed in accordance with the laws of the State of New York, USA, without regards to such state's conflict of law rules. Any legal action, suit or proceeding arising out of or relating to these Terms and Conditions or the breach thereof shall be instituted in a court of competent jurisdiction in New York County in the State of New York in the United States of America and each party hereby consents and submits to the personal jurisdiction of such court, waives any objection to venue in such court and consents to service of process by registered or certified mail, return receipt requested, at the last known address of such party.

### **Wiley Open Access Terms and Conditions**

Wiley publishes Open Access articles in both its Wiley Open Access Journals program [<http://www.wileyopenaccess.com/view/index.html>] and as Online Open articles in its subscription journals. The majority of Wiley Open Access Journals have adopted the [Creative Commons Attribution License](#) (CC BY) which permits the unrestricted use, distribution, reproduction, adaptation and commercial exploitation of the article in any medium. No permission is required to use the article in this way provided that the article is properly cited and other license terms are observed. A small number of Wiley Open Access journals have retained the [Creative Commons Attribution Non Commercial License](#) (CC BY-NC), which permits use, distribution and reproduction in any medium, provided the original work is properly cited and is not used for commercial purposes.

Online Open articles ♦ Authors selecting Online Open are, unless particular exceptions apply, offered a choice of Creative Commons licenses. They may therefore select from the CC BY, the CC BY-NC and the [Attribution-NoDerivatives](#) (CC BY-NC-ND). The CC BY-NC-ND is more restrictive than the CC BY-NC as it does not permit adaptations or modifications without rights holder consent.

Wiley Open Access articles are protected by copyright and are posted to repositories and websites in accordance with the terms of the applicable Creative Commons license referenced on the article. At the time of deposit, Wiley Open Access articles include all changes made during peer review, copyediting, and publishing. Repositories and websites that host the article are responsible for incorporating any publisher-supplied amendments or retractions issued subsequently.

Wiley Open Access articles are also available without charge on Wiley's publishing platform, **Wiley Online Library** or any successor sites.

Conditions applicable to all Wiley Open Access articles:

- The authors' moral rights must not be compromised. These rights include the right of "paternity" (also known as "attribution" - the right for the author to be identified as such) and "integrity" (the right for the author not to have the work altered in such a way that the author's reputation or integrity may be damaged).
- Where content in the article is identified as belonging to a third party, it is the obligation of the user to ensure that any reuse complies with the copyright policies of the owner of that content.
- If article content is copied, downloaded or otherwise reused for research and other purposes as permitted, a link to the appropriate bibliographic citation (authors, journal, article title, volume, issue, page numbers, DOI and the link to the definitive published version on Wiley Online Library) should be maintained. Copyright notices and disclaimers must not be deleted.
  - ♦ Creative Commons licenses are copyright licenses and do not confer any other rights, including but not limited to trademark or patent rights.

- Any translations, for which a prior translation agreement with Wiley has not been agreed, must prominently display the statement: "This is an unofficial translation of an article that appeared in a Wiley publication. The publisher has not endorsed this translation."

### **Conditions applicable to non-commercial licenses (CC BY-NC and CC BY-NC-ND)**

For non-commercial and non-promotional purposes individual non-commercial users may access, download, copy, display and redistribute to colleagues Wiley Open Access articles. In addition, articles adopting the CC BY-NC may be adapted, translated, and text- and data-mined subject to the conditions above.

### **Use by commercial "for-profit" organizations**

Use of non-commercial Wiley Open Access articles for commercial, promotional, or marketing purposes requires further explicit permission from Wiley and will be subject to a fee. Commercial purposes include:

- Copying or downloading of articles, or linking to such articles for further redistribution, sale or licensing;
- Copying, downloading or posting by a site or service that incorporates advertising with such content;
- The inclusion or incorporation of article content in other works or services (other than normal quotations with an appropriate citation) that is then available for sale or licensing, for a fee (for example, a compilation produced for marketing purposes, inclusion in a sales pack)
- Use of article content (other than normal quotations with appropriate citation) by for-profit organizations for promotional purposes
- Linking to article content in e-mails redistributed for promotional, marketing or educational purposes;
- Use for the purposes of monetary reward by means of sale, resale, license, loan, transfer or other form of commercial exploitation such as marketing products
- Print reprints of Wiley Open Access articles can be purchased from: [corporatesales@wiley.com](mailto:corporatesales@wiley.com)

The modification or adaptation for any purpose of an article referencing the CC BY-NC-ND License requires consent which can be requested from [RightsLink@wiley.com](mailto:RightsLink@wiley.com) .

Other Terms and Conditions:

BY CLICKING ON THE "I AGREE..." BOX, YOU ACKNOWLEDGE THAT YOU HAVE READ AND FULLY UNDERSTAND EACH OF THE SECTIONS OF AND PROVISIONS SET FORTH IN THIS AGREEMENT AND THAT YOU ARE IN AGREEMENT WITH AND ARE WILLING TO ACCEPT ALL OF YOUR OBLIGATIONS AS SET FORTH IN THIS AGREEMENT.

**v1.8**

Dear Dr Skiles,

According to the copyright regulations applied by IJAO, authors retain the following rights:

**Retained rights**

Provided the source is fully quoted at all times, Authors are hereby granted the right to:

a) reproduce the manuscript in whole or in part in any printed book or thesis of which they are the author(s).

b) They and any academic institution where they work at the time may reproduce the Manuscript in a reasonable number of copies for the purpose of course teaching. This does not apply if a commercial charge is made for the training course.

c) To post a copy of the Manuscript as accepted for publication after peer review (in Word or Text format) on the Authors' website provided that they also link to the article to the Journal's web site.

d) To reuse figures or tables created by them and contained in the Manuscript in other works created by them.

You may therefore proceed with your dissertation.

With kind regards,

Lucia Steele

Lucia Steele

Permissions

Wichtig Editore Srl | Via Friuli 72 | 20135 Milan (Italy)

Office +39 025455122 ext. 24

Mobile +39 3939129472

lucia.steele@wichtig.it | *Skype: luciasteele62*